FLOODING OF INDIAN RIVER BAY AND REHOBOTH BAY THROUGH INDIAN RIVER INLET AND BY WAVE OVERTOPPING OF BARRIER BEACH

by

Tingting Zhu

A thesis submitted to the Faculty of the University of Delaware in partial fulfillment of the requirements for the degree of Master of Science in Ocean Engineering

Spring 2017

FLOODING OF INDIAN RIVER BAY AND REHOBOTH BAY

THROUGH INDIAN RIVER INLET AND

BY WAVE OVERTOPPING OF BARRIER BEACH

by

Tingting Zhu

Approved: _____

Nobuhisa Kobayashi, Ph.D.
Professor in charge of thesis on behalf of the Advisory Committee

Approved: _____

Harry W. Shenton III, Ph.D.
Chair of the Department of Civil & Environmental Engineering

Approved: _____

Babatunde A. Ogunnaike, Ph.D.
Dean of the College of Engineering

Approved: _____

Ann L. Ardis, Ph.D.
Senior Vice Provost for Graduate and Professional Education

ACKNOWLEDGMENTS

This study was supported by the Delaware Sea Grant No. NOAA SG2016-18 R/OCE-9 and by the U.S. Army Corps of Engineers under Cooperative Agreement No. W912HZ-15-02-0028. I would like to thank all of the little people (especially Chicken Little): my adviser, Nobushia Kobayashi; and my friends and colleagues Hyun Dong Kim, Wanyi Xing and Liangyi Yue. I must also thank my parents and boyfriend, without whom none of this would ever have been possible.

TABLE OF CONTENTS

LIST OF TABLES

LIST OF FIGURES

ABSTRACT

A simple analytical model for a small bay with a tidal inlet channel is developed to predict the peak stillwater elevation in the bay for the given peak stillwater elevation and surge duration in the ocean. The model is applied to the Delaware Atlantic coast where three bay tide gauges together with one ocean tide gauge have been in operation since 2005. 27 storms identified during 2005 – 2015 are used to calibrate a dimensionless parameter related to the inlet and bay characteristics. The calibrated model predicts the peak stillwater elevation within 10% errors at two bay gauges and within 30% errors at the third bay gauge. Wave overtopping and overwash over the barrier beach between the ocean and bay occurred during Hurricane Sandy in 2012. Wave overtopping and barrier beach evolution are predicted using the cross-shore numerical model CSHORE. The analytical model including wave overtopping predicts the peak stillwater elevation increase of 0.1 – 0.2 m in the bay. The coupled approach is useful in evaluating bay flooding risk during extreme storms in efficient manners.

Chapter 1

INTRODUCTION

Low-laying barrier beaches are common along the U.S. East coast. Bays landward of barrier beaches are typically connected with the Atlantic Ocean through tidal inlets. Bay flooding is generally predicted using numerical storm tide (sum of storm surge and tide) models. Cañizares and Irish (2008) developed a simulation methodology to compute storm-induced bay water levels along the south shore of Long Island, New York. The nearshore water level, waves and sediment transport were computed using the software Delft 3D (WL|Delft 2001) which is limited to the submerged area of the computation domain. The simulation of dune crest lowering prior to inundation was performed using the numerical model SBEACH (storm-induced beach change) by Larson and Kraus (1989) which is limited to an emerged dune. The numerical simulations for 1938 and 1992 storms provided realistic results and good agreement with available data after bottom friction and sediment parameters were adjusted and pre-inundation dune lowering was calibrated empirically. Computation was made with and without barrier beach breaching. The comparison of the computed water levels indicated the water level increase of about 1 m and 0.1 m due to breaching for the 1938 and 1992 storms. Irish and Cañizares (2009) also examined the effect of ocean wave setup generated by breaking waves. The bay water level increase was estimated to be 0.1 – 0.2 m for the 1938 and 1992 storms. Their coupled simulation of barrier beach morphodynamics and bay flooding is demanding

computationally and may not be suited for the statistical analysis of extreme water levels for a large number of storms.

Nadal-Caraballo et al. (2016) performed a statistical analysis of extreme water levels for 23 water level stations with a minimum of 30 years of hourly water level measurements throughout the U.S. Atlantic coast. Monthly maxima data were also used to complement the hourly water level data and increase the record length to 38 – 120 years for the 23 stations. The analyzed peak stillwater elevations for recurrence intervals (annual probabilities) of 10, 50, 100, and 500 years (10, 2, 1, and 0.2%) were presented at each station. The Flood Insurance Rate Map (FIRM) of the Federal Emergency Management Agency (FEMA 2011) is based on the peak stillwater elevation during the 100-year storm. Water level measurements in small bays are shorter than 30 years even if such measurements are available. In this study, a simple analytical model is developed to relate the peak stillwater elevations outside and inside of a small bay. The model is applied to Indian River Bay and Rehoboth Bay in Delaware connected to the Atlantic Ocean through the Indian River Inlet. Water level measurements during 2005 to 2015 at 3 stations inside these bays are analyzed and compared with those at Lewes, Delaware located outside the Indian River Inlet. The station at Lewes is one of the 23 stations in the statistical analysis performed by Nadal-Caraballo et al. (2016) who indicated the record length of 94 years at Lewes. The analytical model is compared with 27 high water events during 2005 to 2015. One of the 27 events was caused by Hurricane Sandy on October 29, 2012.

Wave overtopping and overwash of the barrier beach between the ocean and bay occurred during Hurricane Sandy but the barrier beach was not breached. The cross-shore model CSHORE (Kobayashi 2016) is used to compute the barrier beach

profile evolution and wave overtopping rate along 14 cross-shore lines with an alongshore interval of 515 m. The computed profile evolutions indicate no barrier beach breaching. The computed wave overtopping rates indicate a noticeable effect of wave overtopping on bay flooding during Hurricane Sandy. The analytical model is extended to include the contribution of wave overtopping to the bay water level increase, which was not included in the simulation by Cañizares and Irish (2008). The extended analytical model is used to quantify the wave overtopping effect.

The following chapters present the available field data, analytical model without wave overtopping, comparison with the data, wave overtopping and overwash of the barrier beach, analytical model including wave overtopping, and wave overtopping effect on bay flooding, hypothetical storm SandyPlus, and conclusions.

Chapter 2

AVAILABLE FIELD DATA

Figure 2.1 shows the Delaware Atlantic coast with the locations of available data used in this study. The net longshore sand transport along the Delaware Atlantic coast is to the north and the northern end of the coast is Cape Henlopen spit at the mouth of the Delaware Bay. The beaches such as Rehoboth Beach and Dewey Beach are maintained by periodic sand placement (e.g., Figlus and Kobayashi 2008) and by a sand bypassing system to pump sand from the south side of the Indian River Inlet to its north side (e.g., Keshtpoor et al. 2014). Sediment transport within Indian River Inlet was investigated by Keshtpoor et al. (2015). The cross section of the inlet channel is approximately trapezoidal with inclined side slopes protected by rock. The side slope is 1/2 (vertical/horizontal) and the bottom width is about 100 m. The water depth is approximately 20 m below the mean sea level. The cross-sectional area A_C and hydraulic radius R of the inlet channel are $A_C = 2800$ m^2 and $R = 15$ m. The channel length L including rock jetties built on both sides of the channel extending into the ocean is about $L = 1$ km. Measured peak ebb and flood tidal velocities were about 2 m/s (Keshtpoor et al. 2015) and the corresponding discharge is about 5600 m^3/s. The surface areas of Indian River Bay and Rehoboth Bay are almost equal and the combined surface area A_B is approximately 75 km^2. These values of A_C, R, L and A_B are used in the analytical model in the next section.

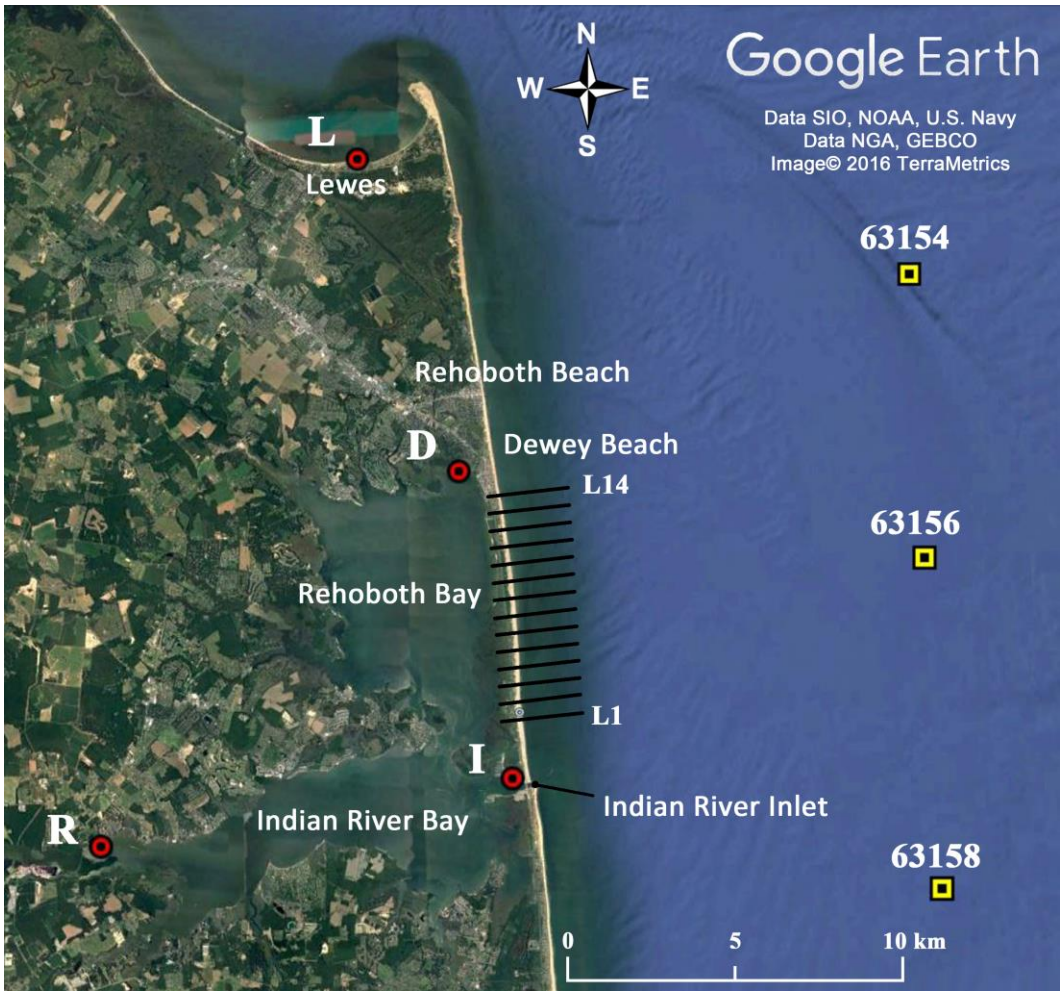

Figure 2.1 Tide gauge at Lewes(L), Indian River Bay Inlet(I), Indian River at Rosedale Beach(R), and Rehoboth Bay at Dewey(D), wave data at WIS63156 station, and barrier beach profiles along 14 cross-shore lines (L1 to L14). Map created using Google Earth® software by Google

2.1 Tide Gauge Data

Tide gauge data at Lewes (L in Figure 2.1) are obtained from the Center for Operational Oceanographic Products and Services at the National Oceanic and Atmospheric Administration (NOAA 2015). The north American Vertical Datum of 1988 (NAVD88) is used as the datum in this study. The mean higher-high water,

mean sea level, and mean lower-low water elevations at gauge L are 0.62, –0.12, and –0.80 m, respectively. The tide gauge data at Indian River Bay Inlet (I), Indian River at Rosedale Beach (R), and Rehoboth Bay at Dewey Beach (D) are obtained from the U.S. Geological Survey (USGS 2016). The water level data inside the Indian River Bay and Rehoboth Bay are available since 2005. The data at gauges L, I, R, and D during 2005 – 2015 are used in the following analysis. The water level data were collected at a sampling rate of 0.1 h.

Nadal-Caraballo et al. (2016) analyzed 94-year record of historical extreme water levels at Lewes statistically. The threshold peak stillwater elevation was chosen to be 1.27 m (NAVD88) at Lewes. The corresponding number of storms per year was 1.5. This threshold elevation of 1.27 m at Lewes is used to identify storms during 2005 – 2015. Table 2.1 lists the date and peak stillwater elevation at Lewes (L) for each of the identified 27 storms and the corresponding peak stillwater elevations at gauges I, R, and D. For storms 1 – 8, the time series of the stillwater elevations at gauges I, R, and D are not available and the listed values are the daily maximum elevations on the day of each storm. The peak stillwater elevation decreased from gauge L seaward of the Indian River Inlet to gauge I and gauge R in Indian River Bay. The peak stillwater elevation was the lowest at gauge D at the northern end of Rehoboth Bay. The highest elevations among the 27 storms in Table 2.1 occurred during storm 20 (Hurricane Sandy). The surge duration T_s listed for each storm is used later in the analytical model in this study.

The 3-day time series of the stillwater elevations at gauges L, I, R, and D are plotted together, starting from one day before the date of each storm listed in Table 2.1. The time series with the sampling rate of 0.1 h are smoothed to reduce small

fluctuations. The smoothed value at given time t is the average value between (t – 0.5 h) and (t + 0.5 h). Figures 2.2 – 2.10 compare the smoothed time series at gauges L, I, R, and D for the 27 storms. The peak stillwater elevations at the ocean gauge L and

Table 2.1 Peak stillwater elevations (NAVD88) at tide gauges L, I, R and D for 27 storms with date and analytical surge duration T_s

Storm	Date			T_s (h)	Peak stillwater elevation (m)			
	Year	Month	Day		L	I	R	D
1	2005	05	24	9.4	1.39	1.12	NA	NA
2	2005	10	12	13.5	1.32	1.12	1.18	0.81
3	2006	01	30	8.1	1.38	1.03	1.00	NA
4	2006	02	11	12.0	1.32	1.21	1.12	0.73
5	2006	10	06	10.2	1.45	1.27	1.36	0.88
6	2006	11	22	11.1	1.32	1.28	1.26	0.90
7	2007	04	17	8.0	1.28	0.97	0.97	0.46
8	2007	06	12	8.7	1.27	0.98	0.99	0.60
9	2008	05	11	12.6	1.60	1.37	1.41	1.00
10	2008	09	24	12.2	1.29	1.21	1.28	0.74
11	2008	10	18	10.6	1.28	1.20	1.05	0.73
12	2009	10	16	10.8	1.45	1.25	1.29	0.95
13	2009	11	12	11.9	1.60	1.54	1.56	1.10
14	2009	12	18	11.7	1.38	1.19	1.33	0.78
15	2010	03	12	12.3	1.30	1.09	1.19	0.80
16	2011	05	16	7.9	1.27	NA	0.92	0.63
17	2011	08	26	10.7	1.70	NA	NA	0.97
18	2011	10	28	9.9	1.56	NA	1.27	0.79
19	2012	06	04	8.8	1.43	1.03	1.09	0.71
20	2012	10	28	13.4	1.85	1.75	1.66	1.34
21	2013	03	05	14.5	1.45	1.32	1.52	0.81
22	2013	03	08	9.5	1.29	1.08	1.05	0.78
23	2014	01	02	8.1	1.28	0.99	0.96	0.60
24	2014	02	12	10.9	1.30	1.02	1.21	0.59
25	2014	04	29	9.1	1.30	1.01	1.13	0.76
26	2014	12	08	11.6	1.36	1.09	1.22	0.94
27	2015	10	01	12.7	1.51	1.26	1.48	0.95
			Min	7.9	1.27	0.97	0.92	0.46
			Max	14.5	1.85	1.75	1.66	1.34

NA = Not Available

the bay gauges I and R occurred within the time interval of 1 h. The time lag of the peak stillwater elevation at gauge D at the northern end of Rehoboth Bay was about 2 h and noticeable. For storms 1 – 8, daily maximum and minimum elevations at gauges I, R and D are plotted in the middle of each day. Data are not available at gauge I for storms 16 – 18, and at gauge R for storm 17.

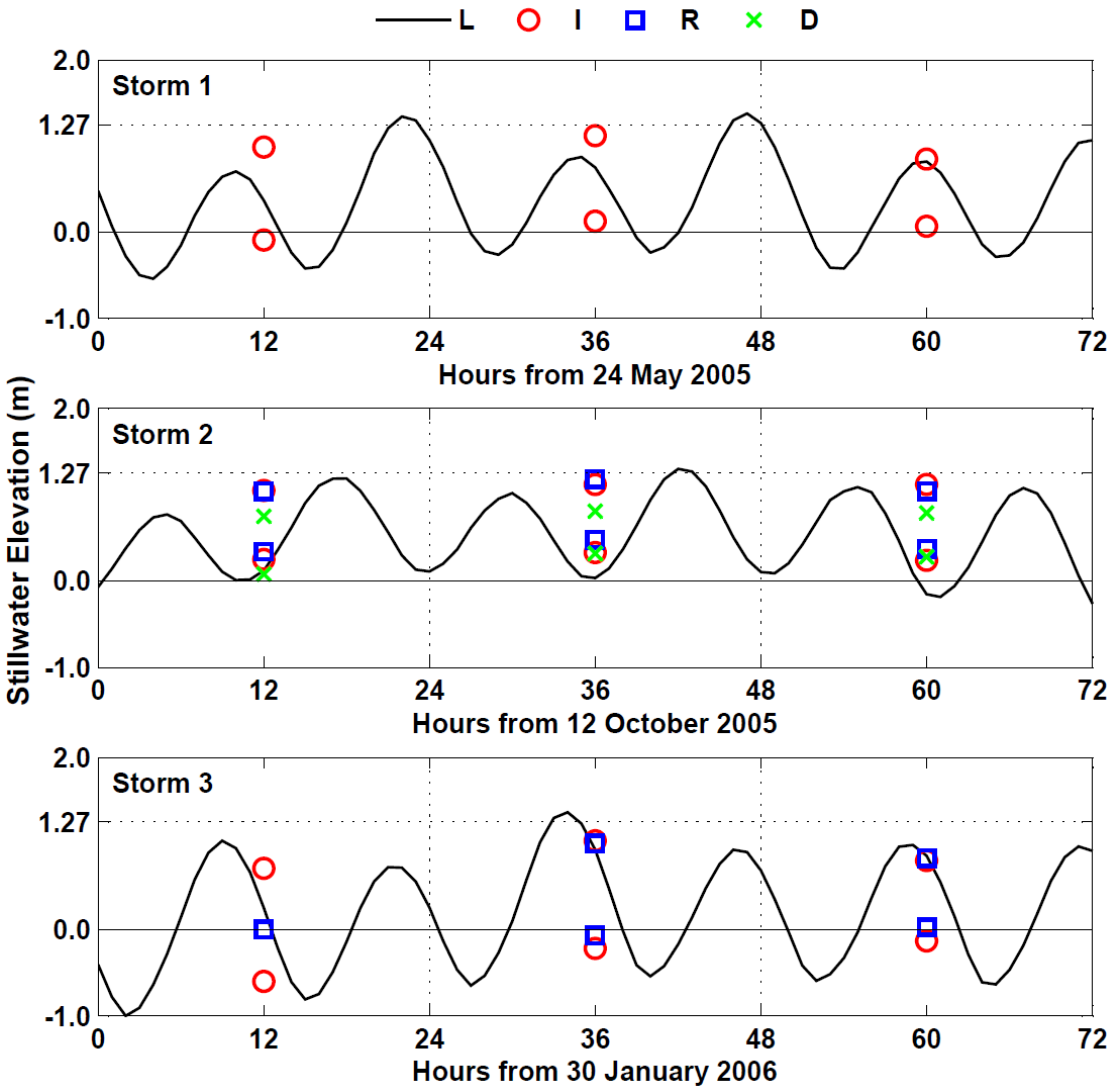

Figure 2.2 3-day time series of stillwater elevations at 4 tide gauges for storms 1, 2 and 3 where daily maximum and minimum elevations at gauges I, R and D are plotted in the middle of each day

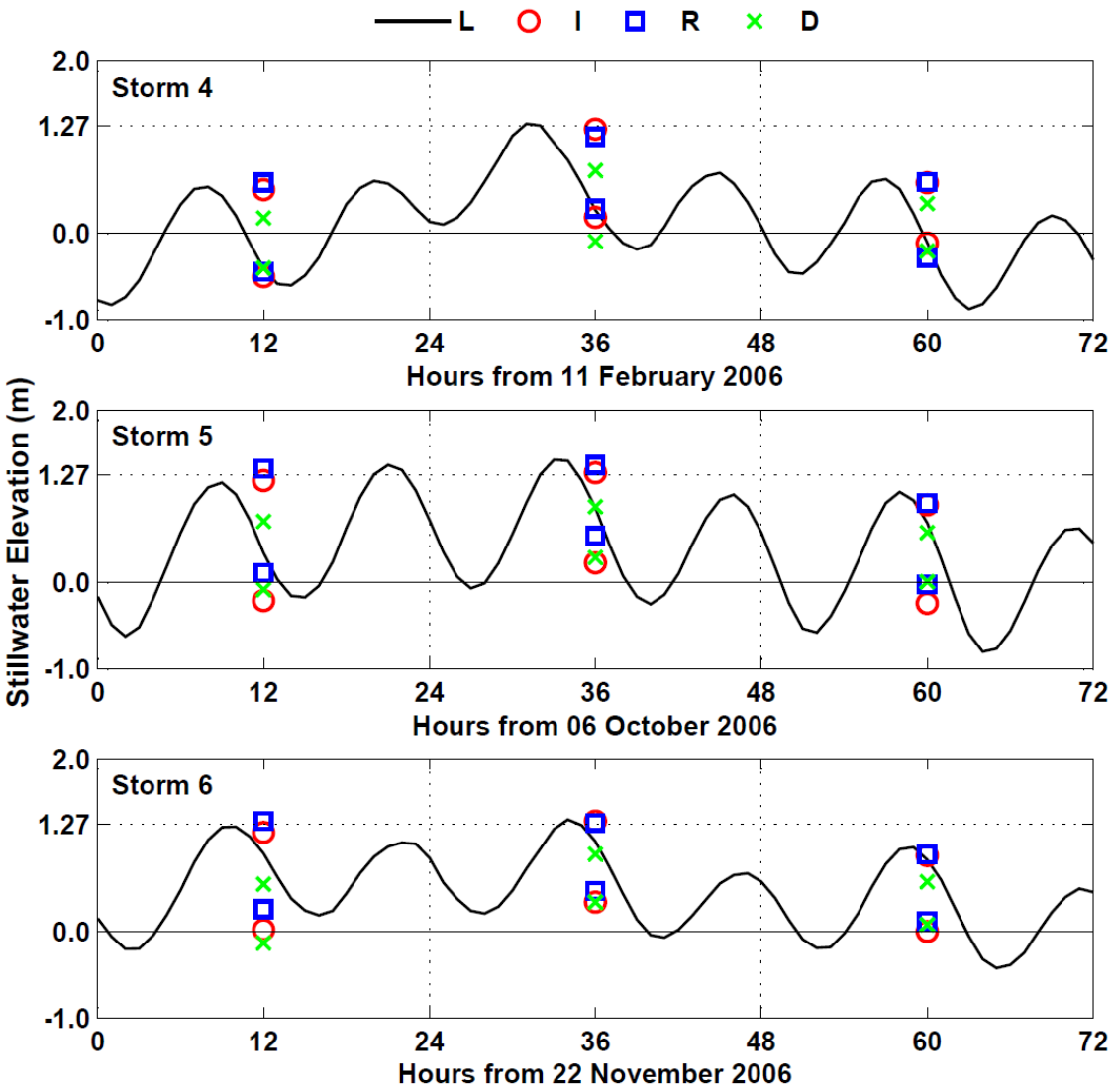

Figure 2.3 3-day time series of stillwater elevations at 4 tide gauges for storms 4, 5 and 6 where daily maximum and minimum elevations at gauges I, R and D are plotted in the middle of each day

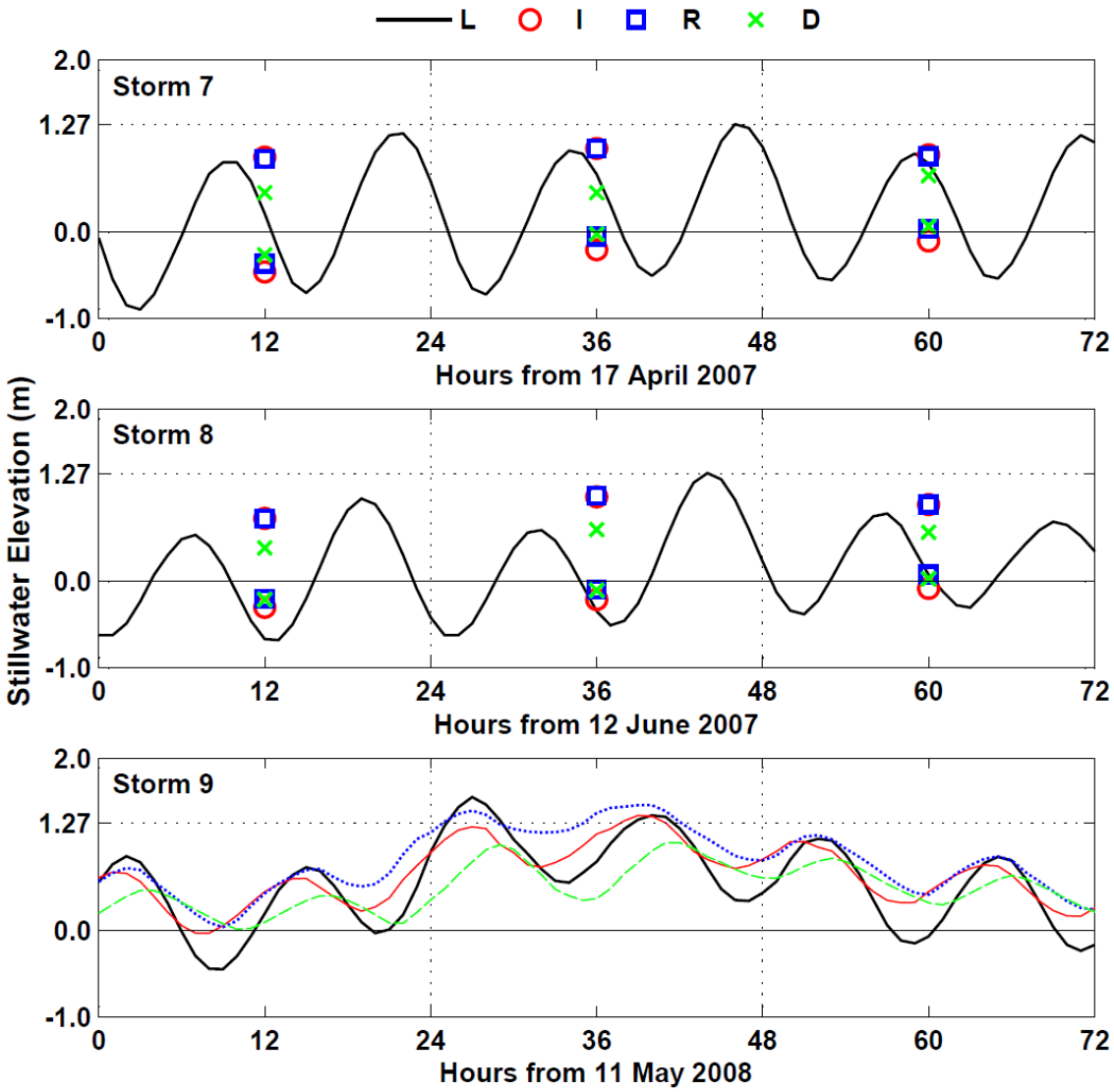

Figure 2.4 3-day time series of stillwater elevations at 4 tide gauges for storms 7, 8 and 9 where daily maximum and minimum elevations at gauges I, R and D are plotted in the middle of each day

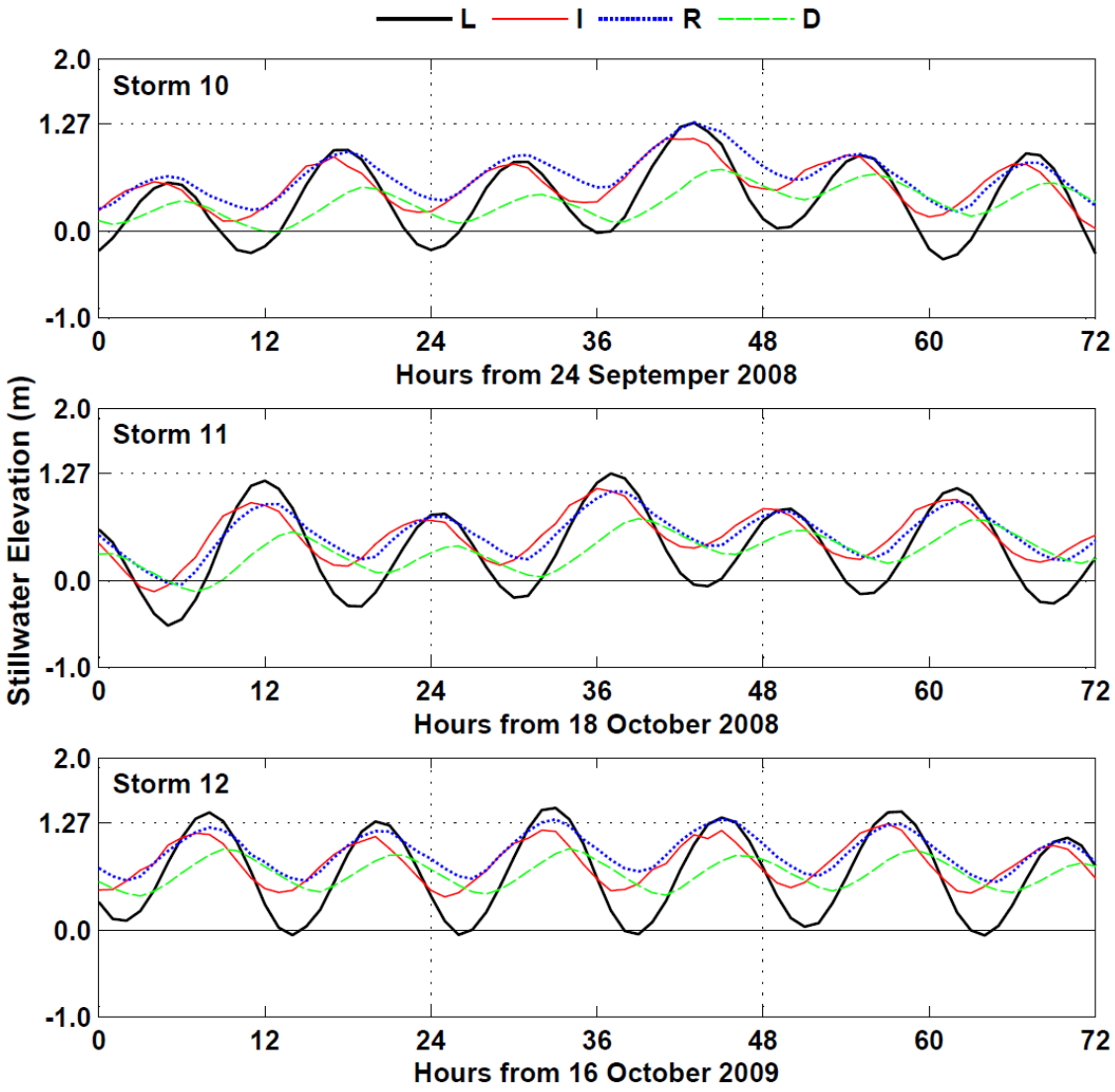

Figure 2.5 3-day time series of stillwater elevations at 4 tide gauges for storms 10, 11 and 12

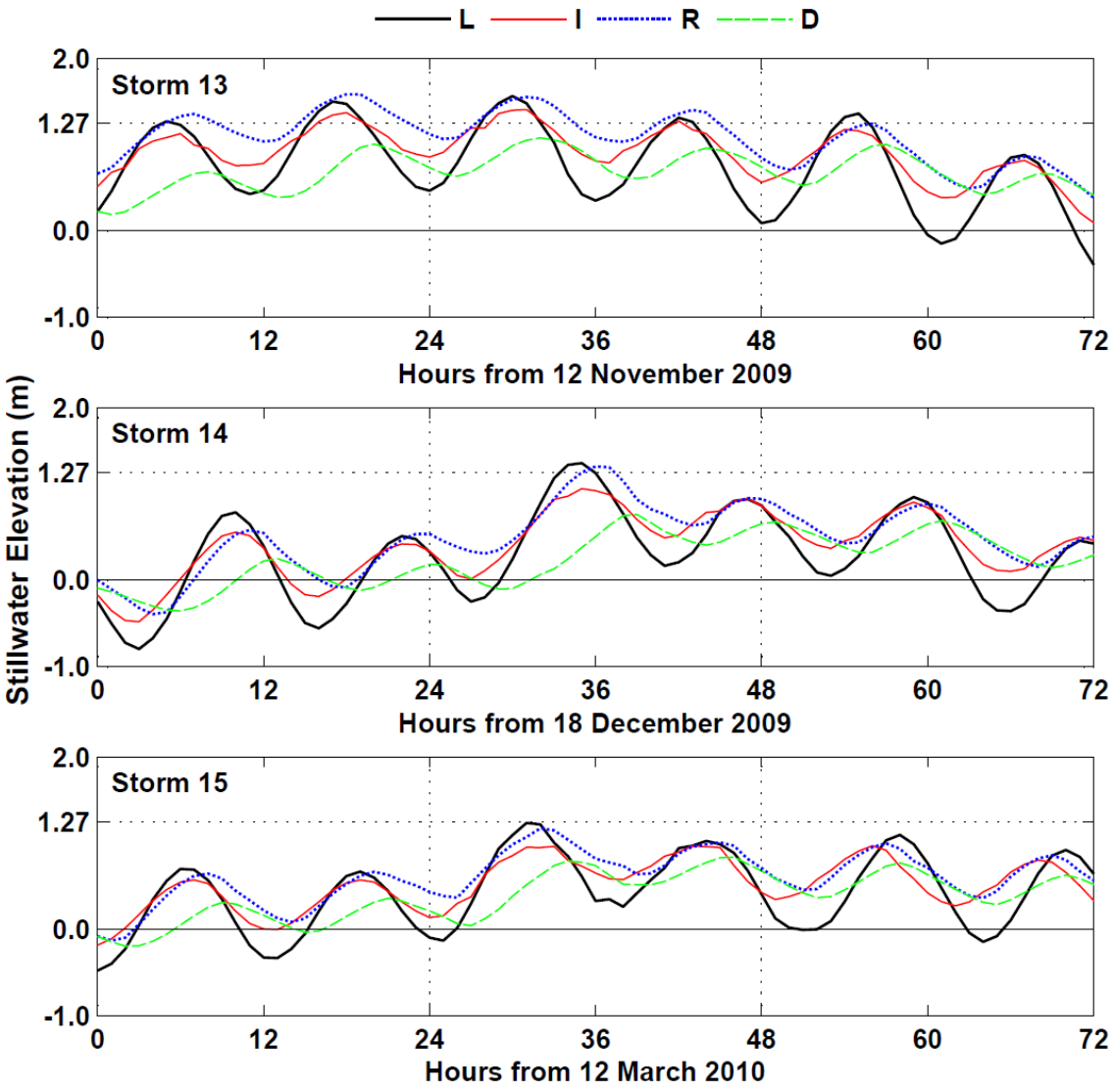

Figure 2.6 3-day time series of stillwater elevations at 4 tide gauges for storms 13, 14 and 15

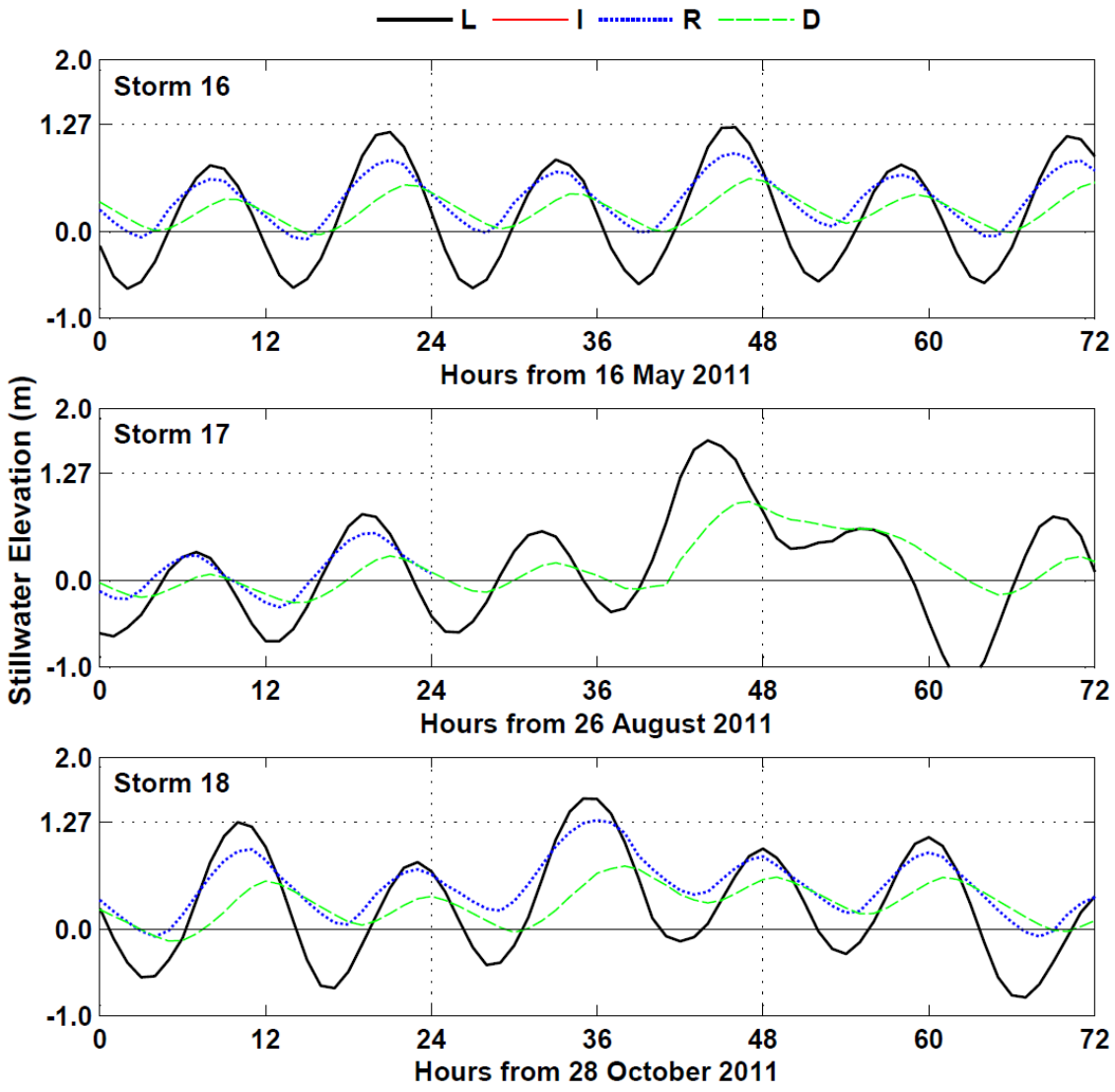

Figure 2.7 3-day time series of stillwater elevations at 4 tide gauges for storms 16, 17 and 18 where no data at gauge I for storms 16, 17, and 18, and at gauge R for storm 17

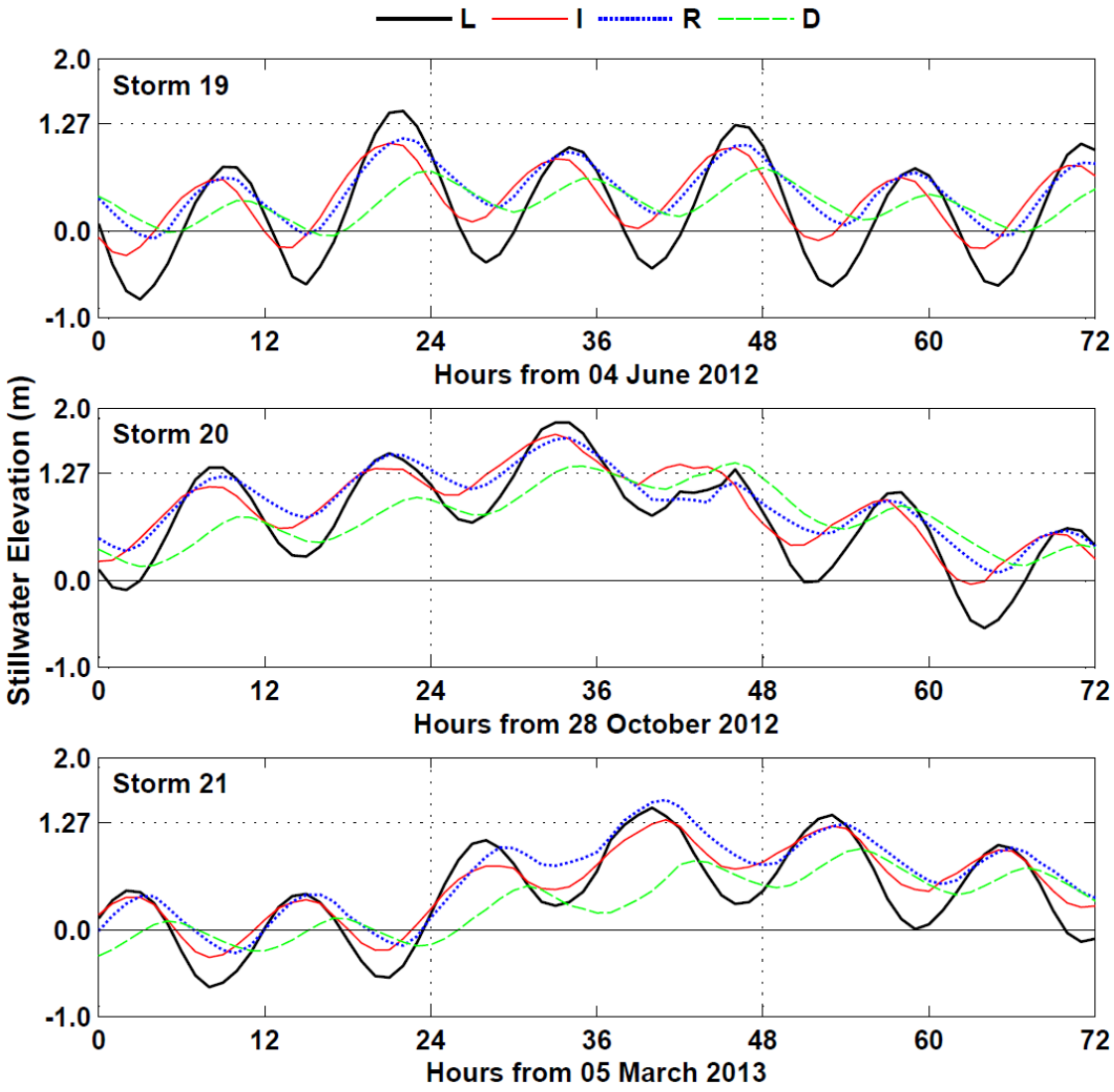

Figure 2.8 3-day time series of stillwater elevations at 4 tide gauges for storms 19, 20 and 21

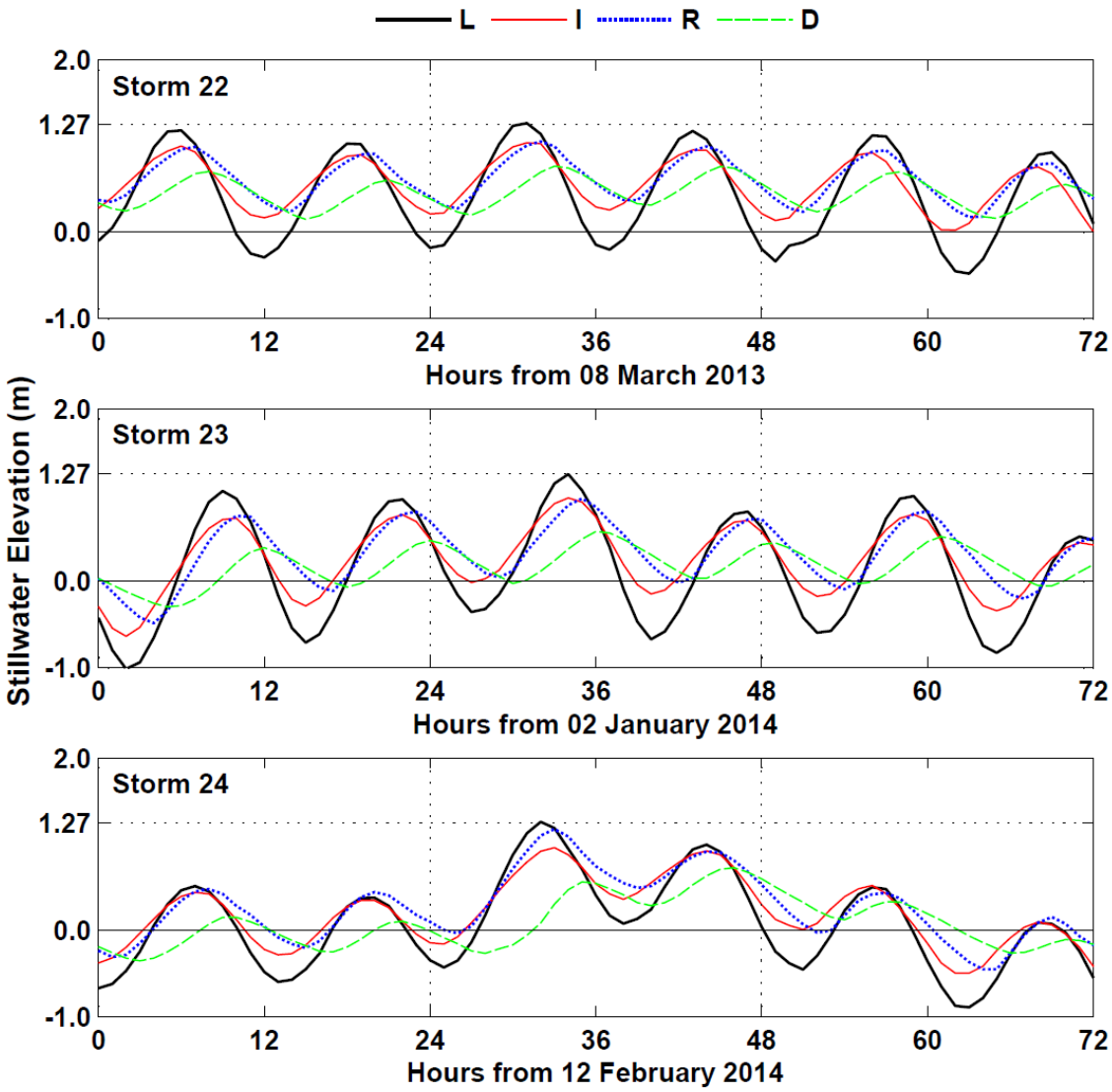

Figure 2.9 3-day time series of stillwater elevations at 4 tide gauges for storms 22, 23 and 24

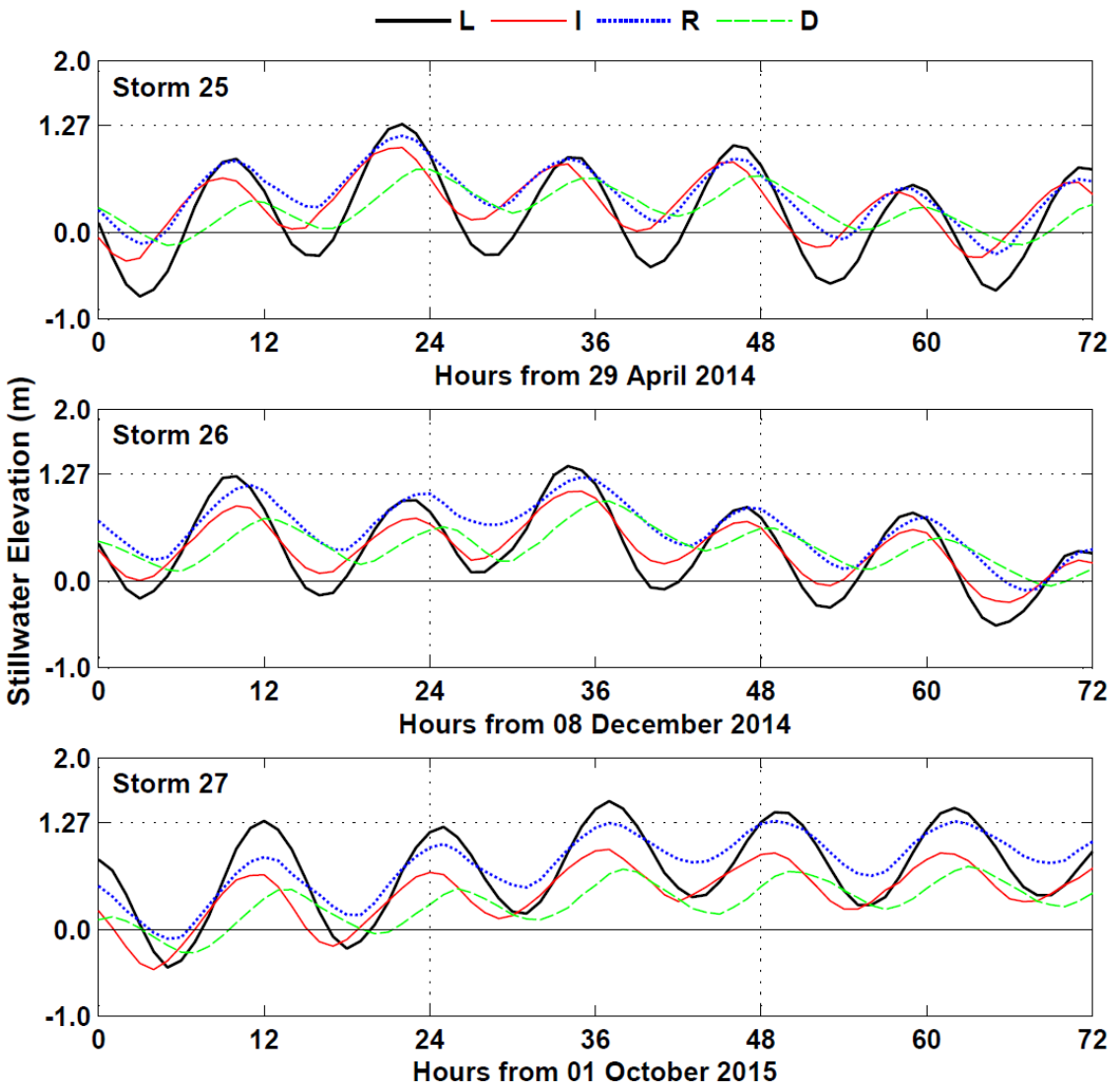

Figure 2.10 3-day time series of stillwater elevations at 4 tide gauges for storms 25, 26 and 27

2.2 River Discharge Data

Daily mean discharge data at the Millsboro Pond Outlet (USGS 2016) upstream of gauge R in Figure 2.11 are used to estimate the river discharge contribution to the water level in Indian River Bay. The daily mean discharge on the day of the 27 storms in Table 2.2 was less than 12 m^3/s except for storm 13 with its daily mean discharge of 30 m^3/s. In the following, the river discharge into Indian River Bay and Rehoboth Bay is assumed to be negligible in comparison to the discharge through the Indian River Inlet.

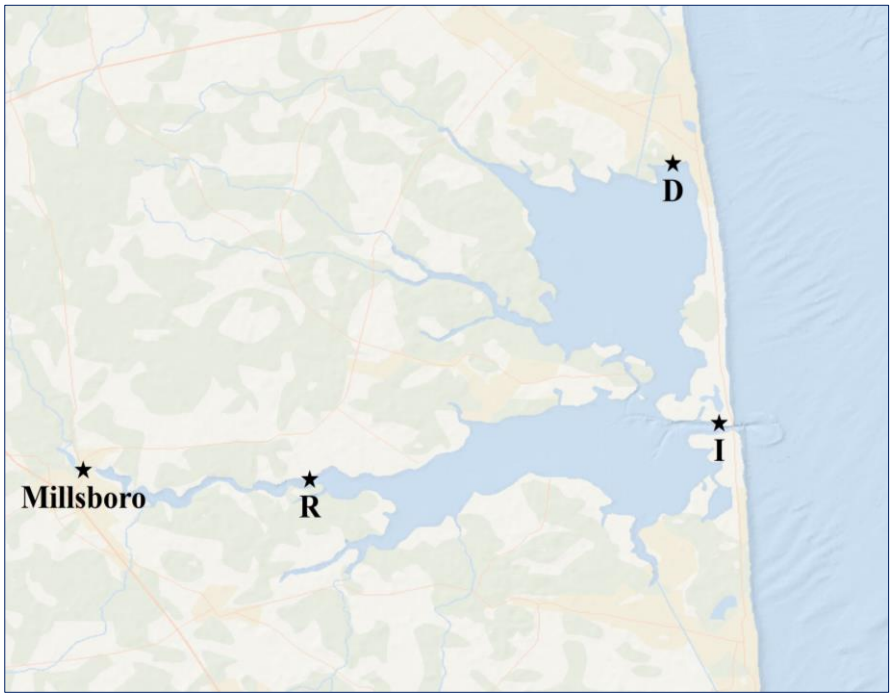

Figure 2.11 Discharge data at Millsboro Pond Outlet

Table 2.2 Daily mean discharge at Millsboro Pond Outlet

Storm	Daily Mean Discharge (m^3/s)	Storm	Daily Mean Discharge (m^3/s)
1	4.36	**15**	11.63
2	2.43	**16**	1.44
3	4.61	**17**	1.10
4	5.69	**18**	1.73
5	3.54	**19**	0.91
6	9.00	**20**	8.77
7	6.59	**21**	5.58
8	1.36	**22**	8.09
9	4.30	**23**	4.27
10	0.88	**24**	5.63
11	0.48	**25**	4.30
12	2.80	**26**	3.00
13	30.00	**27**	3.45
14	7.42		

2.3 Offshore Wave Data

Offshore wave data are obtained from the Wave Information Study Stations (WIS) of the U.S. Army Corps of Engineers (USACE 2016). The locations of WIS 63154, 63156, and 63158 are indicated in Figure 2.1. The wave conditions during each storm are represented by the hourly time series of the spectral significant wave height H_{mo}, spectral peak period T_p and vector mean wave angle θ (positive clockwise) from the normal to the straight barrier beach shoreline with the cross-shore lines L1 – L14 in Figure 2.1. The shoreline is inclined at an angle of 6.38° counterclockwise from the north. The alongshore wave variations are examined by comparing the time series of H_{mo}, T_p and θ at WIS 63154, 63156, and 63158. The wave height differences are less than 10%. In the following, the wave data at WIS 63156 in water depth of 20 m are assumed to represent the incident waves for lines L1 – L14.

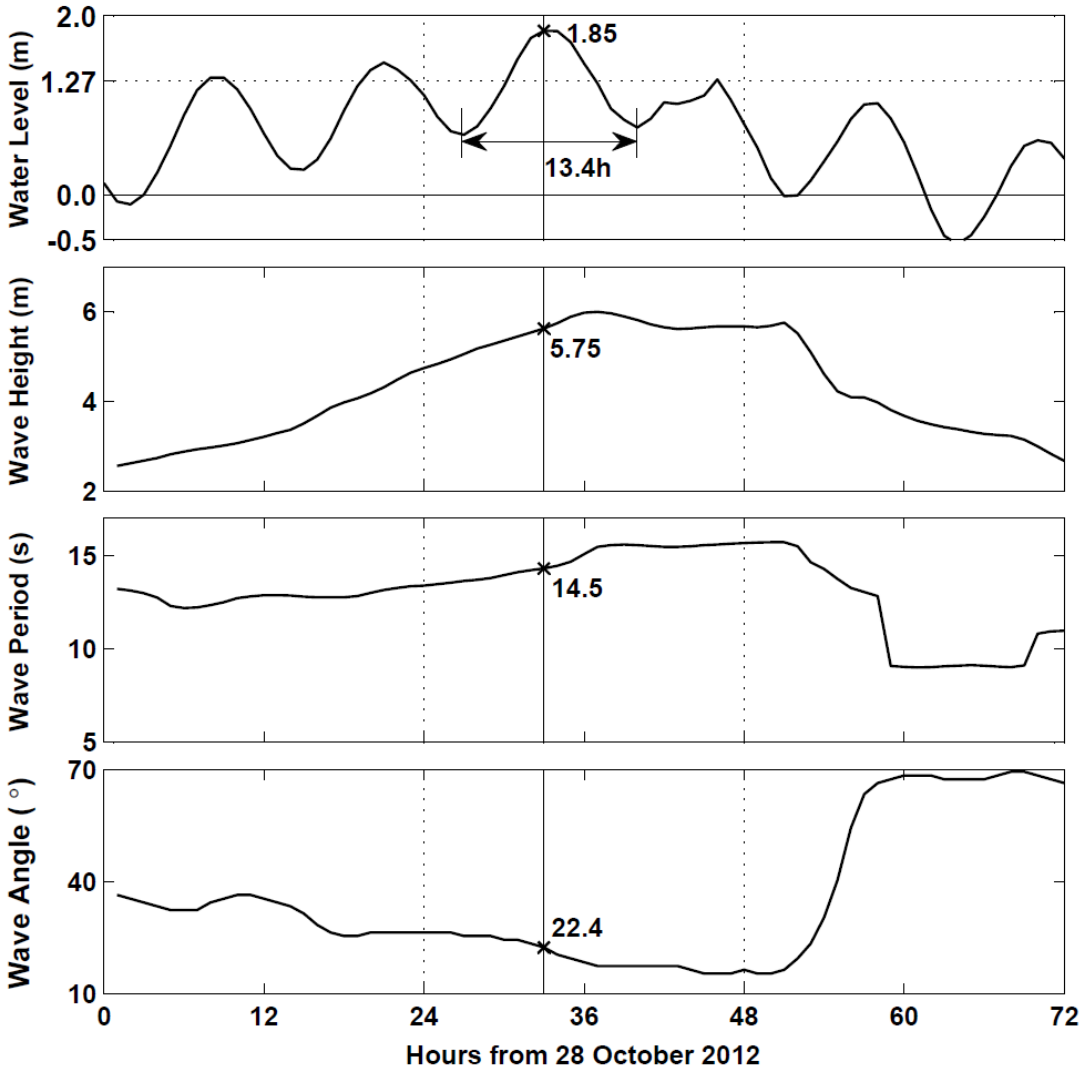

Figure 2.12 3-day time series of stillwater elevation η_o at tide gauge L, and the wave height H_{mo}, period T_p, and angle θ at WIS 63156 station for storm 20

Figure 2.12 shows the 3-day time series of the stillwater elevation η_o at the ocean gauge L and the wave height H_{mo}, period T_p, and angle θ at WIS 63156 for storm 20 (Hurricane Sandy). The maximum η_m of η_o varying with time is 1.85 m and the vertical line in Figure 2.12 indicates the time of $\eta_o = \eta_m$. The wave conditions at

Table 2.3 Spectral significant wave height H_{mo}, spectral peak period T_p, and wave angle θ (positive clockwise) from the normal to the straight barrier beach shoreline at the time of the peak stillwater elevation η_m at Lewes

Storm	Peak Water Level η_m (m)	Wave Height H_{mo} (m)	Wave Period T_p (s)	Wave Angle θ (°)
1	1.39	1.88	10.5	-6.6
2	1.32	2.53	10.9	4.4
3	1.38	0.89	8.1	69.4
4	1.32	1.15	4.5	7.4
5	1.45	4.19	11.3	3.4
6	1.32	4.59	12.0	9.4
7	1.28	1.71	10.8	-12.6
8	1.27	0.99	8.1	-3.6
9	1.60	1.46	10.3	13.4
10	1.29	4.51	12.9	16.4
11	1.28	2.94	9.7	-10.6
12	1.45	2.65	9.7	-0.6
13	1.60	5.48	13.2	9.4
14	1.38	1.32	4.8	-18.6
15	1.30	2.14	6.5	3.4
16	1.27	1.70	6.7	38.4
17	1.70	3.00	14.3	42.4
18	1.56	1.54	5.5	-12.6
19	1.43	0.67	6.6	13.4
20	1.85	5.75	14.5	22.4
21	1.45	3.05	7.9	-10.6
22	1.29	2.09	14.9	-29.6
23	1.28	1.86	4.9	-60.6
24	1.30	1.91	6.0	3.4
25	1.30	1.88	6.6	3.4
26	1.36	2.94	13.4	-3.6
Min	1.27	0.67	4.5	-60.6
Max	1.85	5.75	14.9	69.4

the time of the peak stillwater elevation η_m at Lewes for storm 20 are given by H_{mo} = 5.75 m, T_p = 14.5 s, and θ = 22.4°. The values of η_m at gauge L for storms 1 – 27 are tabulated in Table 2.1 and Table 2.3. At the time of the peak stillwater elevation at Lewes, H_{mo} = 0.67 – 5.75 m, T_p = 4.5 – 14.9 s, and θ = (–60.6) – 69.4° for storms 1 – 26 in Table 2.3 where wave data for storm 27 are not available yet. Hurricane Sandy generated the largest storm tide and waves among the 27 storms. The top panel in Figure 2.12 depicts the surge duration T_s = 13.4 h between the two low water levels adjacent to the peak stillwater level at gauge L. The duration T_s introduced in this study is related to the time scale of the peak stillwater level. The value of T_s is obtained from the time series of η_o above the datum (NAVD88) in the vicinity of the peak stillwater level, and the definition of T_s will be presented in Chapter 3.

2.4 Beach Profile Data

The merged bathymetry and topography data of the barrier beach are obtained from the Hurricane Sandy Digital Elevation Model (DEM) of the National Centers for Environmental Information of the National Oceanic and Atmospheric Administration (NOAA 2016). The cross-shore profiles along lines L1 – L14 depicted in Figures 2.13 – 2.15 at an alongshore interval of 515 m are plotted as a function of the onshore coordinate x with $x = 0$ at the location of WIS 63156 in water depth of 20 m and the bottom elevation z_b. The landward end of each cross-shore line is situated near x = 13 km on the bay side slightly above or below NAVD88. The water depth along the bay boundary is about 1 m and very shallow. The seaward end of each line in Figures 2.13 – 2.15 is located near x = 11 km in water depth of about 10 m. The bottom slope of each line between $x = 0$ and seaward end point is assumed to be uniform. The cross-

shore resolution along lines L1 – L14 between the seaward and landward end points is 8 m. Table 2.4 lists the barrier beach width W_b above the datum (NAVD88) with the range of 450 – 850 m, and the dune crest (highest) elevation z_c above the datum with the range of 2.92 – 6.62 m for lines L1 – L14. The dune crest elevation of each line is above the peak stillwater elevation of 1.85 m for Hurricane Sandy. The beach profile data are used as input to the subsequent computation of wave overtopping of the barrier beach during Hurricane Sandy.

Table 2.4 Alongshore distance y, dune crest elevation z_c, and barrier beach width W_b at NAVD88 along each of 14 cross-shore lines

Line	**y (m)**	$\boldsymbol{z_c}$ **(m)**	$\mathbf{W_b}$ **(m)**
1	0	3.12	530
2	515	3.13	560
3	1030	4.06	600
4	1546	6.62	610
5	2061	4.24	810
6	2576	5.11	580
7	3091	3.47	850
8	3606	2.92	610
9	4122	4.19	530
10	4637	5.63	450
11	5152	3.96	470
12	5667	5.55	490
13	6182	5.01	540
14	6698	3.26	460
	Min	2.92	450
	Max	6.62	850

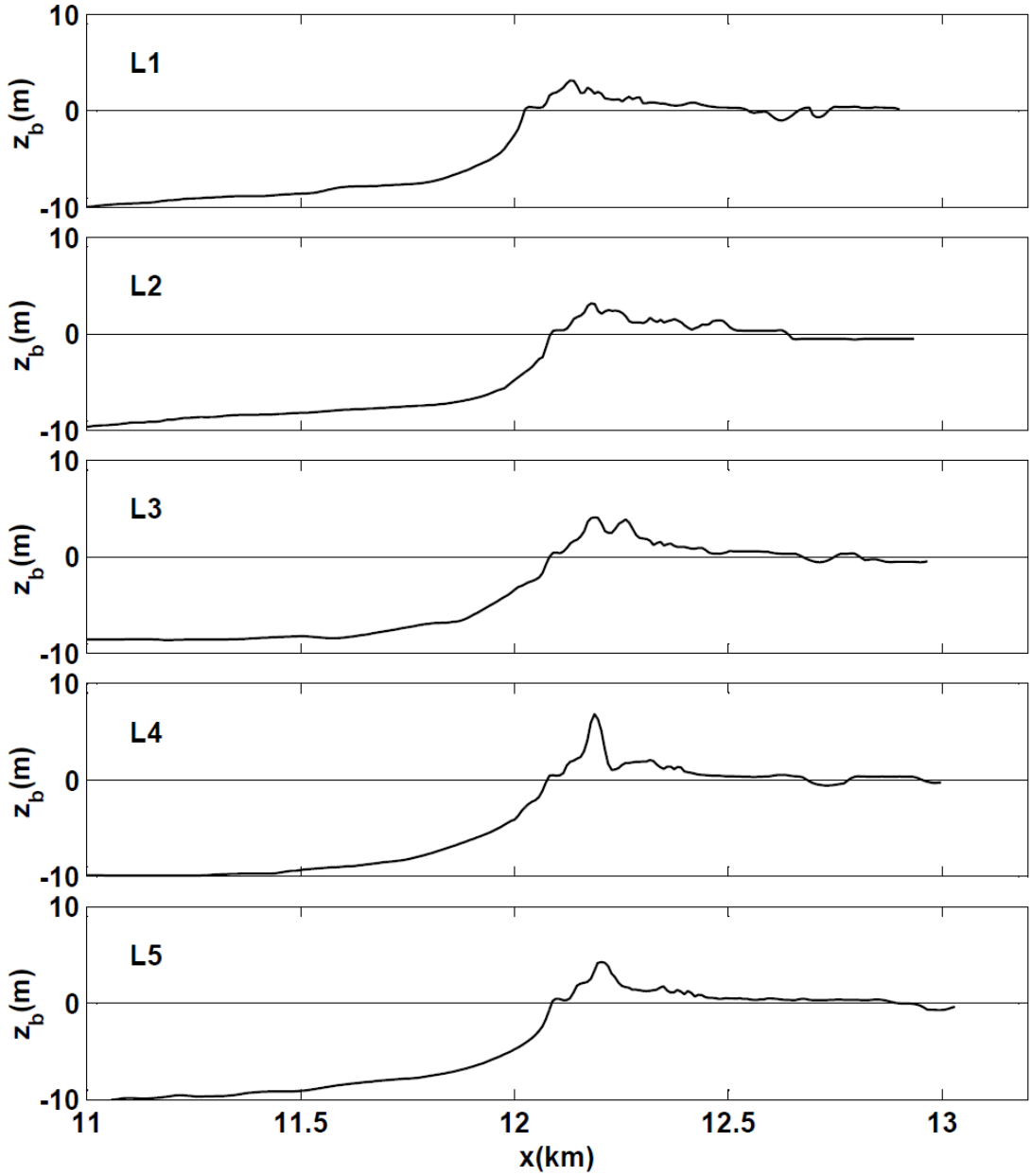

Figure 2.13 Bottom elevation z_b along cross-shore lines L1, L2, L3, L4 and L5

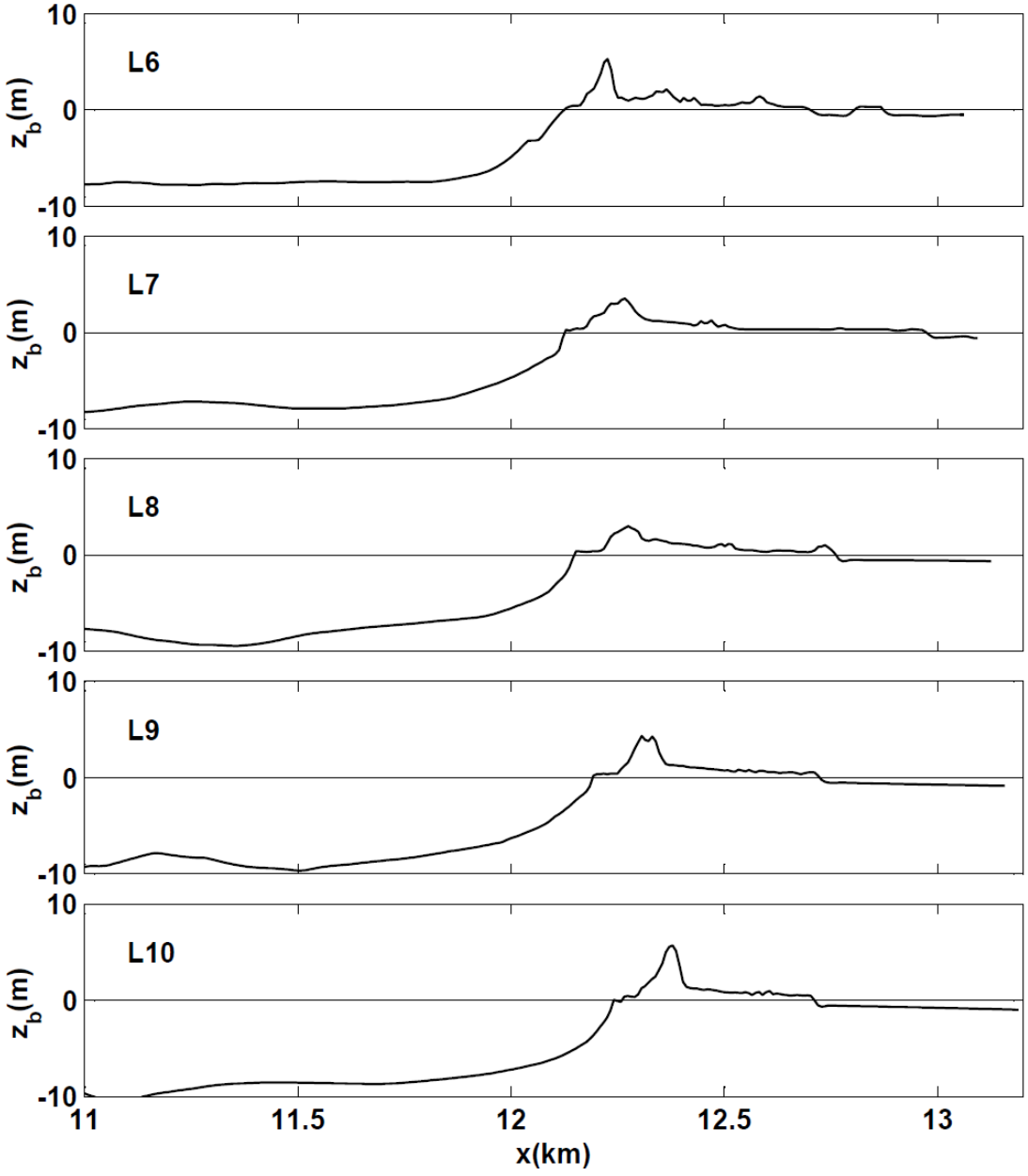

Figure 2.14 Bottom elevation z_b along cross-shore lines L6, L7, L8, L9 and L10

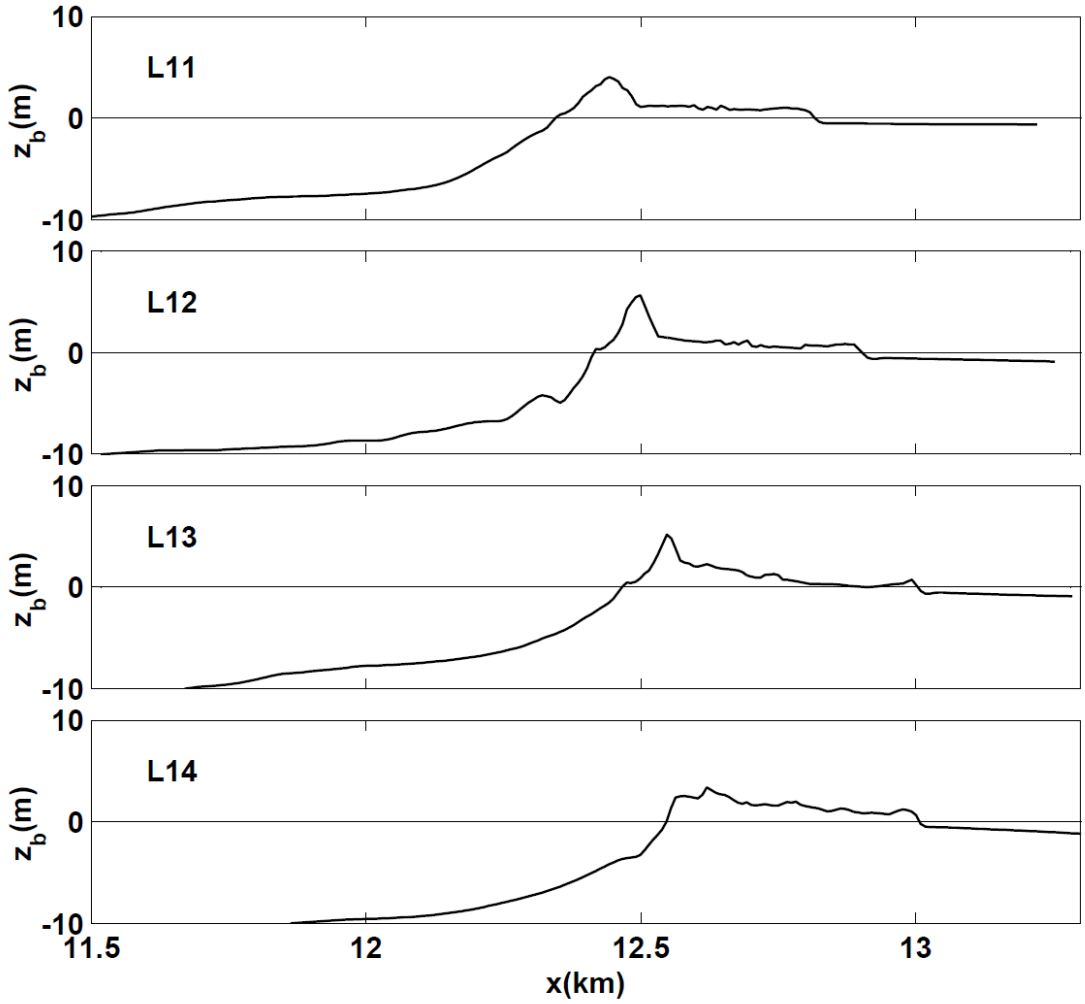

Figure 2.15 Bottom elevation z_b along cross-shore lines L11, L12, L13 and L14

Chapter 3

ANALYTICAL MODEL FOR PEAK STILLWATER ELEVATIONS

An analytical model is developed to predict the peak stillwater elevation in a small bay with a narrow inlet for the given ocean storm tide characterized by the peak elevation η_m and the surge duration T_s. The model is based on tidal hydraulics modeling (e.g., Dean and Dalrymple 2002). The stillwater elevation $\eta_B(t)$ above the datum in the bay varies with time t but is assumed to be invariant horizontally.

3.1 Governing Equations

The conservation of water volume in the bay is expressed as

$$A_B \frac{d\eta_B}{dt} = A_C U(t) + Q_w(t) \tag{1}$$

where A_B = bay surface area; A_C = inlet channel cross-sectional area; U = average velocity over the area A_C; and Q_w = wave overtopping rate over the barrier beach. A_B and A_C are assumed constant. Q_w needs to be estimated separately. The difference between the stillwater elevations η_o and η_B in the ocean and bay is assumed to cause water flow in the inlet channel

$$\eta_o(t) - \eta_B(t) = K \frac{|U(t)|U(t)}{2g} \tag{2}$$

with

$$K = K_{en} + K_{ex} + \frac{f_D L}{4R} \tag{3}$$

where g = gravitational acceleration; K_{en} = entrance loss coefficient; K_{ex} = exit loss coefficient; f_D = Darcy-Weisbach friction factor; L = inlet channel length; and R =

hydraulic radius in the channel. The combined loss coefficient K is assumed constant and expected to be of the order of 2.

Eq. (2) is linearized using an equivalent linearization method (Mei 1989)

$$\eta_o(t) - \eta_B(t) = K\frac{U_c U(t)}{2g} \tag{4}$$

where U_c = constant positive velocity. The mean square of error $(|U|U - U_c U)$ is minimized with respect to U_c to obtain the following equation for U_c

$$U_c = \left(\int_0^{T_s} |U|^3 dt\right)\left(\int_0^{T_s} U^2 dt\right)^{-1} \tag{5}$$

where the square of the error is minimized during $t = 0$ to $t = T_s$.

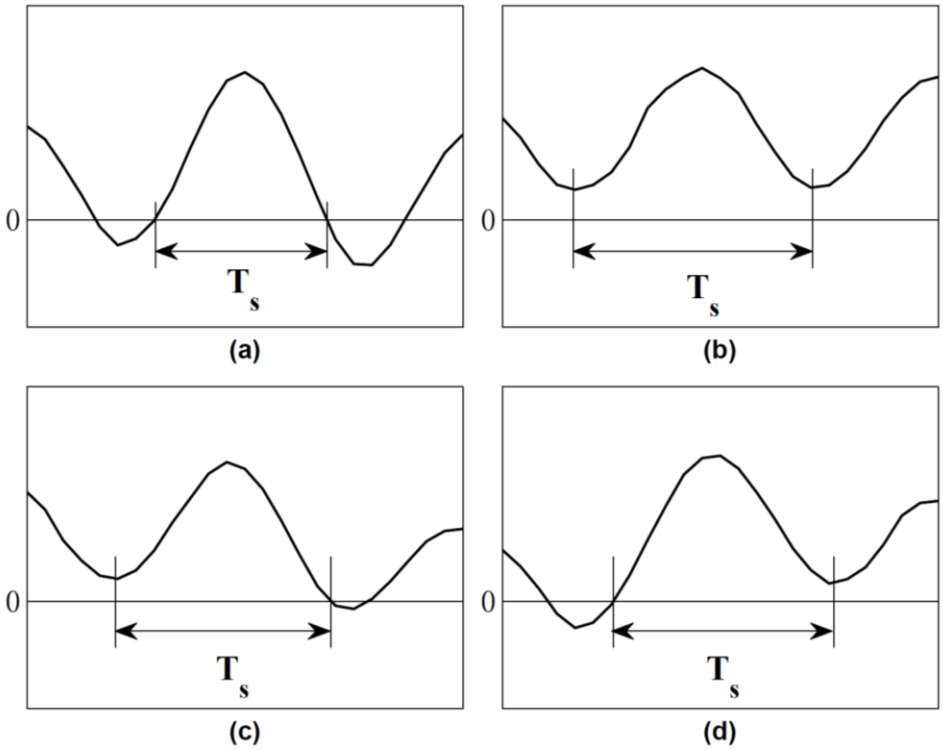

Figure 3.1 Definition of surge duration T_s : (a) zero-upcrossing and zero-downcrossing points; (b) no zero-upcrossing and no zero-downcrossing points; (c) no zero-upcrossing and zero-downcrossing points; (d) zero-upcrossing and no zero-downcrossing points.

3.2 Analytical Solution without Wave Overtopping

The stillwater elevation η_o in the ocean is assumed to be given by

$$\eta_o(t) = \eta_m \sin\left(\frac{\pi t}{T_s}\right) \quad \text{for} \quad 0 \le t \le T_s \tag{6}$$

where η_m = peak stillwater elevation; and T_s = surge duration. Eq. (6) implies that $\eta_o = \eta_m$ at $t = (T_s/2)$ and $\eta_o = 0$ at $t = 0$ and T_s, corresponding to the zero-upcrossing and zero-downcrossing points in the time series of $\eta_o(t)$. Figure 3.1 shows the definition used in this study. For the case of no zero-upcrossing, $t = 0$ at the time of the low water level before $t = (T_s/2)$. For the case of no zero-downcrossing, $t = T_s$ at the time of the low water level after $t = (T_s/2)$. Eq. (6) may not represent the measured time series of $\eta_o(t)$ near $t = 0$ and T_s but this analytical model is intended for the prediction of the peak stillwater elevation in a small bay.

For the case of no wave overtopping of the barrier beach, Eq. (1) with $Q_w = 0$ and Eq. (4) with η_o given by Eq. (6) for $0 \le t \le T_s$ can be solved analytically. The bay stillwater elevation η_B and the inlet velocity U can be expressed as

$$\eta_B(t) = \eta_p \sin\left(\frac{\pi t}{T_s} - \varepsilon\right) \quad ; \quad U(t) = U_m \cos\left(\frac{\pi t}{T_s} - \varepsilon\right) \tag{7}$$

where η_p = peak stillwater elevation in the bay; ε = phase shift; and U_m = maximum velocity in the inlet channel. The time lag between $\eta_B(t)$ and $\eta_o(t)$ is equal to $(\varepsilon T_s/\pi)$. This analytical model may be appropriate if the phase shift ε is small and the time lag is short in comparison to the surge duration T_s. Eq. (5) yields $U_c = (8/3\pi)\, U_m = 0.85\, U_m$. The following concise expressions of ε, η_p, and U_m in Eq. (7) are obtained after algebraic manipulations:

$$\tan\varepsilon = \beta \; ; \; \eta_p = \frac{\eta_m}{\sqrt{1+\beta^2}} \; ; \; U_m = \left(\frac{3\pi\beta g \eta_m}{4K\sqrt{1+\beta^2}}\right)^{1/2} \tag{8}$$

The parameter β related to the phase shift ε is given by

$$\beta = \left(\frac{\sqrt{1+C^2} - 1}{2} \right)^{1/2} \quad ; \quad C = K^* \eta_m^* \tag{9}$$

The inlet and bay parameter K^* and the surge steepness parameter η_m^* are defined as

$$K^* = \frac{8\pi K}{3} \left(\frac{A_B}{A_C} \right)^2 \times 10^{-10} \quad ; \quad \eta_m^* = \frac{\eta_m}{g T_s^2} \times 10^{10} \tag{10}$$

The dimensionless parameters K^* and η_m^* are of the order of unity and β is of the order of 0.5 in this study.

3.3 Peak Stillwater Elevation and Maximum Velocity in Inlet Channel

The ratio (η_p / η_m) between the peak stillwater elevations in the bay and ocean in Eq. (8) depends on β only and is less than unity, which is showed in Figure 3.2. The inlet and bay parameter K^* is assumed constant in this simple model. The value of β is affected by the surge steepness parameter η_m^* because the linearized equation (4) includes the velocity $U_c = 0.85\, U_m$ which depends on the value of η_m. When the surge duration T_s becomes large, η_m^* approaches zero. If $\eta_m^* = 0$, $\beta = 0$, $\varepsilon = 0$, $\eta_p = \eta_m$, and $U_m = 0$ because there is enough time to fill the bay with water. As T_s decreases, η_m^* and β increase, resulting in the increase of the phase shift ε and the decrease of (η_p / η_m) because the surge duration is too short to fill the bay. The normalized maximum velocity, $U_m / \sqrt{g \eta_m}$, decreases with the increase of the combined loss coefficient K and with the decrease of β as shown in Figure 3.3. For $K = 2$ and $\beta = 0.5$, $U_m = 0.7\sqrt{g \eta_m}$. In short, Eqs. (8) – (10) appear to be reasonable physically and are easy to use for field applications.

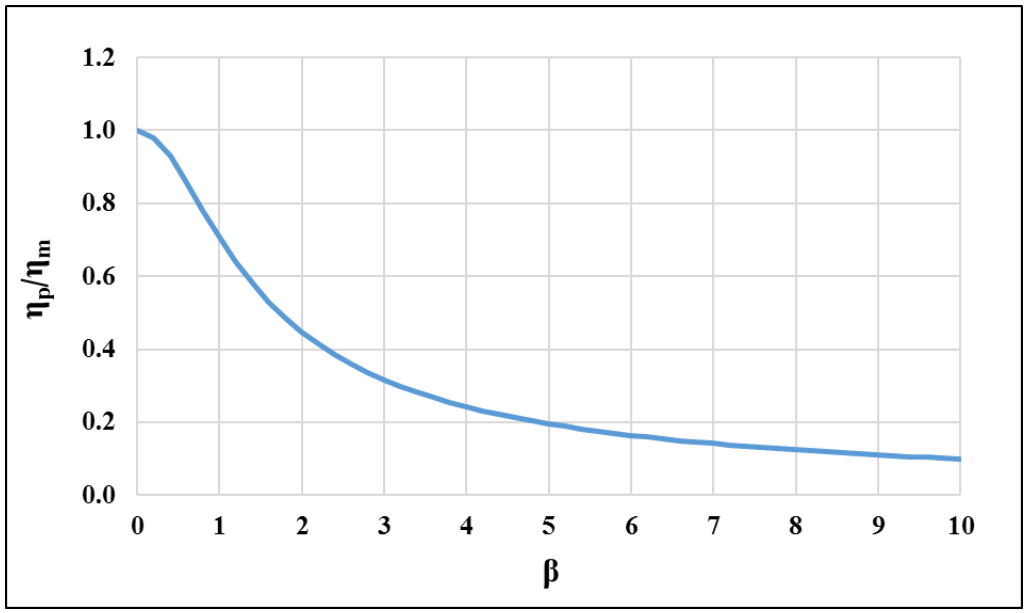

Figure 3.2 Ratio (η_p/η_m) of the peak stillwater elevations in the bay and ocean as a function of β

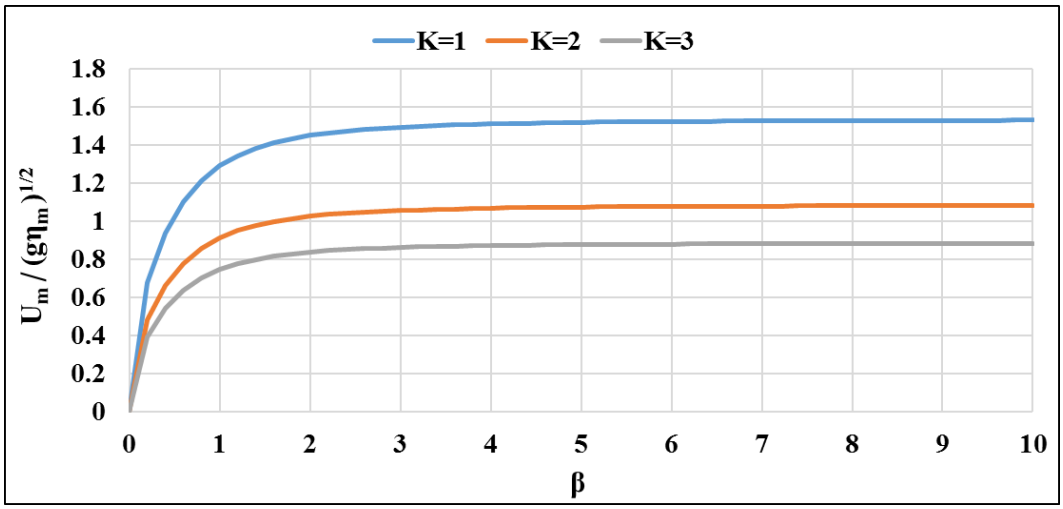

Figure 3.3 Normalized maximum velocity $U_m / \sqrt{g\eta_m}$ as a function of β for the combined loss coefficient K = 1, 2, and 3

Chapter 4

COMPARISON WITH FIELD DATA

The analytical model in section 3.2 is compared with the tide gauge data in section 2.1 in the following.

4.1 Measured and Fitted Ocean Stillwater Elevations

The accuracy of the analytical model depends on the degree of agreement between the measured time series $\eta_o(t)$ and Eq. (6) with the measured values of η_m and T_s listed in Table 2.1. The comparisons for storms 1 – 27 are shown in Figures 4.1 – 4.7.

Figures 4.1 – 4.7 clearly explain the surge duration T_s for each storm. For storms 1 in Figure 4.1, $t = 0$ and $t = T_s = 9.4$ h are corresponding to the zero-upcrossing and zero-downcrossing points, respectively, corresponding to Figure 3.1(a). Eq. (6) fits the measured time series of $\eta_o \geq 0$ well. For storm 6 in Figure 4.2, $t = 0$ is at the low water level and $t = T_s = 11.1$ h is at the zero-downcrossing point, corresponding to Figure 3.1(c). For storm 9 in Figure 4.3, $t = 0$ is at the zero-upcrossing point and $t = T_s = 12.6$ h is at the low water level, corresponding to Figure 3.1(d). For storm 20 (Hurricane Sandy) in Figure 4.5, both $t = 0$ and $t = T_s = 13.4$ h are at the low water levels, in the same way as in Figure 3.1 (b). The exact time of the low water level is somewhat ambiguous and the points of $t = 0$ and $t = T_s$ are chosen to obtain the agreement near the peak at $t = (T_s/2)$. As a result, the surge duration T_s is somewhat uncertain.

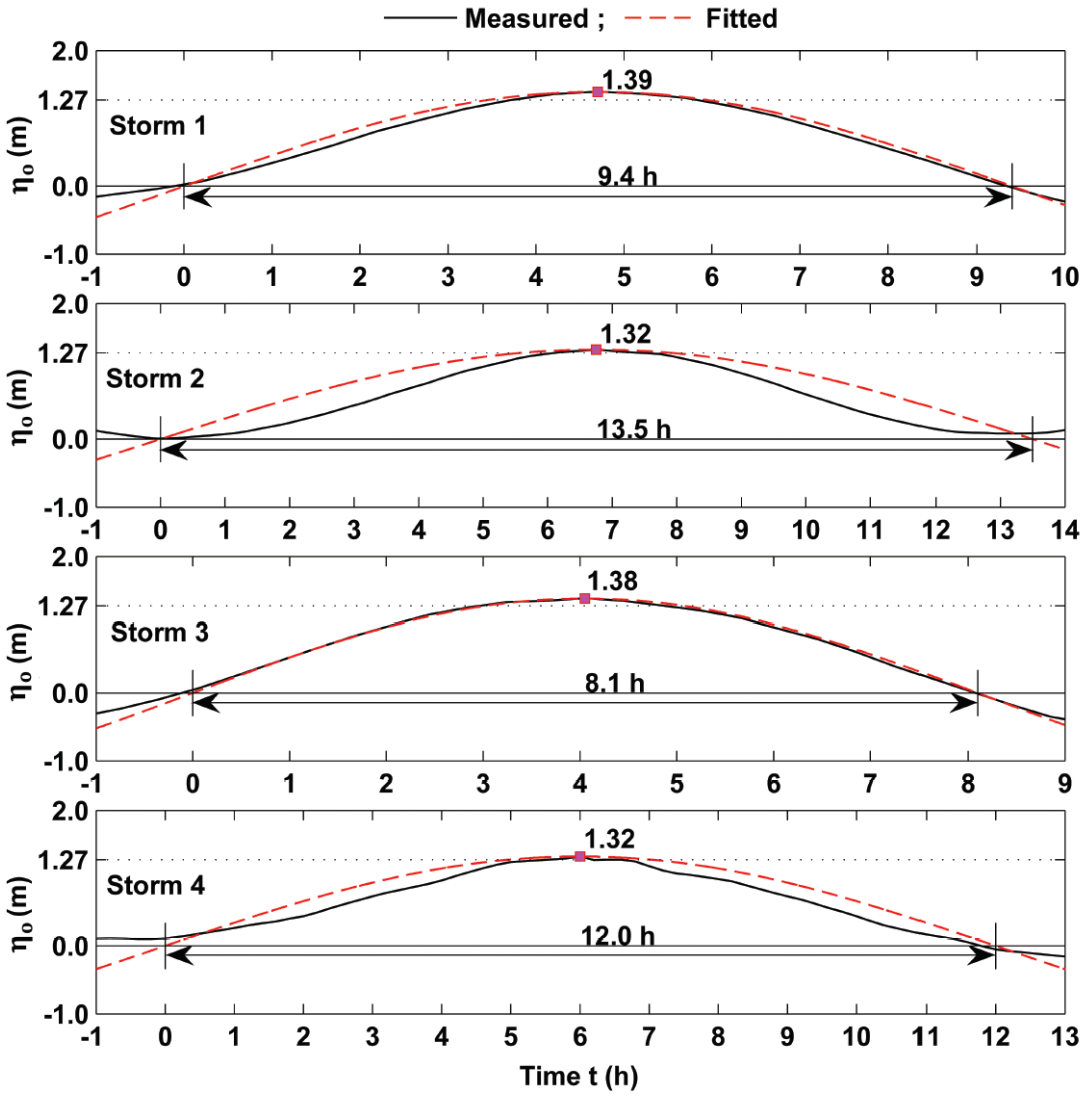

Figure 4.1 Measured and fitted temporal variations of ocean stillwater elevation $\eta_o(t)$ with its peak η_m at time $t = (T_s/2)$ for storms 1, 2, 3, and 4

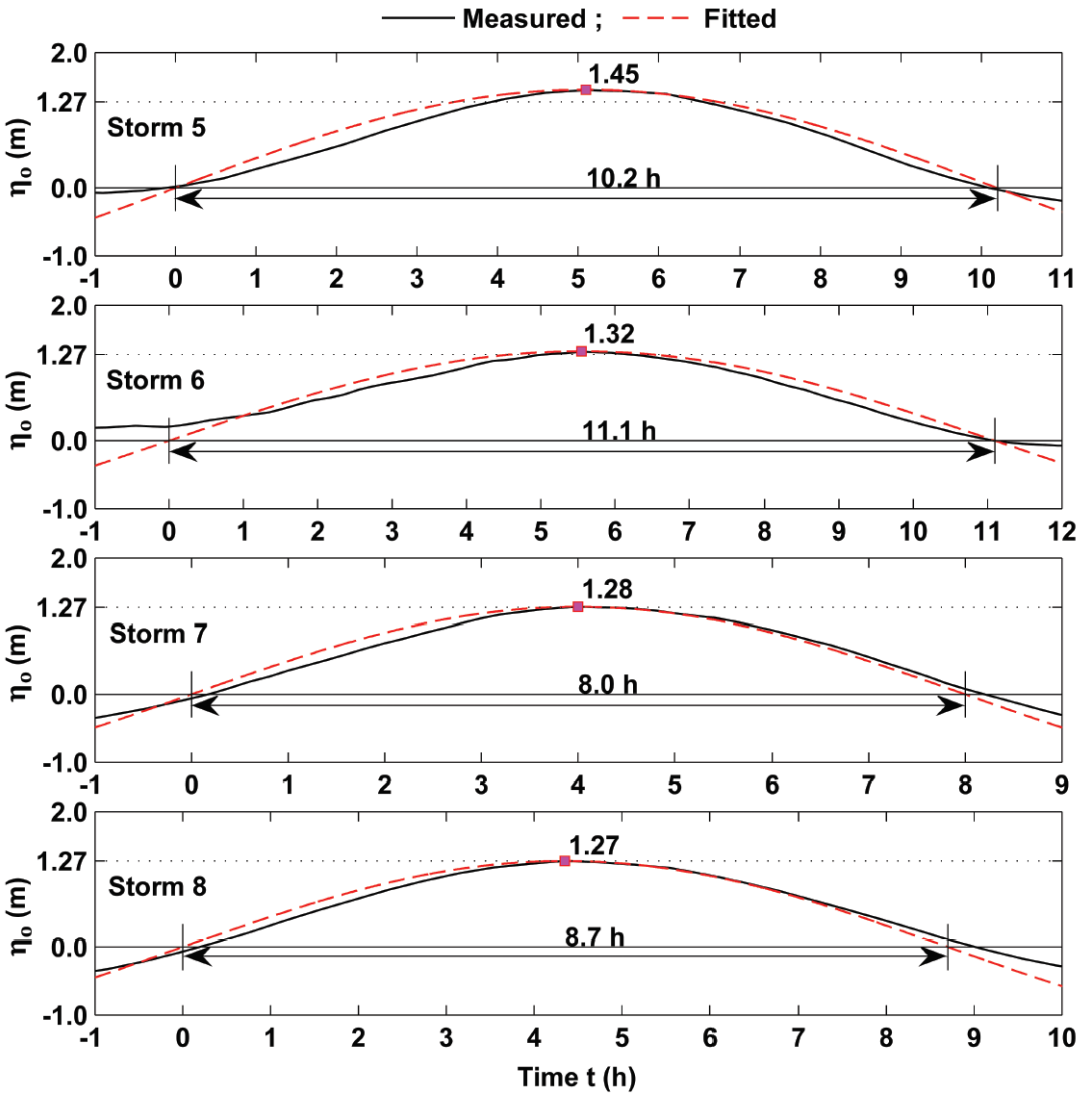

Figure 4.2 Measured and fitted temporal variations of ocean stillwater elevation $\eta_o(t)$ with its peak η_m at time $t = (T_s/2)$ for storms 5, 6, 7, and 8

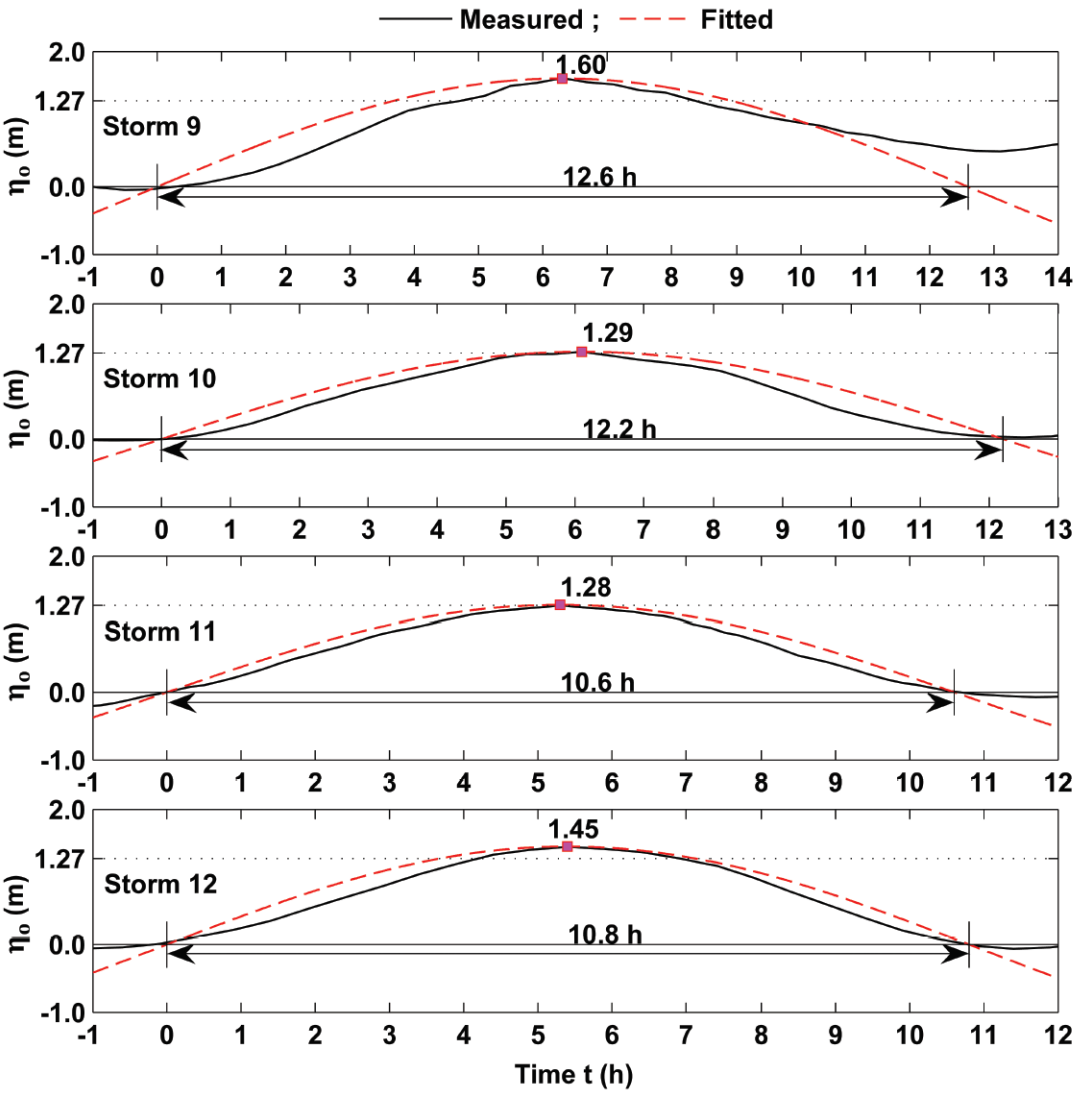

Figure 4.3 Measured and fitted temporal variations of ocean stillwater elevation $\eta_o(t)$ with its peak η_m at time $t = (T_s/2)$ for storms 9, 10, 11, and 12

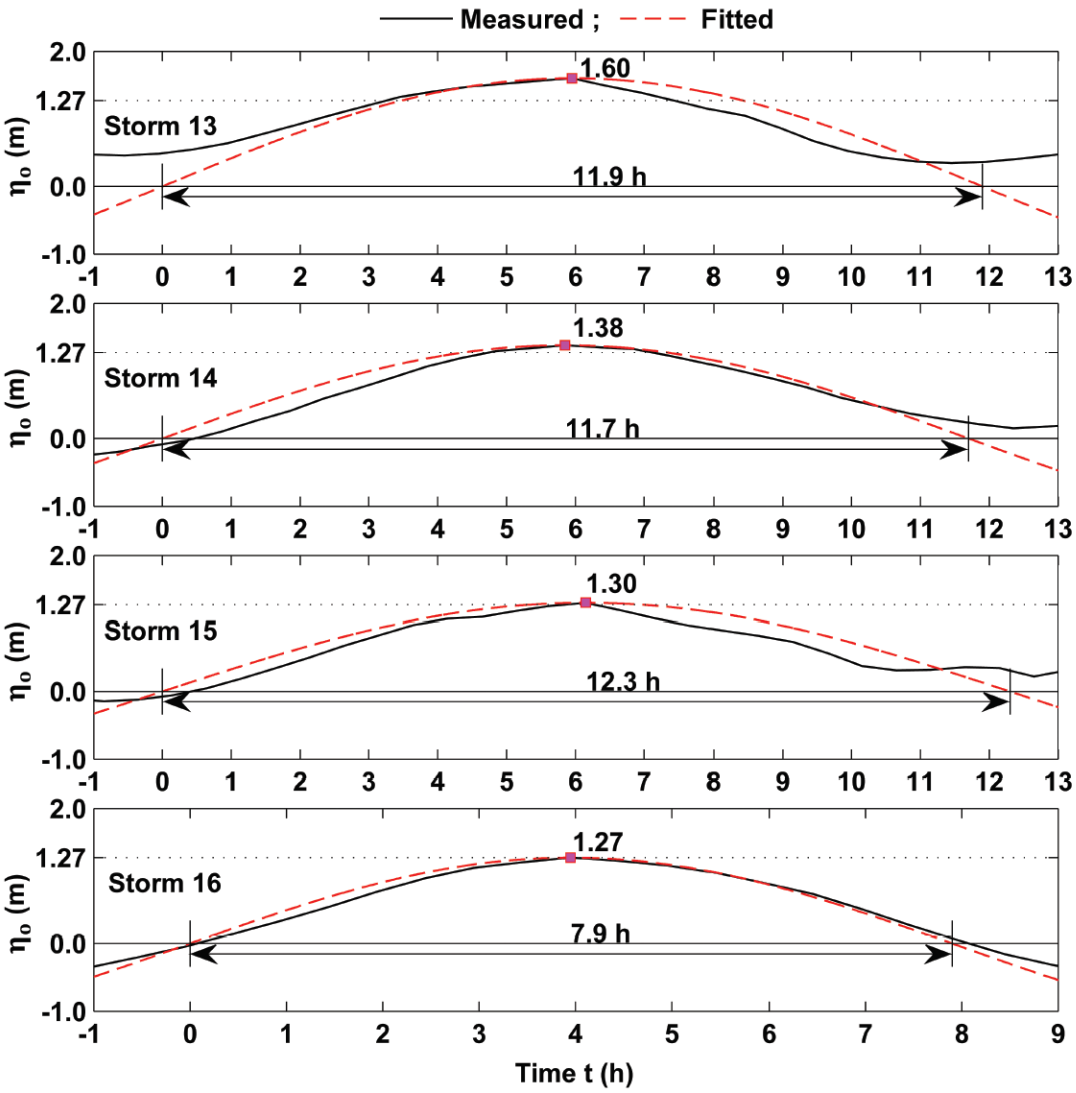

Figure 4.4 Measured and fitted temporal variations of ocean stillwater elevation $\eta_o(t)$ with its peak η_m at time $t = (T_s/2)$ for storms 13, 14, 15, and 16

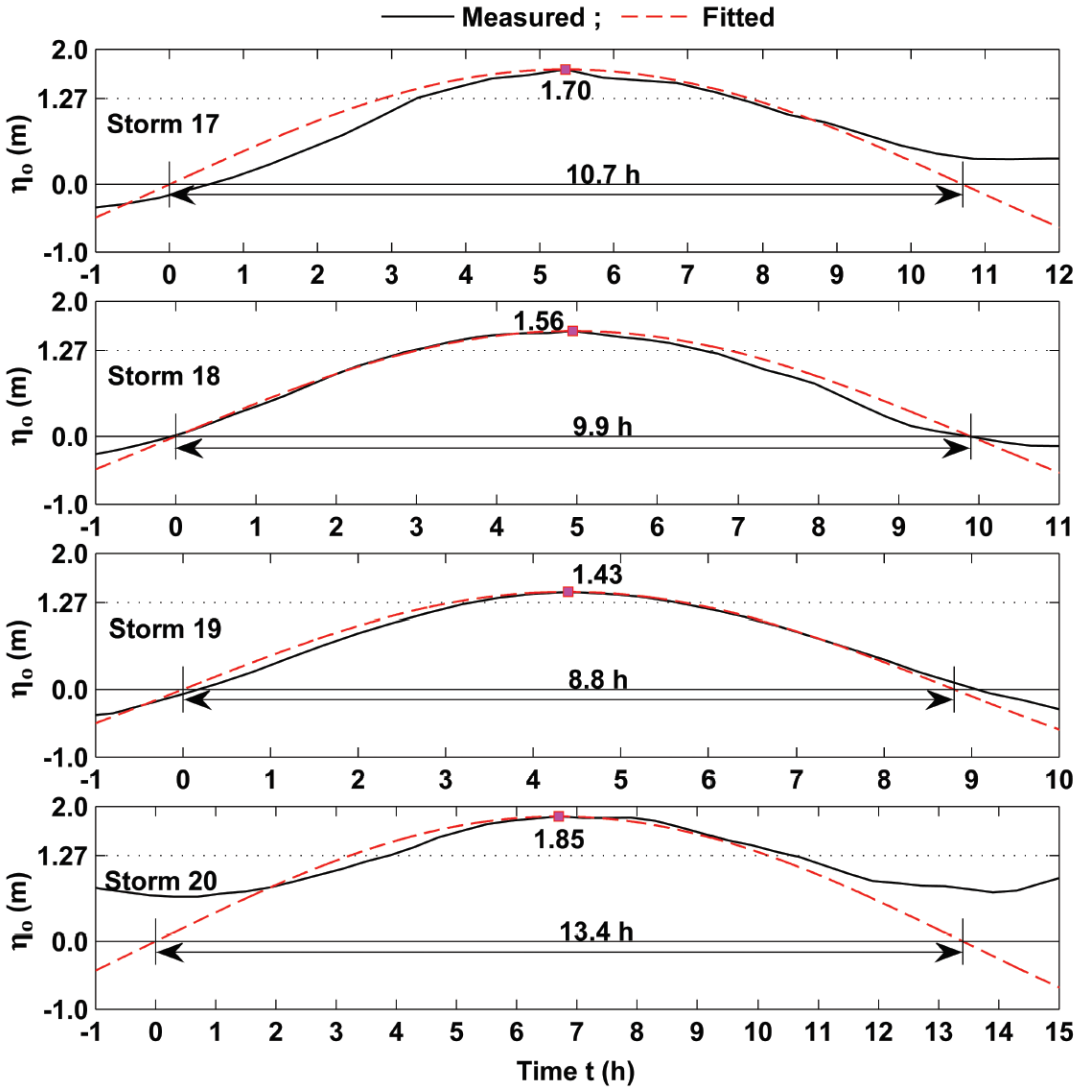

Figure 4.5 Measured and fitted temporal variations of ocean stillwater elevation $\eta_o(t)$ with its peak η_m at time $t = (T_s/2)$ for storms 17, 18, 19, and 20

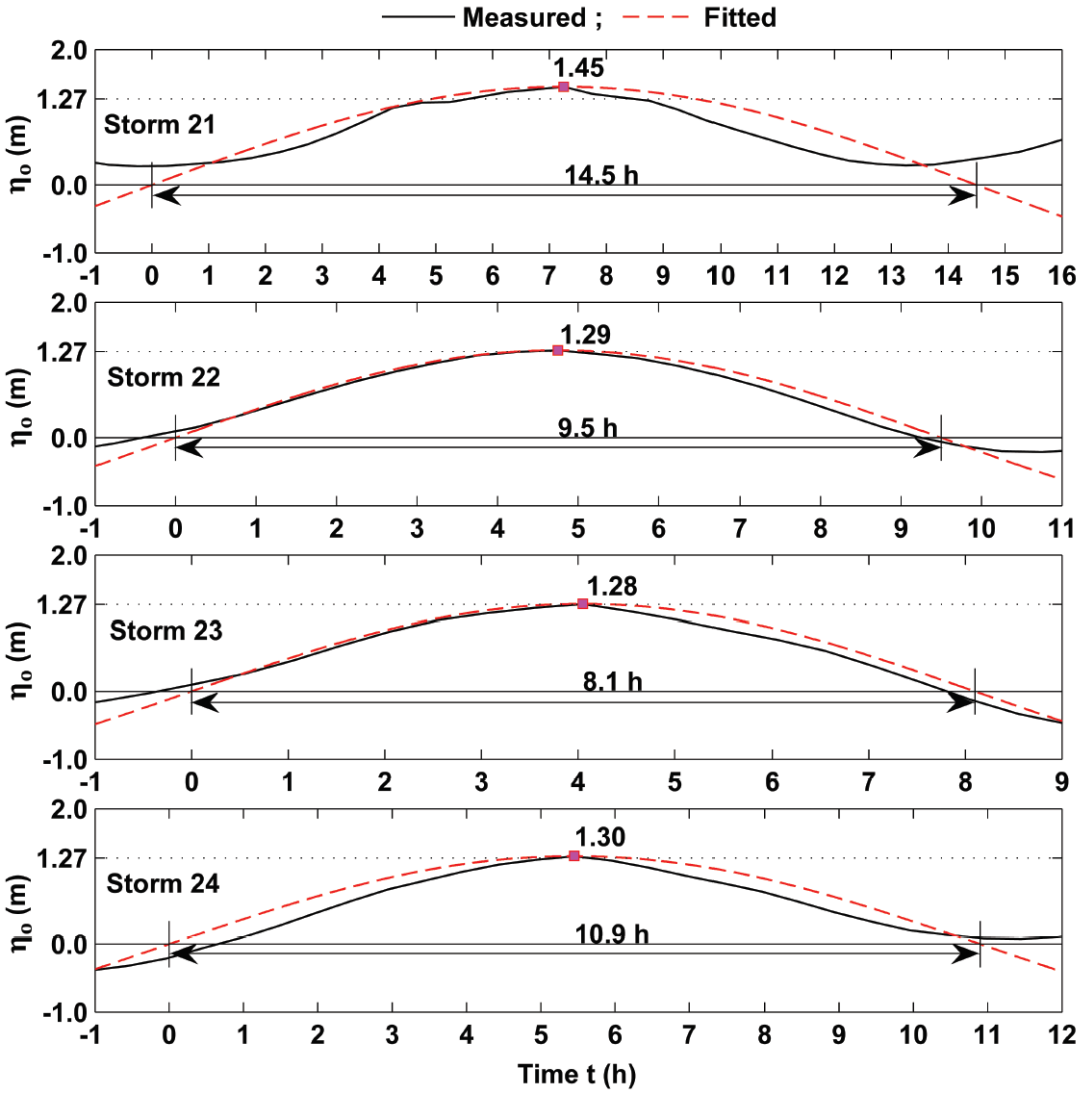

Figure 4.6 Measured and fitted temporal variations of ocean stillwater elevation $\eta_o(t)$ with its peak η_m at time $t = (T_s/2)$ for storms 21, 22, 23, and 24

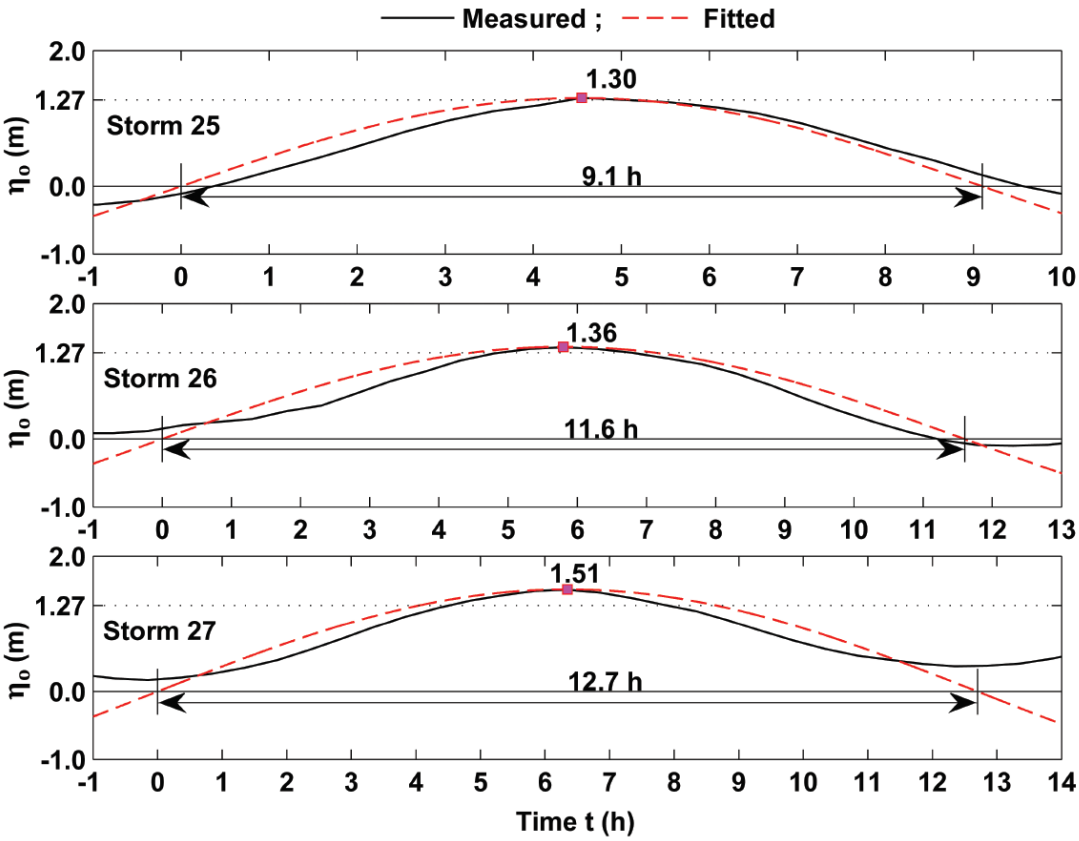

Figure 4.7 Measured and fitted temporal variations of ocean stillwater elevation $\eta_o(t)$ with its peak η_m at time $t = (T_s/2)$ for storms 25, 26, and 27

4.2 Calibration of Inlet and Bay Parameter K^*

The combined loss coefficient K defined by Eq. (3) is estimated as $K = 2.3$ using typical values of $K_{en} = 0.3$, $K_{ex} = 1.0$, and $f_D = 0.06$ (Dean and Dalrymple 2002) and approximate values of $L = 1$ km and $R = 15$ m for the Indian River Inlet channel with two jetties. The inlet and bay parameter K^* defined in Eq. (10) is estimated as K^*

= 1.4 using K = 2.3, A_B = 75 km^2 and A_C = 2800 m^2. The surge steepness parameter η_m^* is in the range of 0.54 – 1.66 for the 27 storms.

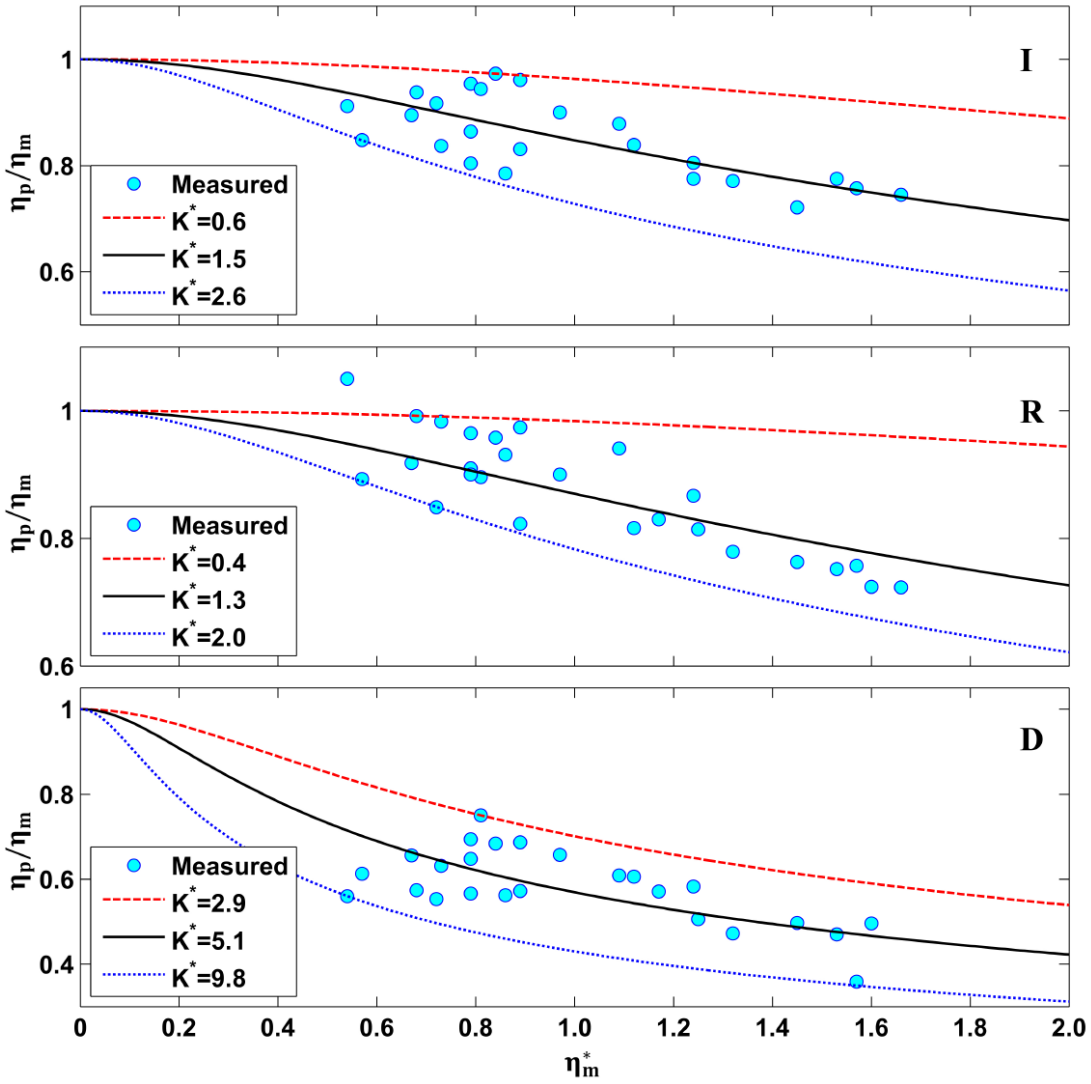

Figure 4.8 Measured and analytical ratios (η_p/η_m) as a function of surge steepness parameter η_m^* for range of inlet and bay parameter K^* at tide gauges I, R, and D

The measured values of T_s, η_m at gauge L, and η_p at gauges I, R, and D are listed in Table 2.1. The assumption of the uniform stillwater level in both Indian River Bay and Rehoboth Bay is not accurate. As a result, the values of K^* at gauges I, R, and D are calibrated separately. The measured values of (η_p/η_m) and η_m^* for each storm are plotted for each gauge in Figure 4.8. Eqs. (8) and (9) are used to obtain the fitted value of K^* for each storm at each gauge. The analytical relationship between (η_p/η_m) and η_m^* is shown using the minimum, average, and maximum values of the fitted K^* at each gauge. The data point with (η_p/η_m) = 1.05 for storm 21 at gauge R is excluded from the calibration of K^*. The ranges of K^* = 0.6 – 2.6 at gauge I and K^* = 0.4 – 2.0 at gauge R may be regarded to be consistent with the estimated values of K^* = 1.4 based on the bay and inlet characteristics. The values of K^* = 2.9 – 9.8 at gauge D are much larger than K^* = 1.4. The large fitted K^* at gauge D might be related to the additional loss from gauge I to gauge D but the fitted K^* decreases slightly from gauge I to gauge R.

4.3 Comparison for Bay Peak Stillwater Elevations

Figure 4.9 compares the measured and analytical values of the peak stillwater elevation η_p at gauges I, R, and D. Use is made of the average K^* = 1.5, 1.3, and 5.1 at gauges I, R, and D, respectively. The root-mean-square relative error E is calculated separately for each gauge, where E is the standard deviation of the relative error $(A_i - M_i)/M_i$ with A_i and M_i = analytical and measured values for the i-th data point for each gauge. The dashed lines in Figure 4.9 indicate 10% (30% for gauge D) deviations from the solid line of perfect agreement. The reason for the larger deviations for gauge D is unknown and under investigation. The analytical time series of the stillwater elevation $\eta_B(t)$ in Eq. (7) are compared with the measured time series at

gauges I, R, and D. The analytical model tends to overpredict the phase shift ε and does not predict $\eta_B(t)$ well in comparison with the measured and fitted time series of $\eta_o(t)$ shown in Figures 4.1 – 4.7. This analytical model is still useful in predicting the

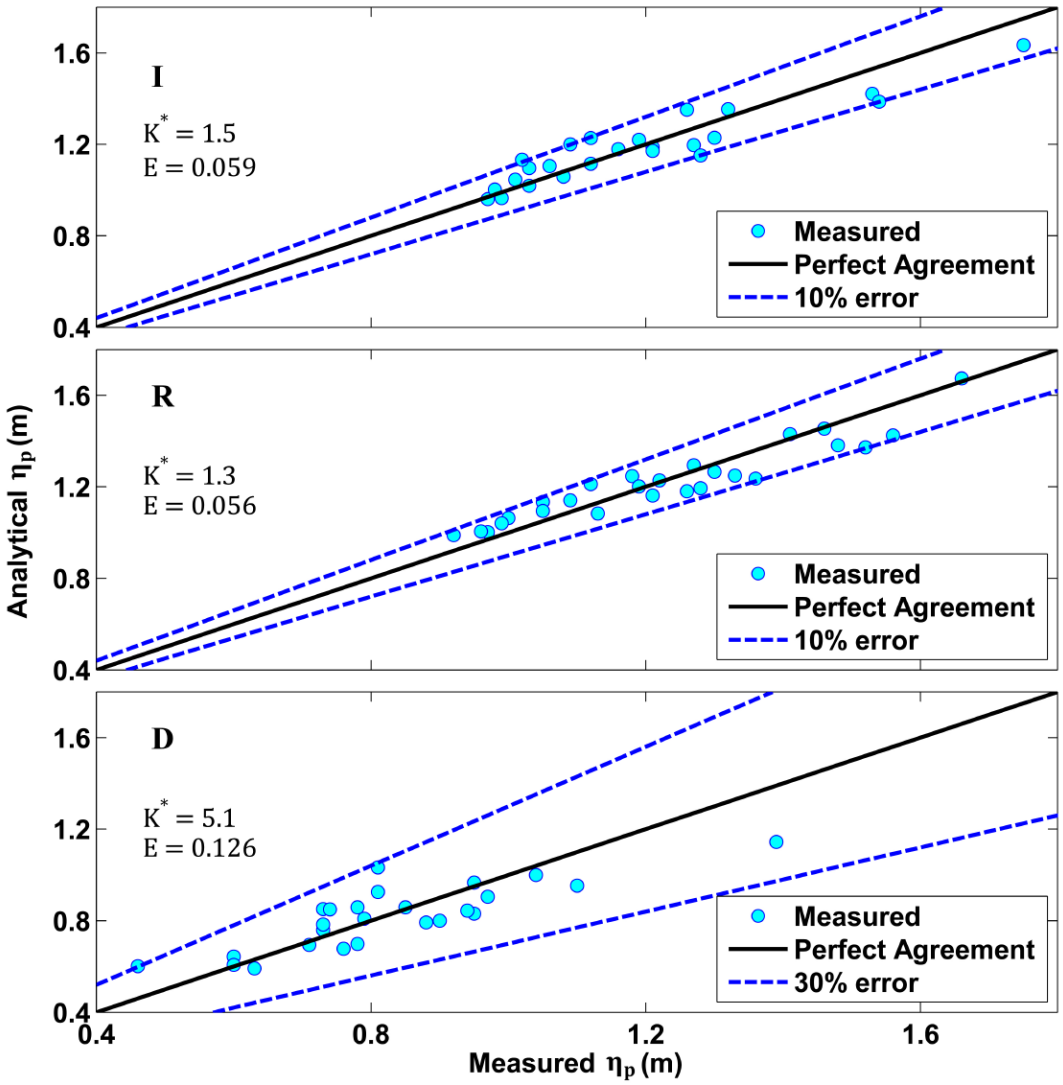

Figure 4.9 Measured and analytical peak elevations η_p in bay at tide gauges I (K^* = 1.5), R (K^* = 1.3), and D (K^* = 5.1) with 10% or 30% error range and root-mean-square relative error E

peak stillwater elevation η_p in the bay for the given peak stillwater elevation η_m in the ocean.

4.4 Statistical Extreme Stillwater Elevations

Table 4.1 lists the values of η_m at a function of the recurrence interval T_r based on the statistical analysis of the 94-year historical extreme water levels at Lewes by Nadal-Caraballo et al. (2016). The value of η_m = 1.85 m for storm 20 (Hurricane Sandy) is close to η_m = 1.88 m for T_r = 50 yr (2% annual probability). The 11-year historical extreme water levels at gauges I, R, and D are used to calibrate the inlet and bay parameter K^* at each gauge. The analytical model with this calibrated K^* is used to estimate the values of η_p at gauges I, R, and D for T_r = 1, 10, 25, 50, 100, and 500 yr. The statistical analysis by Nadal-Caraballo et al. (2016) did not include the surge duration T_s. The surge steepness parameter η_m^* is in the range of 0.54 – 1.66 during 2005 – 2015. The analytical values of η_p for the given η_m^* = 0.54 and 1.66 at gauges I, R, and D are listed in Table 4.1 to show the sensibility of η_p to η_m^* where η_m^* = 0.81 for Hurricane Sandy. The difference of η_p between gauges I and R is within the 10%

Table 4.1 Estimated extreme stillwater elevation η_p at tide gauges I, R, and D with η_m^* = 0.54 and 1.66 for recurrence interval T_r = 1 - 500 yr

T_r (yr)	η_m(m)	η_p (m) for η_m^* = 0.54			η_p (m) for η_m^* = 1.66		
		I	R	D	I	R	D
1	1.32	1.23	1.25	0.94	0.97	1.02	0.60
10	1.65	1.54	1.57	1.18	1.22	1.27	0.76
25	1.78	1.66	1.69	1.27	1.31	1.37	0.82
50	1.88	1.76	1.78	1.34	1.39	1.45	0.86
100	1.99	1.86	1.89	1.42	1.47	1.53	0.91
500	2.25	2.10	2.13	1.61	1.66	1.73	1.03

error of the analytical model. The difference of η_p between gauges I and D is as large as that between T_r = 10 and 100 yr at each gauge and that between η_m^* = 0.54 and 1.66. The surge duration T_s and the spatial variation of η_p are as important as the recurrence interval T_r.

The increase of η_p from T_r = 50 yr to T_r = 100 yr at each gauge for given η_m^* is about 0.1 m in Table 4.1. As a result, the peak stillwater elevations at gauges I, R, and D measured during Hurricane Sandy may be fairly close to those for T_r = 100 yr. However, wave overtopping and overwash of the barrier beach occurred during Hurricane Sandy. Eqs. (7) and (8) are based on the assumption of no wave overtopping. The wave overtopping rate $Q_w(t)$ in Eq. (1) during Hurricane Sandy is predicted in the following.

Chapter 5

WAVE OVERTOPPING OF BARRIER BEACH DURING HURRICANE SANDY

The cross-shore numerical model CSHORE (Kobayashi 2016) is used to predict wave overtopping and overwash along the cross-shore lines L1 – L14 in Figure 2.1. Figlus et al. (2011) compared CSHORE with three small-scale tests with different dune geometries in front of a low-crested vertical wall. Johnson et al. (2012) evaluated CSHORE using severe beach and dune erosion data at seven sites on the mid-Atlantic east coast. Kobayashi and Jung (2012) compared CSHORE with beach erosion and recovery data along 16 cross-shore lines spanning 5 km alongshore on Rehoboth Beach and Dewey Beach in Figure 2.1. The input parameters required for the CSHORE computation are kept the same as those used by Kobayashi and Jung (2012). The median diameter of the beach sand was 0.33 mm. A bay was not included in the computation domain in the above comparisons. Kobayashi et al. (2013) extended CSHORE to the landward wet zone and computed wave transmission over and through a porous breakwater. This extended CSHORE is modified for an impermeable barrier beach with a bay.

5.1 Computation Domain and Input

Figure 5.1 shows the computation domain in this study. The onshore coordinate x extends from WIS 63156 in 20-m water depth at $x = 0$ to the bay near $x =$ 13 km. The 72-h hourly series of the stillwater level η_o and the wave height H_{mo}, period T_p and angle θ shown in Figure 2.12 are specified as the seaward boundary

conditions. The 72-h hourly series of the stillwater level η_B at tide gauge I shown in Figure 2.8 (Storm 20 for Hurricane Sandy) is specified as the landward boundary condition to account for the stillwater level difference in the ocean and bay. The vertical coordinate z is positive upward with $z = 0$ at NAVD88. The initial bottom elevation z_b at computation time $t_c = 0$ is specified as the initial condition. The barrier beach is assumed to consist of 0.33-mm sand without regard to vegetation and a paved road. The cross-shore grid spacing is 3 m. It is noted that the computation time $t_c = 0$ is different from the analytical time t defined in relation to Eq. (6). The bottom elevation $z_b(x,t_c)$ varies with time t_c due to cross-shore sediment transport. The cross-shore variation of $z_b(x, t_c)$ includes undulations. The seaward stillwater shoreline at time t_c is located at the most seaward intersection point between $\eta_o(t_c)$ and $z_b(x,t_c)$. The landward stillwater shoreline at time t_c is located at the most landward intersection point between $\eta_B(t_c)$ and $z_b(x,t_c)$. The wet and dry zone is situated between the seaward and landward stillwater shorelines. The dune crest elevation

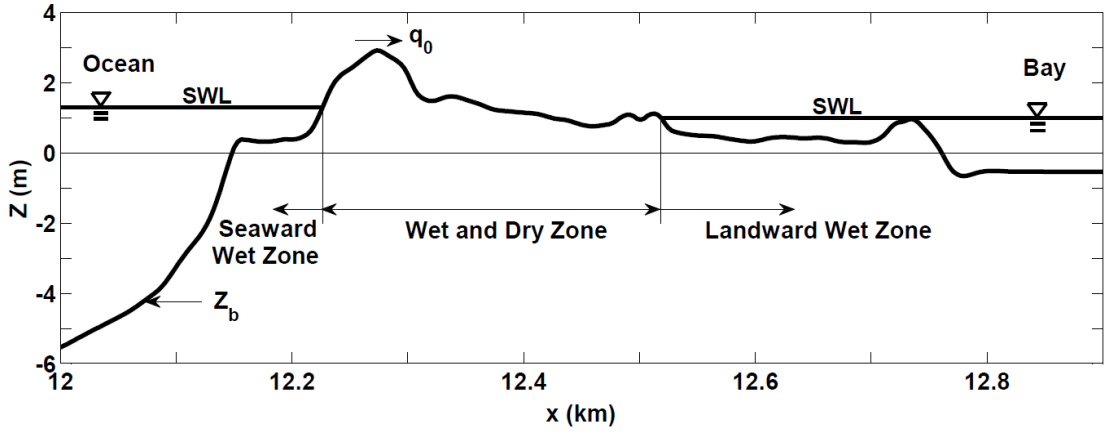

Figure 5.1 Computation for wave overtopping of evolving barrier beach using CSHORE with seaward wet zone, wet and dry zone, and landward wet zone based on still water level (SWL) in ocean and bay

$z_c(t_c)$ at given t_c is defined as the highest elevation of $z_b(x,t_c)$ with respect to x. The wave overtopping rate $q_o(t_c)$ is computed on the dune crest. If $z_c(t_c)$ becomes less than $\eta_o(t_c)$ during the 72-h computation, the dune crest becomes submerged and the seaward wet zone is assumed to reach the landward end of the computation domain. The specified $\eta_B(t_c)$ in the bay is ignored when the dune crest becomes submerged. The barrier beach was not submerged during Hurricane Sandy but submergence is allowed during this CSHORE computation.

5.2 Computed Beach Profile Evolution

The computed beach profile evolution along each of L1 – L14 is examined by plotting the cross-shore variations of $z_b(x,t_c)$ at t_c = 0, 24, 48, and 72 h in Figures 5.2 – 5.4. The computed profile changes occur mostly during the day of the storm peak during t_c = 24 – 48 h. For the cross-shore line of minor wave overtopping and overwash (e.g. L4, L6 and L10), the computed beach profile change is essentially limited to the seaward side of the dune crest. For the cross-shore line of major wave overtopping and overwash (e.g. L1, L2, L7, L8 and L14), the dune crest lowering and overwash deposit are noticeable.

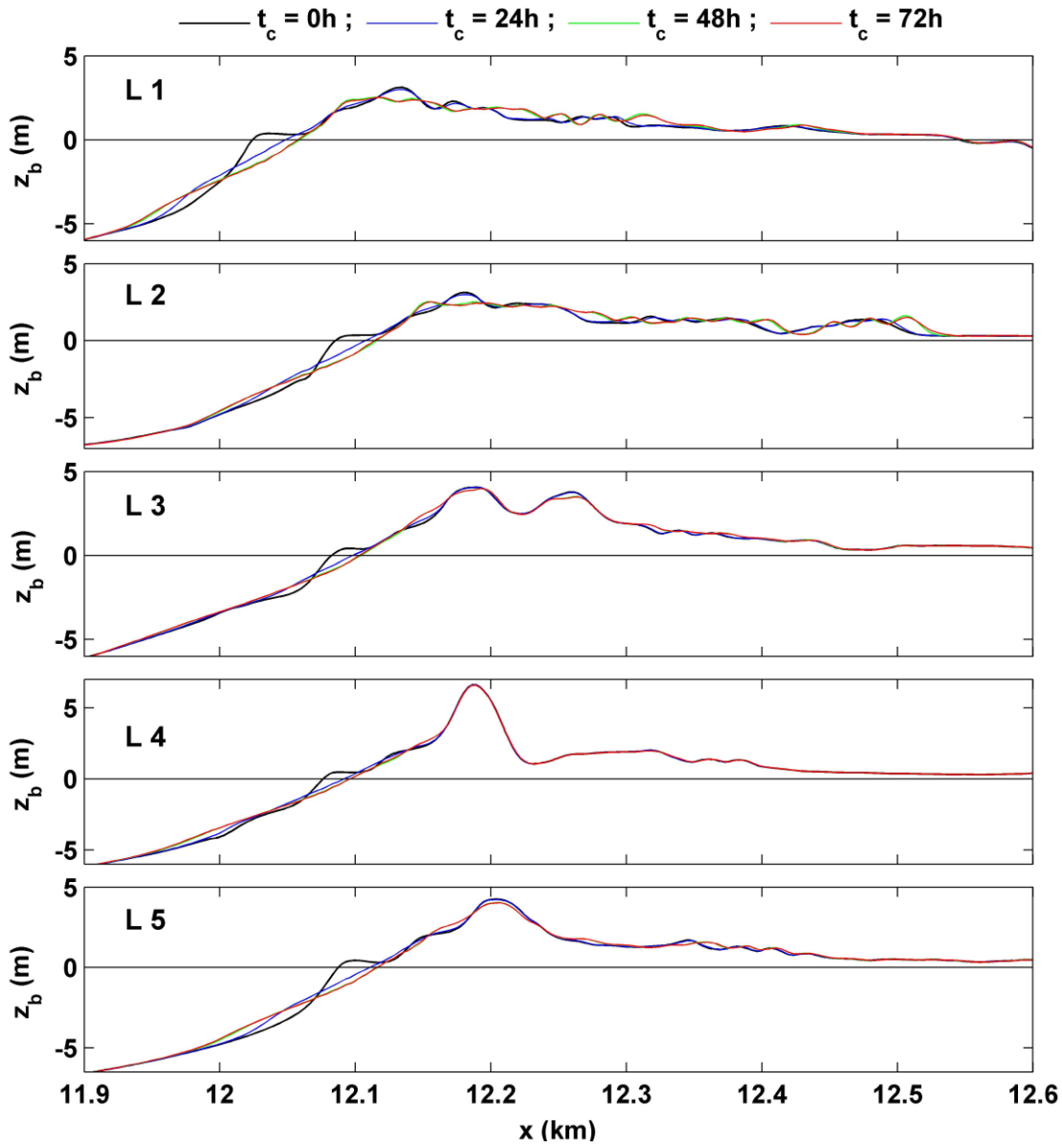

Figure 5.2 Initial (t_c = 0) and computed beach profiles at computation time t_c = 24, 48, and 72h along cross-shore lines L1, L2, L3, L4 and L5

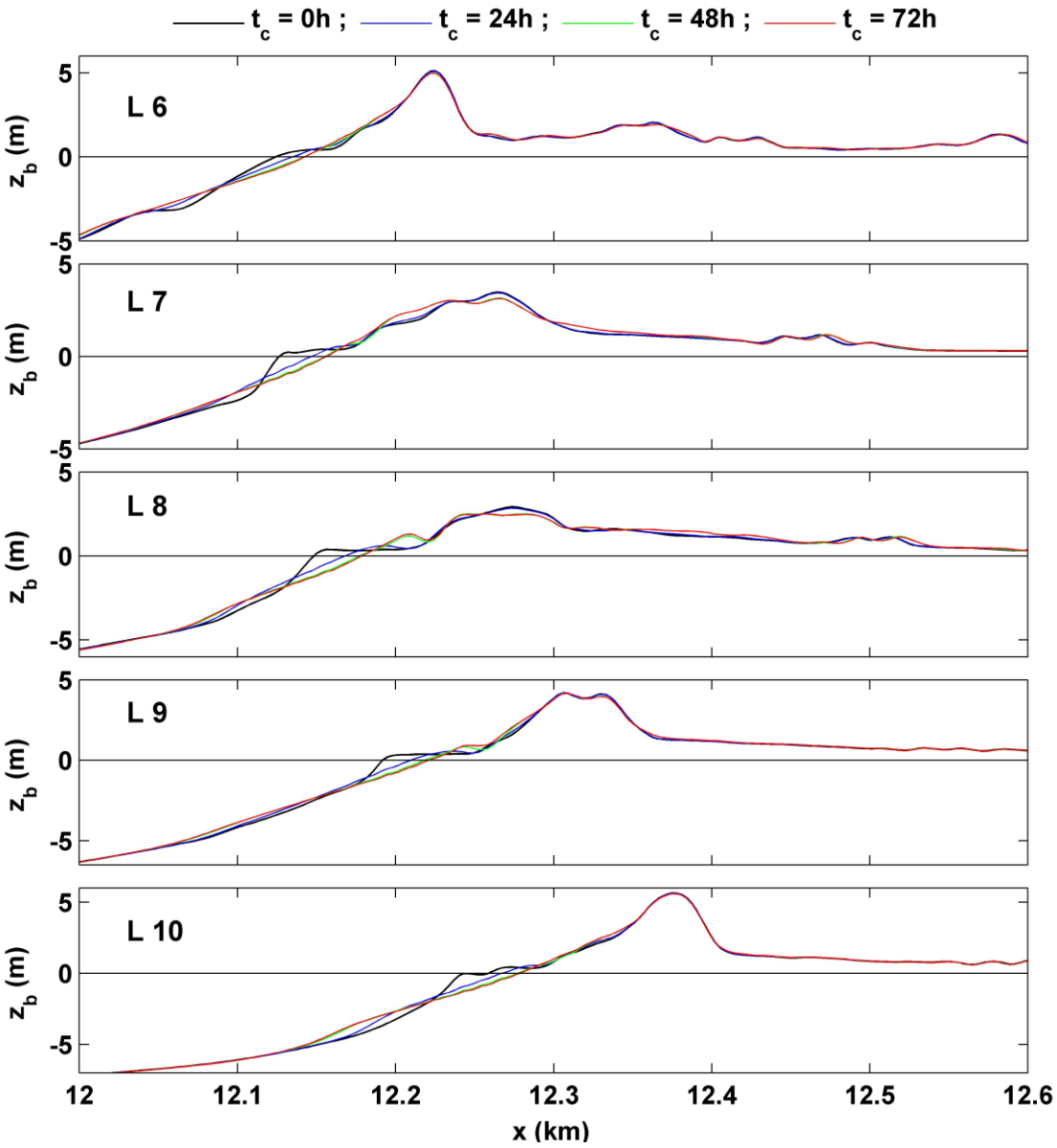

Figure 5.3 Initial (t_c = 0) and computed beach profiles at computation time t_c = 24, 48, and 72h along cross-shore lines L6, L7, L8, L9, and L10

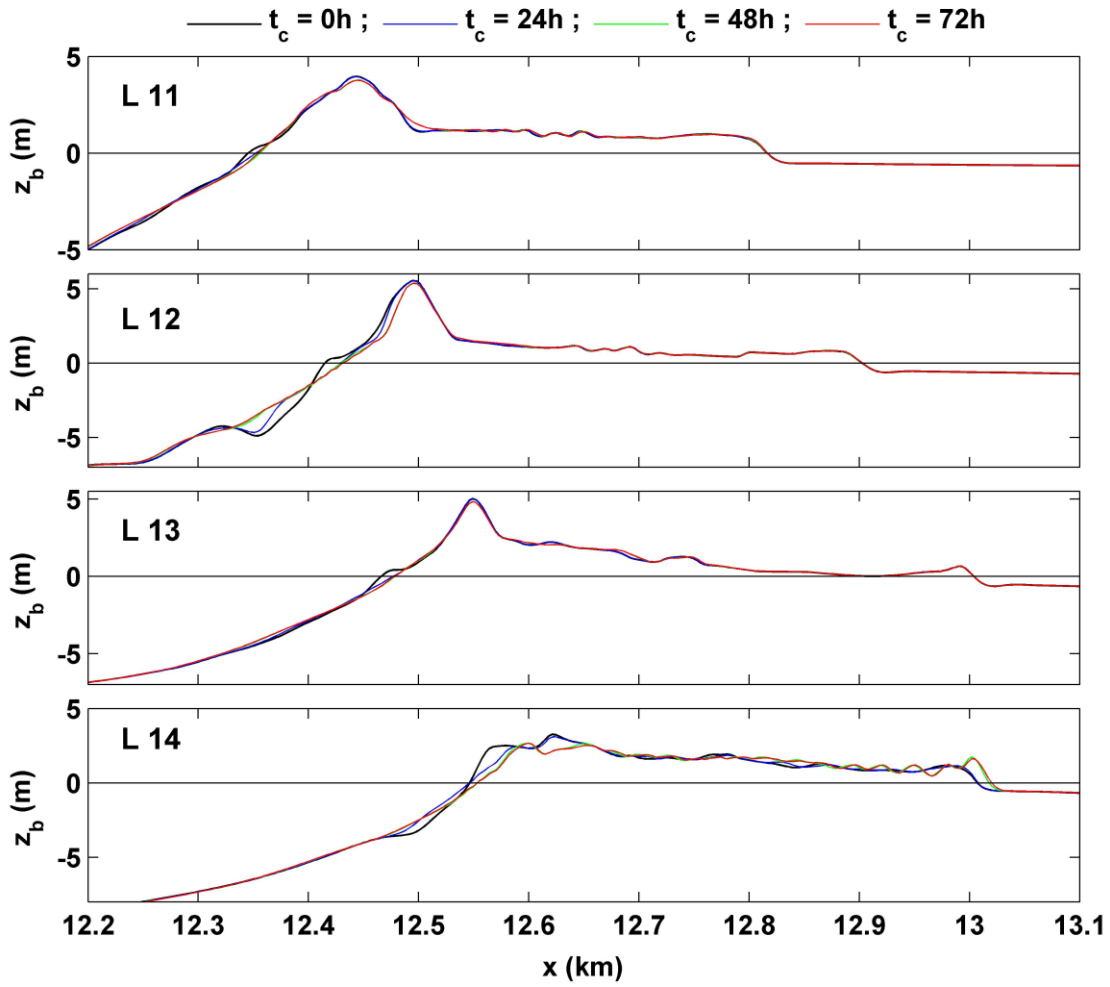

Figure 5.4 Initial (t_c = 0) and computed beach profiles at computation time t_c = 24, 48, and 72h along cross-shore lines L11, L12, L13, and L14

5.3 Cross-shore and Longshore Sand Transport

Figures 5.5 – 5.11 show the initial ($t_c = 0$) and final (t_c = 72 h) profiles along L1 – L14. The computed cross-shore bed load and suspended load transport rates per unit width are integrated for the 72-h computation duration to obtain the bed load volume, v_{bx}, suspended load volume v_{sx}, and net volume $v_x = (v_{bx} + v_{sx})$ per unit width. The computed longshore bed load and suspended load transport rates are also integrated to obtain the bed load volume v_{by}, suspended load volume v_{sy}, and net volume $v_y = (v_{by} + v_{sy})$ for the 72-h duration. The cross-shore bed load transport is positive (onshore). The cross-shore suspended load transport is negative (offshore) in the zone affected little by onshore water flux caused by wave overtopping and becomes positive in the affected zone. The computed net cross-shore transport is slightly positive in the offshore zone of dominant bed load (e.g., Kobayashi and Jung 2012) and becomes negative in the zone dominated by suspended sand transported offshore by return (undertow) current induced by breaking waves. The value of v_x is positive in the zone of wave overtopping and onshore water flux. On the other hand, longshore bed load and suspended load transport are positive (northward) under the incident waves from the southeast during Hurricane Sandy. The computed longshore sand transport takes place predominantly seaward of the dune crest even in the presence of major wave overtopping and overwash. The longshore transport volume v_y is much larger than the magnitude of the cross-shore transport volume v_x on the beach seaward of the dune crest.

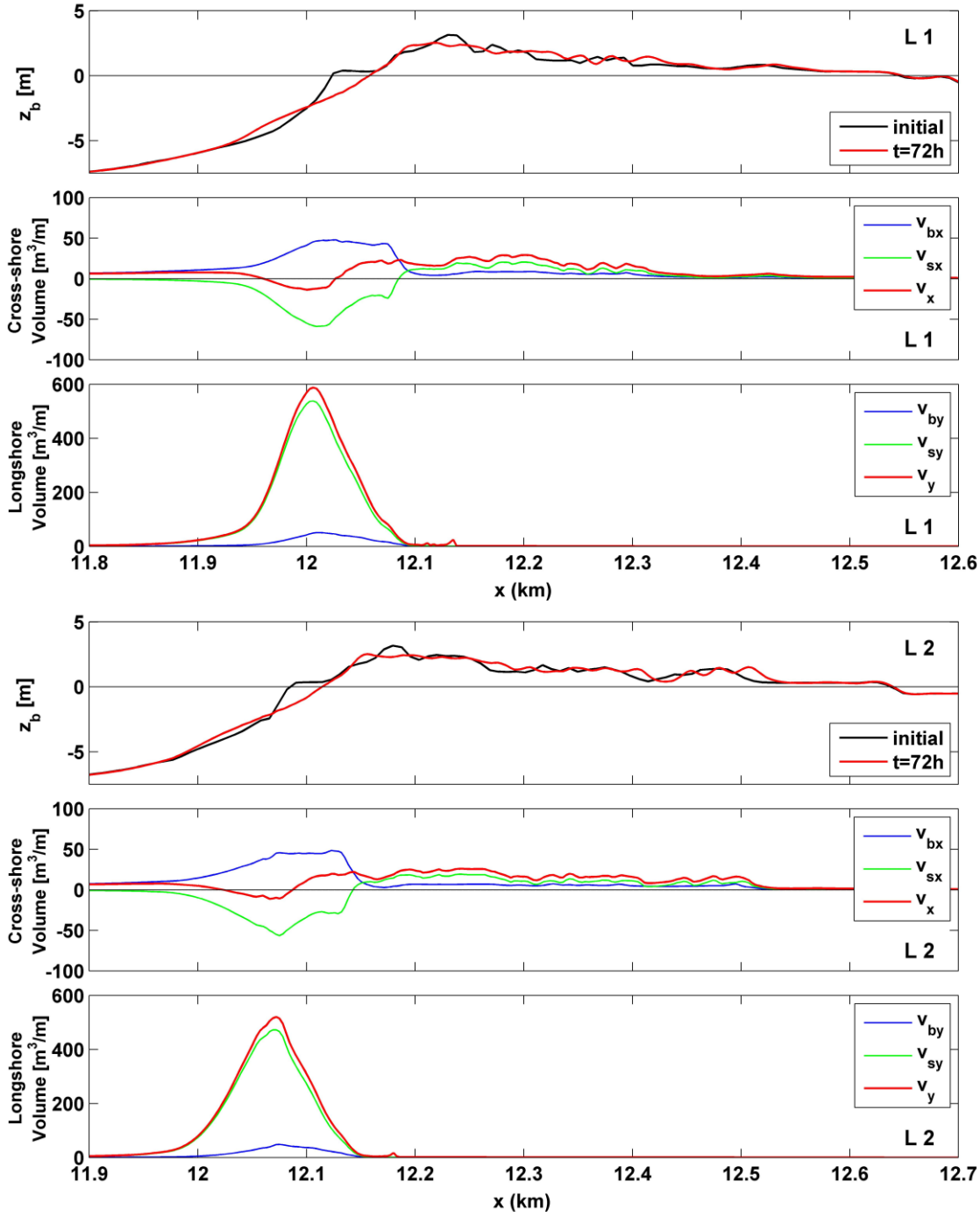

Figure 5.5 Initial and final profiles z_b, cumulative cross-shore sand transport volumes v_{bx}, v_{sx}, and v_x per unit width and cumulative longshore sand transport volumes v_{by}, v_{sy}, and v_y per unit width for cross-shore lines L1 and L2

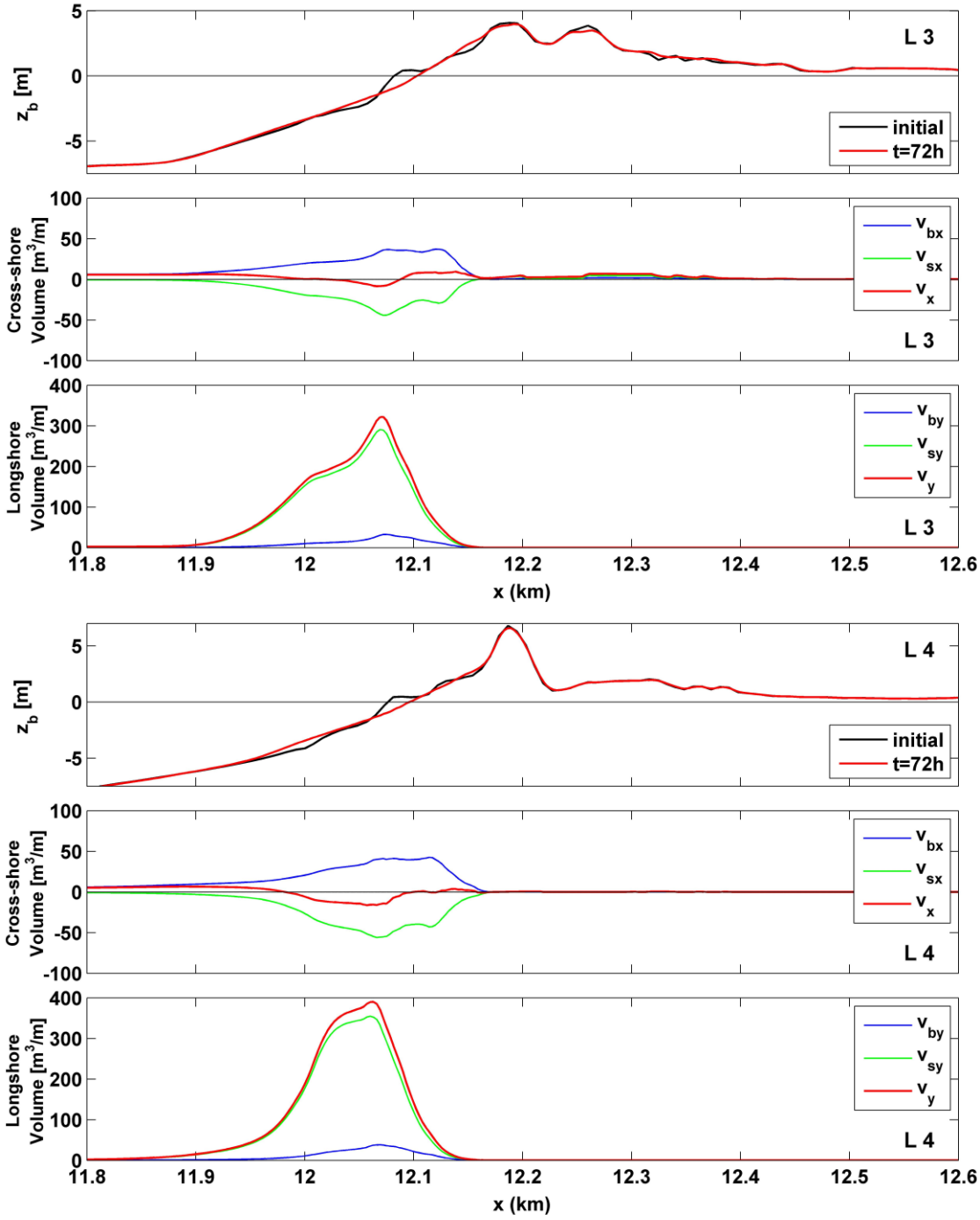

Figure 5.6 Initial and final profiles z_b, cumulative cross-shore sand transport volumes v_{bx}, v_{sx}, and v_x per unit width and cumulative longshore sand transport volumes v_{by}, v_{sy}, and v_y per unit width for cross-shore lines L3 and L4

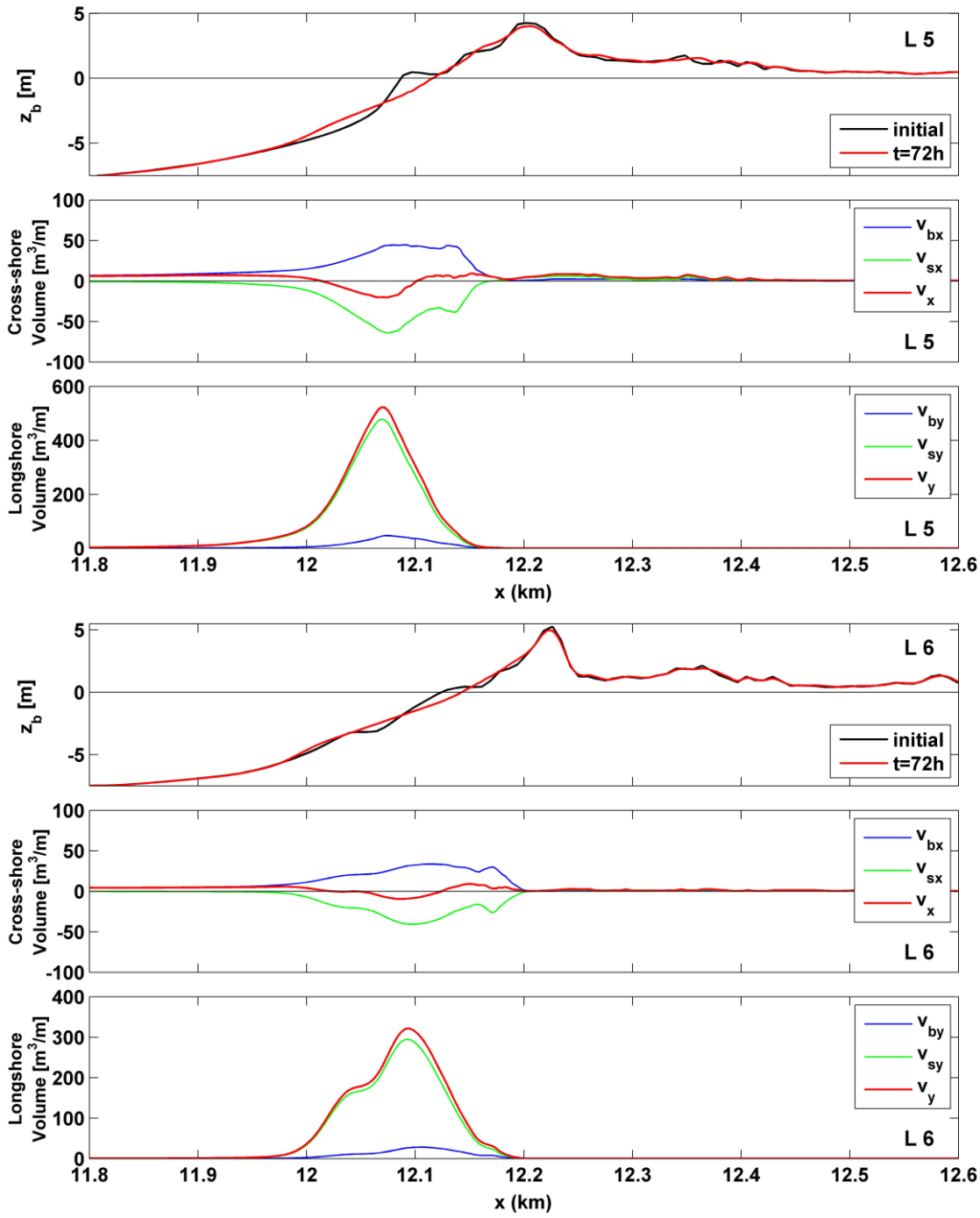

Figure 5.7 Initial and final profiles z_b, cumulative cross-shore sand transport volumes v_{bx}, v_{sx}, and v_x per unit width and cumulative longshore sand transport volumes v_{by}, v_{sy}, and v_y per unit width for cross-shore lines L5 and L6

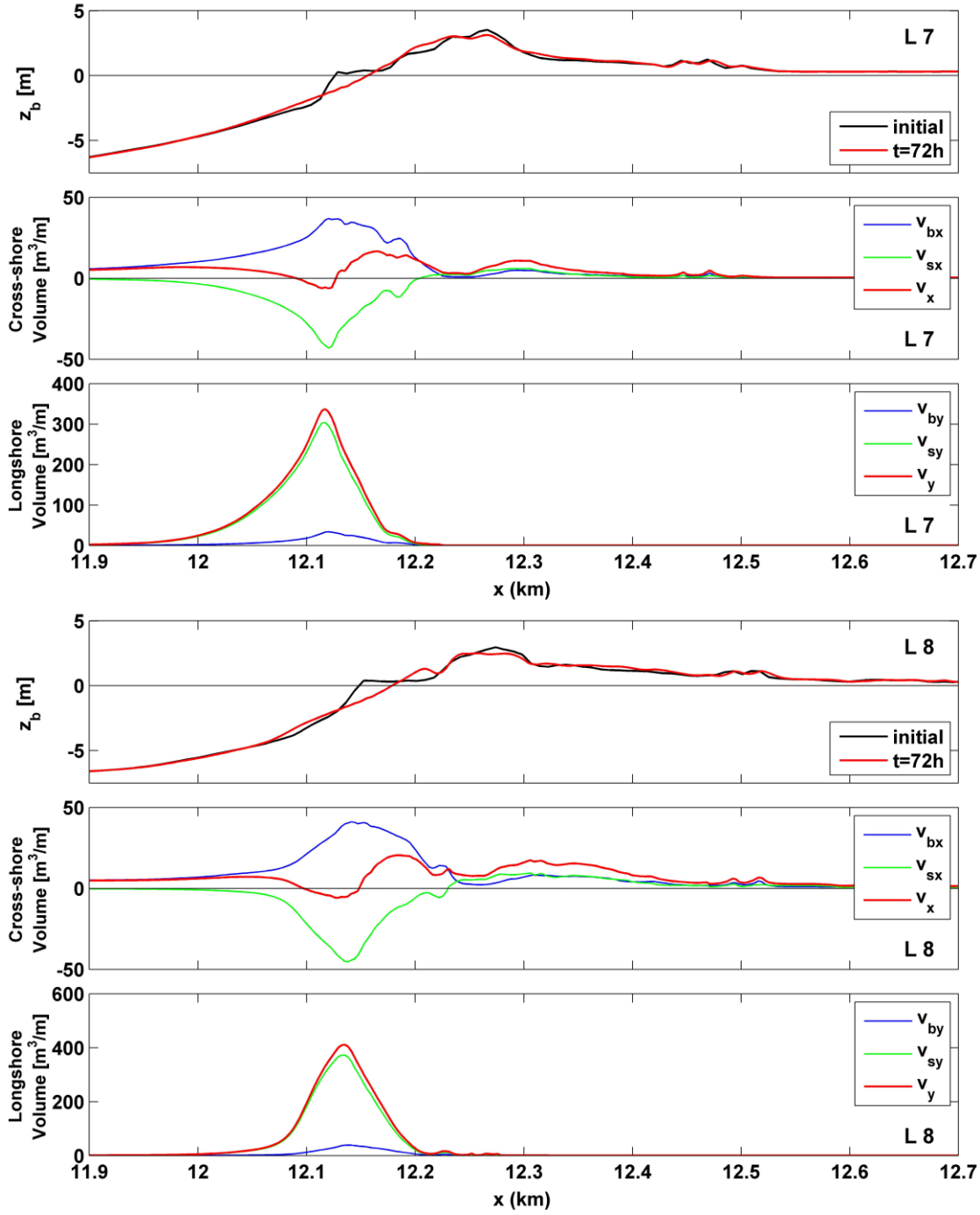

Figure 5.8 Initial and final profiles z_b, cumulative cross-shore sand transport volumes v_{bx}, v_{sx}, and v_x per unit width and cumulative longshore sand transport volumes v_{by}, v_{sy}, and v_y per unit width for cross-shore lines L7 and L8

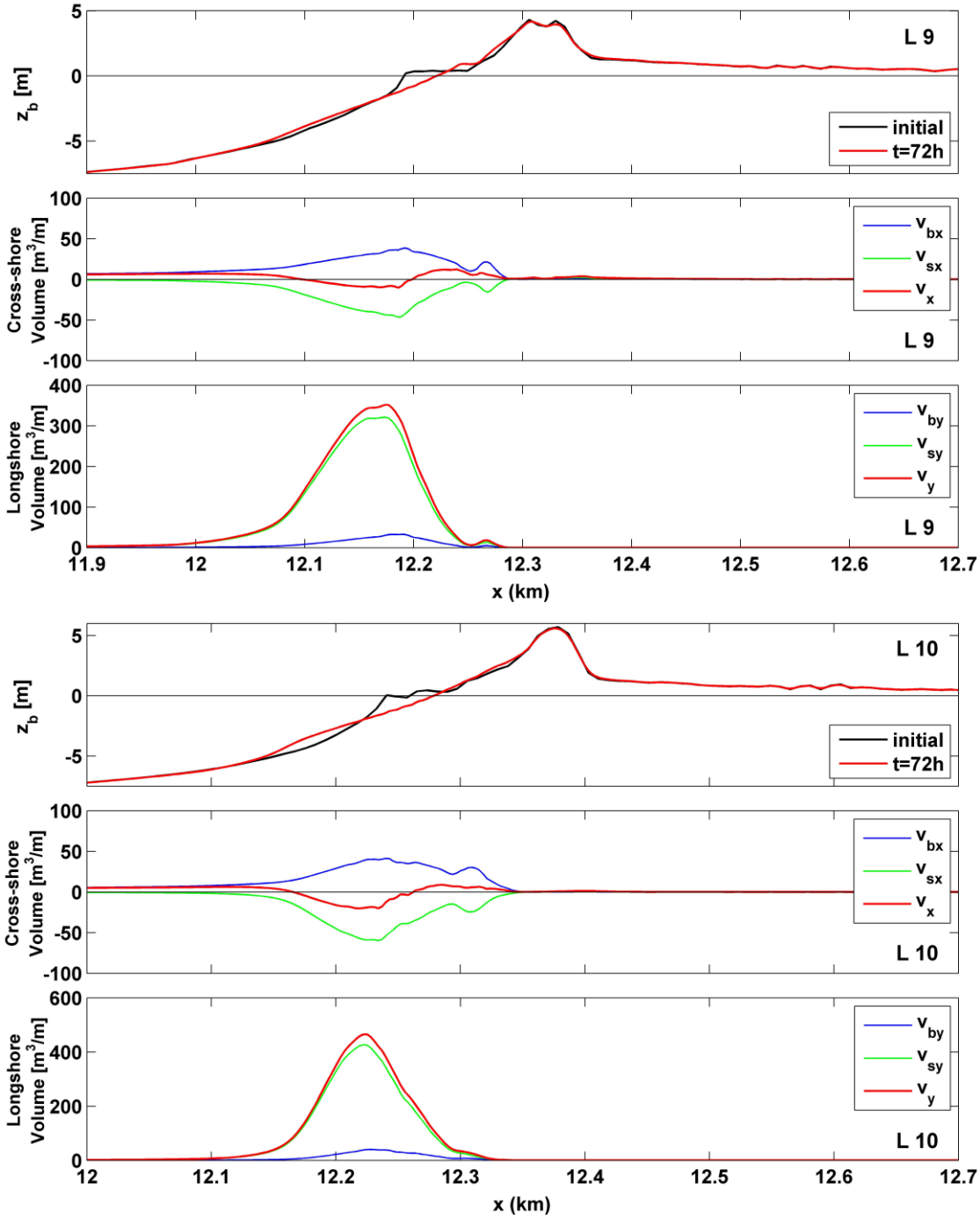

Figure 5.9 Initial and final profiles z_b, cumulative cross-shore sand transport volumes v_{bx}, v_{sx}, and v_x per unit width and cumulative longshore sand transport volumes v_{by}, v_{sy}, and v_y per unit width for cross-shore lines L9 and L10

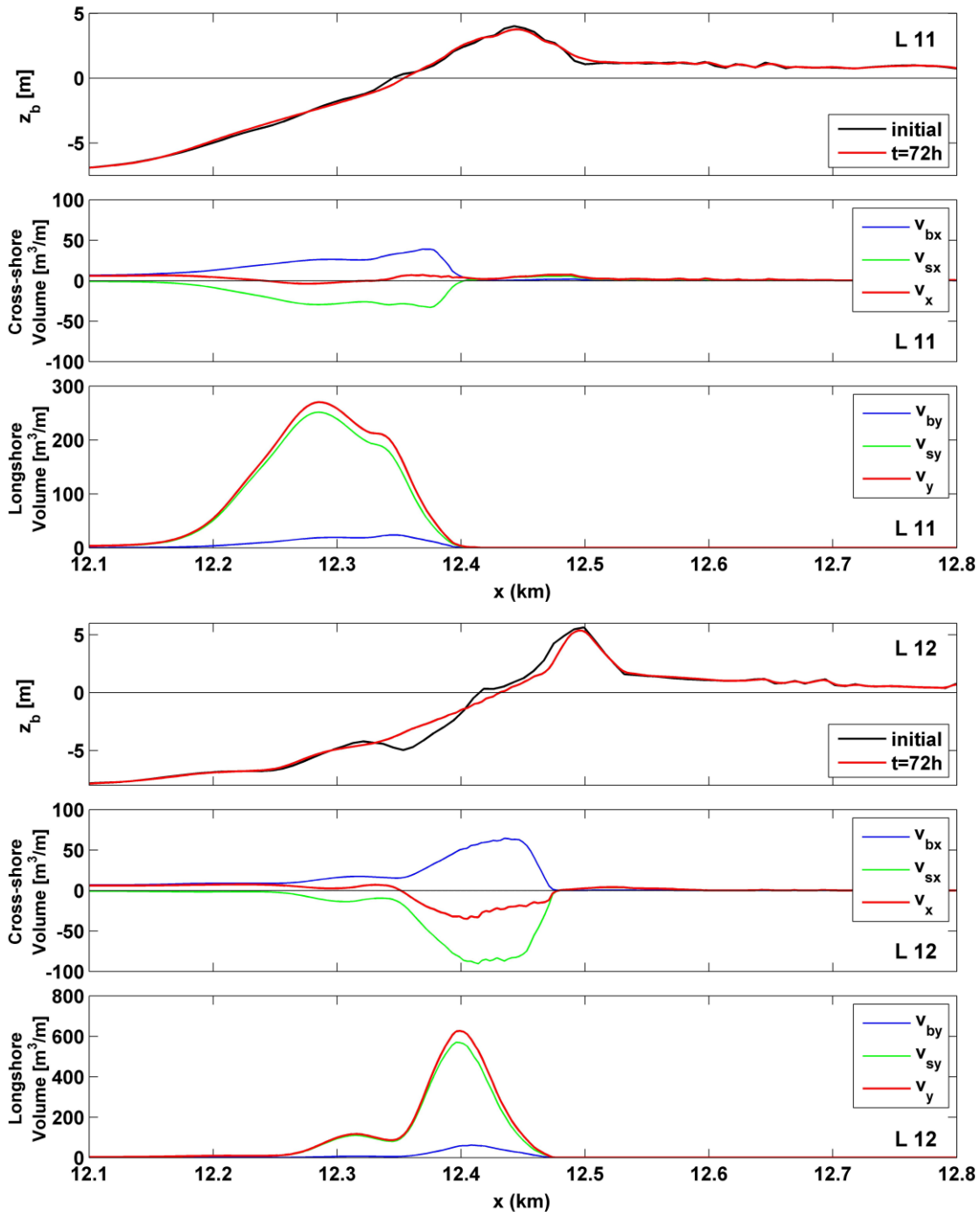

Figure 5.10 Initial and final profiles z_b, cumulative cross-shore sand transport volumes v_{bx}, v_{sx}, and v_x per unit width and cumulative longshore sand transport volumes v_{by}, v_{sy}, and v_y per unit width for cross-shore lines L11 and L12

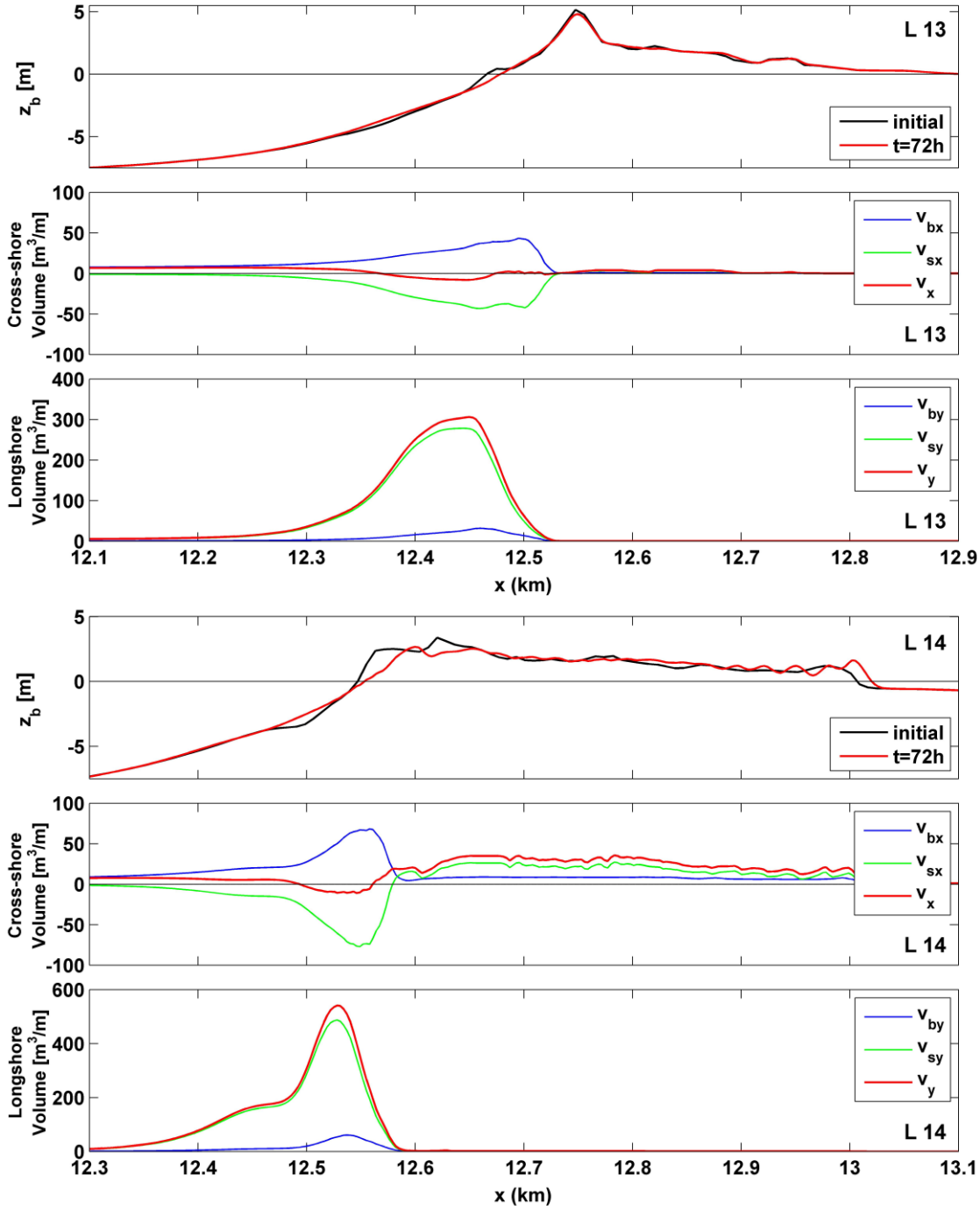

Figure 5.11 Initial and final profiles z_b, cumulative cross-shore sand transport volumes v_{bx}, v_{sx}, and v_x per unit width and cumulative longshore sand transport volumes v_{by}, v_{sy}, and v_y per unit width for cross-shore lines L13 and L14

5.4 Computed Wave Overtopping Rates

The hourly wave overtopping rate q_o is computed by averaging the overtopped water volume per unit alongshore length for the duration of 1 h, corresponding to the hourly water level and wave data (Figure 2.12). The hourly variation of q_o is plotted for each of L1 – L14 in Figures 5.12 – 5.14. As in Section 5.2, the hourly variations of q_o for L4, L6 and L10 are typical examples of minor wave overtopping. The hourly variations of q_o for L1, L2, L7, L8 and L14 are typical examples of major wave overtopping. The computed variation of q_o exhibits fluctuations because wave overtopping is sensitive to the detailed topography near the dune crest. The computed wave overtopping occurs mostly during t_c = 24 – 48 h on the day of the storm peak. The computed q_o of the order of 0.1 m^2/s (100 l /s/m) may have increased the bay water level.

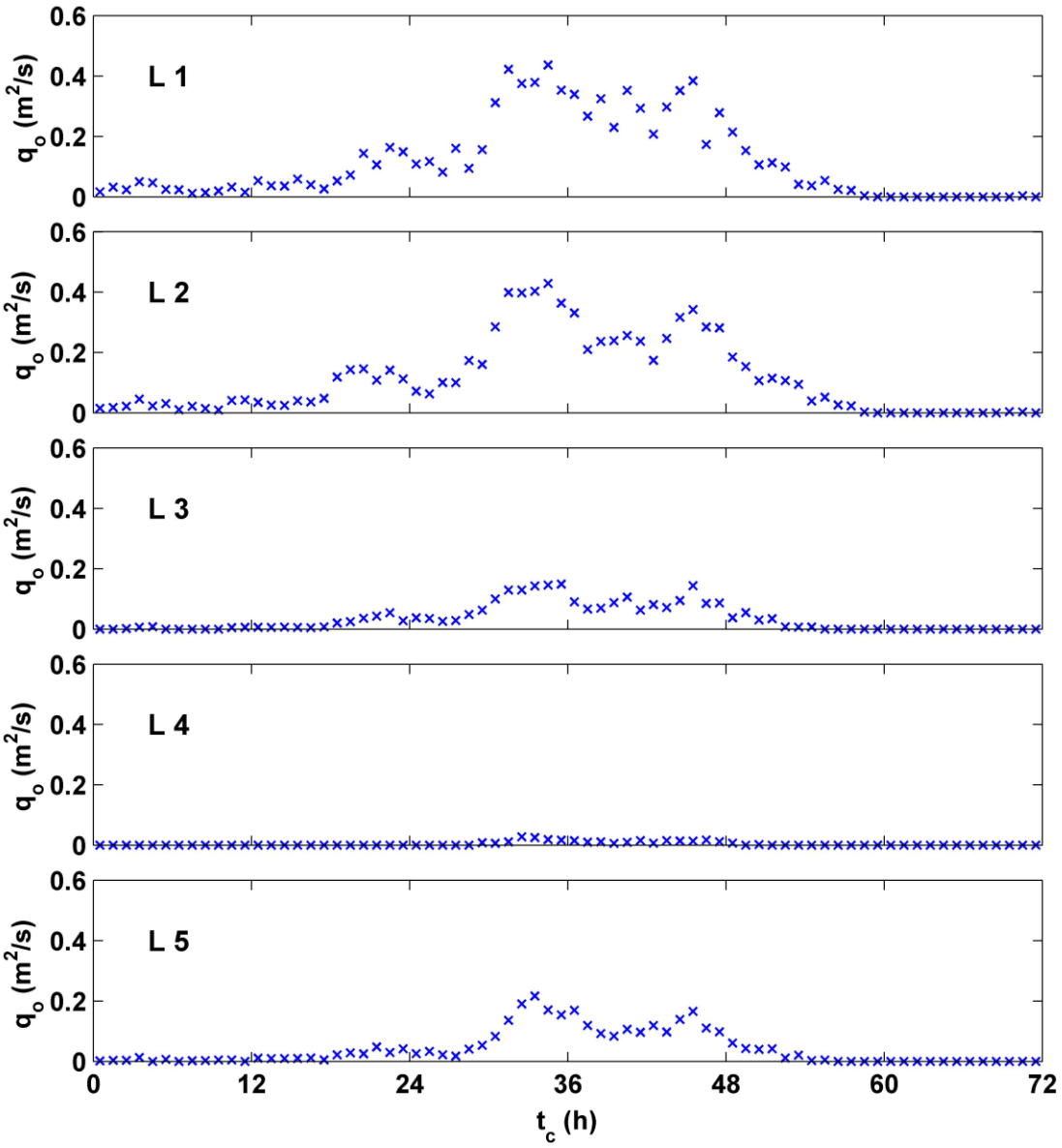

Figure 5.12 Computed temporal variation of hourly wave overtopping rate q_o per unit width along cross-shore lines L1, L2, L3, L4, and L5

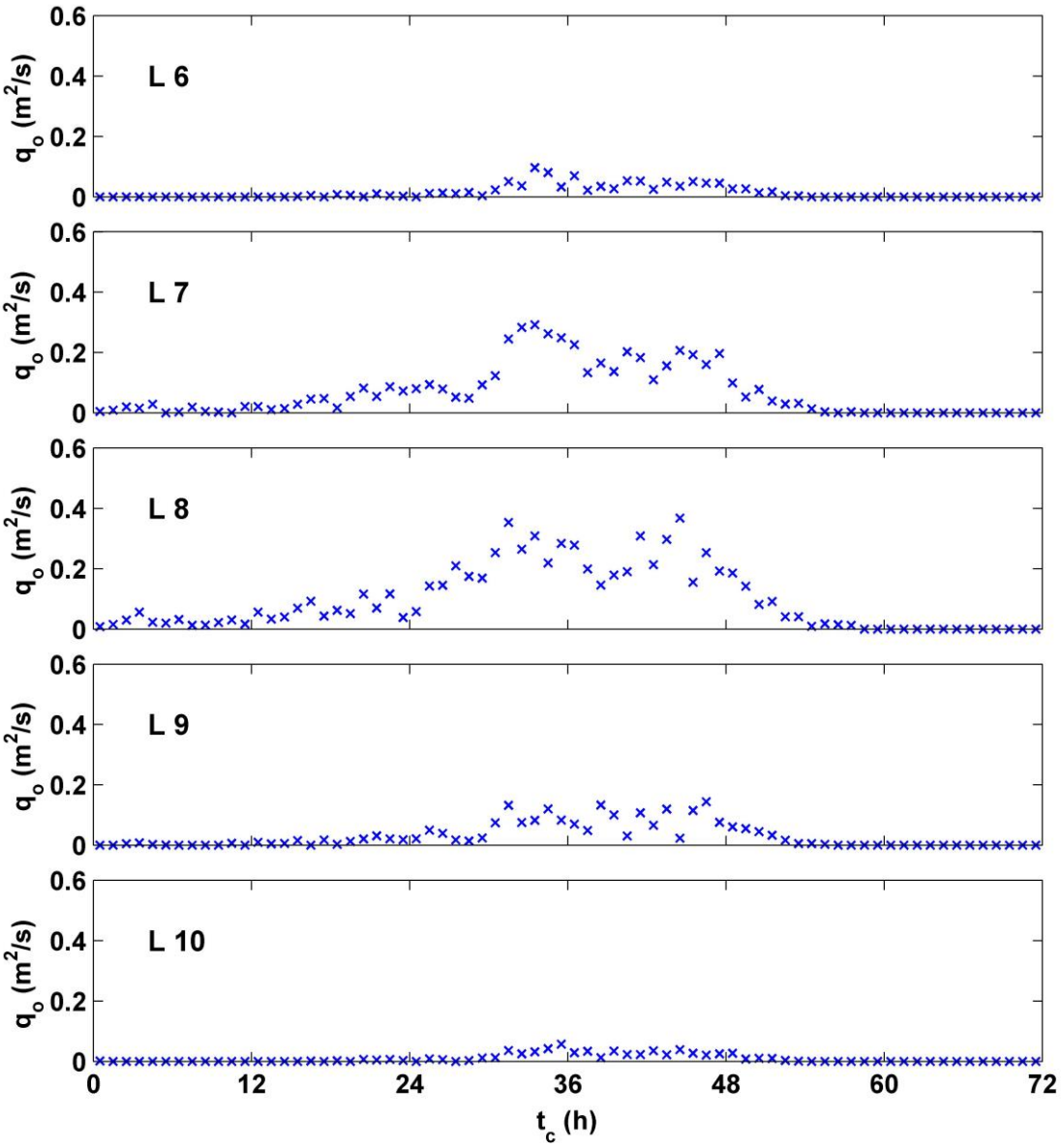

Figure 5.13 Computed temporal variation of hourly wave overtopping rate q_o per unit width along cross-shore lines L6, L7, L8, L9, and L10

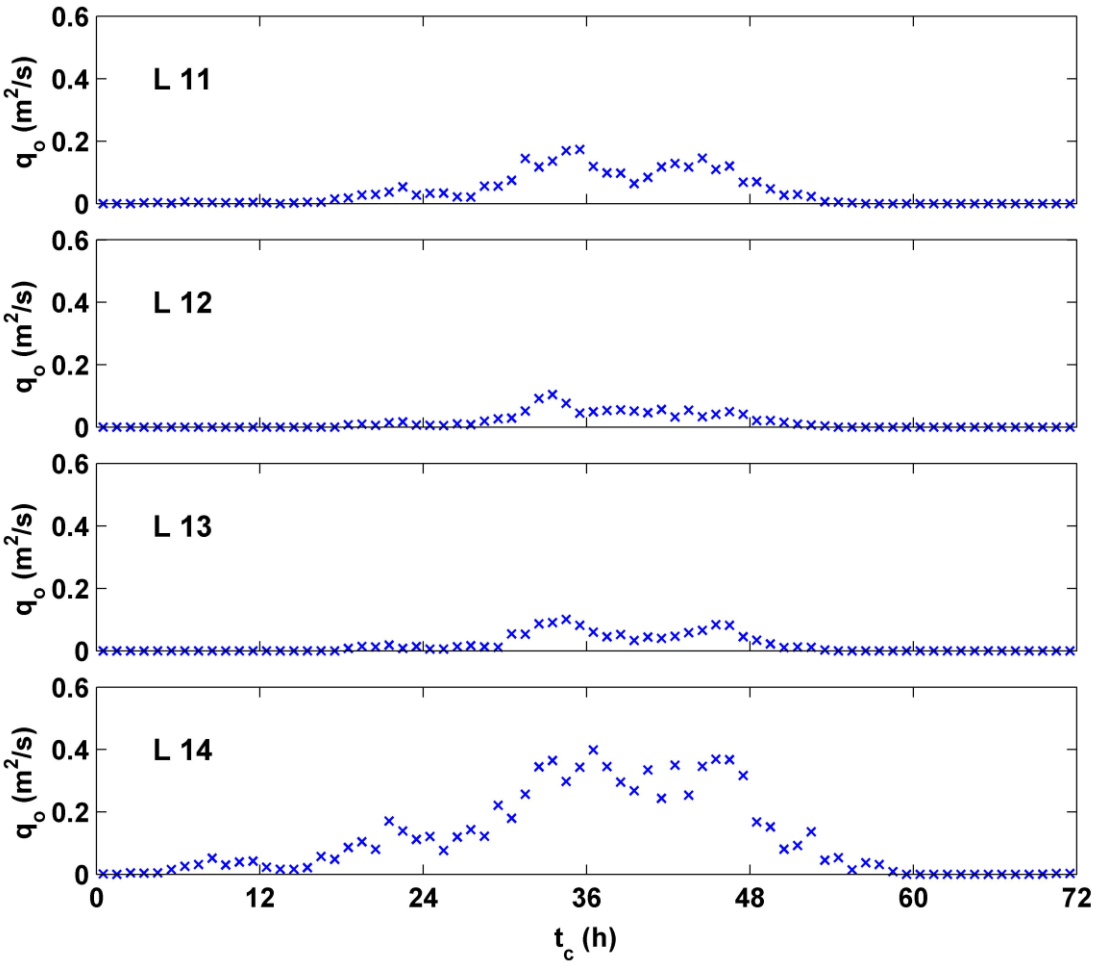

Figure 5.14 Computed temporal variation of hourly wave overtopping rate q_o per unit width along cross-shore lines L11, L12, L13, and L14

5.5 Dune Crest Lowering and Cross-sectional Area

Table 5.1 summarizes the computed profile change and wave overtopping volume v_o per unit alongshore length for L1 – L14 where v_o is obtained by adding the hourly rate q_o over the 72-h duration. The initial and final dune profiles are characterized by the dune crest elevation z_c and the dune cross-sectional area A_d defined as the area above the peak stillwater elevation η_m in the ocean and seaward of the dune crest as shown in Figure 5.15. CSHORE predicts the dune crest lowering in the range of 0.04 – 0.61 m and the decrease (increase) of A_d for the lines with the dune crest lowering larger (smaller) than about 0.2 m. For Hurricane Sandy, η_m = 1.85 m

Table 5.1 Alongshore variation of dune crest elevation z_c (m), dune cross-sectional area A_d (m^2), and wave overtopping volume v_o (m^3/m) per unit width for storm 20 (Hurricane Sandy)

Line	Initial Profile		Final Profile		Overtopping
	z_c (m)	A_d (m^2)	z_c (m)	A_d (m^2)	v_0 (m^2)
1	3.12	26.4	2.53	14.3	30996
2	3.13	17.8	2.52	5.4	29814
3	4.06	53.5	3.98	66.5	9087
4	6.62	99.8	6.58	103.6	949
5	4.24	55.5	4.02	66.6	10994
6	5.11	62.0	4.97	66.2	3607
7	3.47	50.6	3.03	30.4	17897
8	2.92	24.0	2.50	13.2	25416
9	4.19	35.9	4.15	47.0	7769
10	5.63	91.0	5.59	98.1	2301
11	3.96	61.6	3.77	61.9	9968
12	5.55	80.1	5.36	52.2	4209
13	5.01	51.6	4.81	48.5	4869
14	3.26	39.3	2.67	8.6	30325

and the computed final z_c is in the range of 2.50 – 6.58 m. The dune survival or complete destruction criterion used by the Federal Emergency Management Agency (FEMA 2011) is based on the threshold of A_d = 100 m^2 above the 100-year (1% annual probability) peak stillwater elevation. Judge et al. (2003) evaluated dune erosion vulnerability indicators including z_c and A_d. The dune of 2.92 to 6.62-m height on the barrier beach of 450 to 850-m width in this study is computed to be durable even though the initial A_d is much less than 100 m^2. It is more realistic to predict wave overtopping and assess flooding risk.

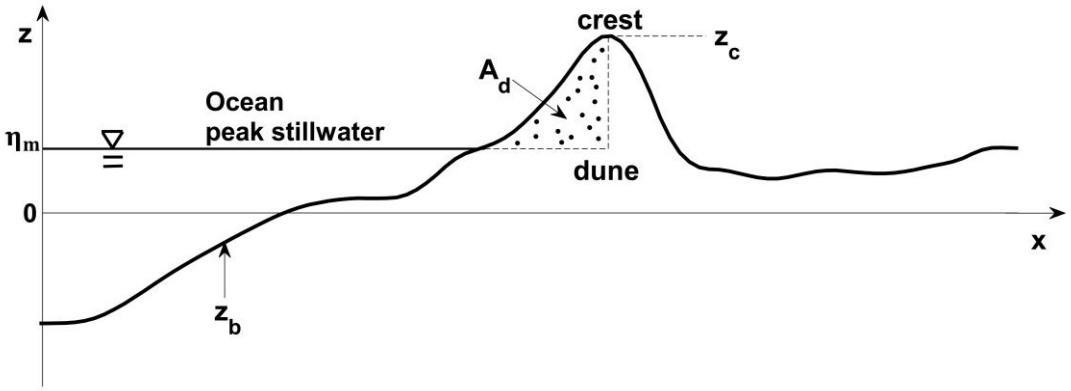

Figure 5.15 Definition sketch of dune cross-sectional area A_d above ocean peak stillwater elevation η_m and seaward of dune crest at elevation z_c for arbitrary beach profile $z_b(x)$

The computed overtopping volume v_o in Table 5.1 decreases with the increase of z_c and A_d as shown in Figure 5.16. The differences between the initial and final values of z_c and A_d increase with the increase of v_o. The computed values of v_o for L1 – L14 are added and multiplied by the alongshore length of 515 m represented by each

line to obtain the total overtopping volume $V_o = 97 \times 10^6$ m^3 over the barrier beach of 7.2-km alongshore length. The bay surface area is approximately $A_B = 75$ km^2. The stillwater elevation in the bay would have increased by $(V_o/A_B) = 1.3$ m if the bay had no tidal inlet.

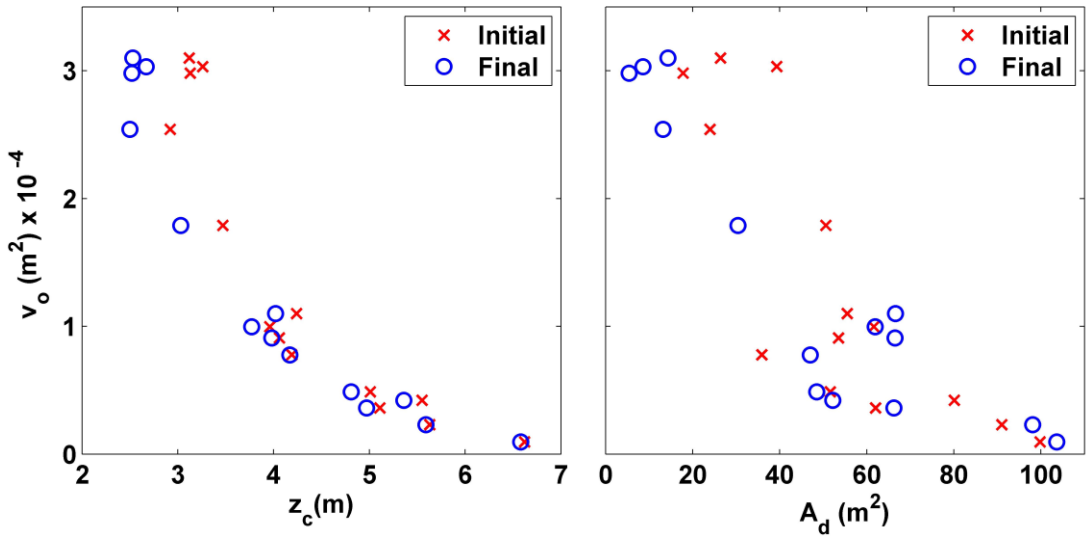

Figure 5.16 Wave overtopping volume v_o as a function of initial and final values of dune crest elevation z_c and dune cross-sectional area A_d

Chapter 6

ANALYTICAL MODEL INCLUDING WAVE OVERTOPPING

The analytical model in Chapter 3 is extended to include the wave overtopping rate Q_w in the following.

6.1 Wave Overtopping Rate Q_w

The wave overtopping rate Q_w over the barrier beach in Eq. (1) needs to be specified to solve Eqs. (1) and (4). The overtopping rate Q_o is obtained by adding the computed wave overtopping rate q_o per unit length and multiplying the added value by 515 m. Figure 6.1 shows the measured stillwater elevation η_o for storm 20 and the

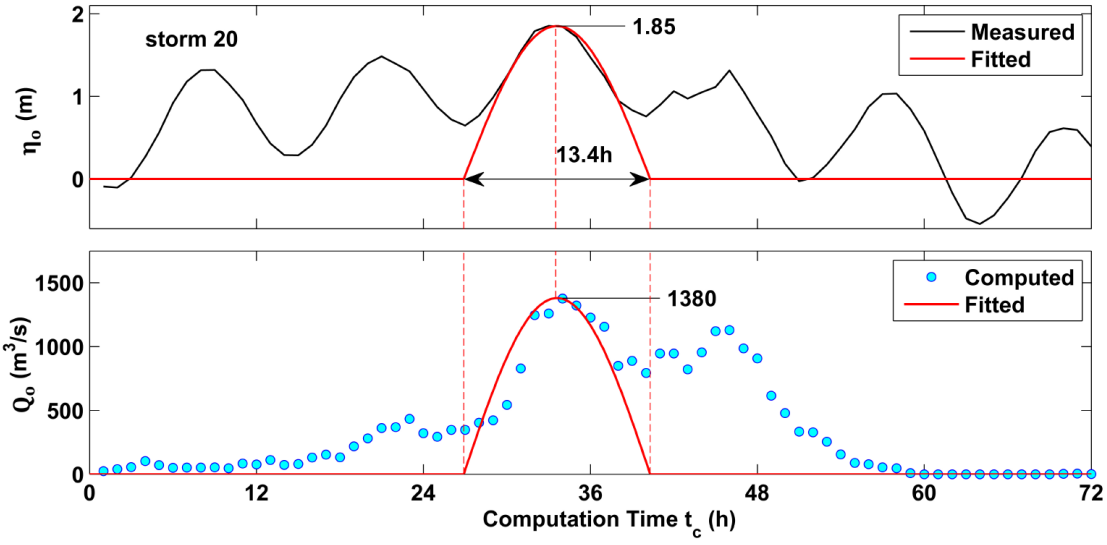

Figure 6.1 Measured and fitted ocean stillwater elevation η_o and computed and fitted wave overtopping rate Q_o over barrier beach of 7.2-km alongshore length

corresponding rate Q_o as a function of the computation time t_c to show the correlation of η_o and Q_o where the offshore wave conditions for storm 20 are presented in Figure 2.12. The fitted η_o in the form of Eq. (6) is also plotted in Figure 6.1. To obtain a simple analytical solution, the rate Q_w in Eq. (1) is assumed to be in phase with the fitted η_o

$$Q_w(t) = Q_m \sin\left(\frac{\pi t}{T_s}\right) \quad \text{for} \quad 0 \le t \le T_s \tag{11}$$

where t = analytical time associated with the fitted η_o; T_s = surge duration; Q_m = maximum wave overtopping rate of the computed Q_o. For storm 20, η_m = 1.85 m, T_s = 13.4 h, and Q_m = 1380 m^3/s.

6.2 Analytical Solution Including Wave Overtopping

The constant velocity U_c in Eq. (4) is not estimated using Eq. (5) to obtain a simple solution. Instead, use is made of the expression of U_c for $Q_w = 0$ where $U_c = (8/3\pi)U_m$ with U_m given in Eq. (8). Using Eqs. (9) and (10), U_c is given by

$$U_c = \frac{2g\beta T_s A_C}{\pi K A_B} \tag{12}$$

where β give in Eq. (9) depends on K^* *and* η_m^* in Eq. (10). Combining Eqs. (1) and (4) and using Eq. (12), the bay stillwater elevation $\eta_B(t)$ is expressed as

$$A_B \frac{d\eta_B}{dt} = \frac{\pi A_B}{\beta T_s}\left[\eta_o(t) - \eta_B(t)\right] + Q_w(t) \tag{13}$$

The positive Q_w increases η_B but the increased η_B reduces the stillwater elevation difference and water flux from the ocean to the bay.

Substitution of Eqs. (6) and (11) into Eq. (13) yields the equation of $\eta_B(t)$ in the same form as in Eq. (7) with the peak stillwater elevation η_p given by

$$\eta_p = \frac{\eta_m}{\sqrt{1+\beta^2}}\left(1+\frac{\beta Q_m^*}{\pi}\right) \quad ; \quad Q_m^* = \frac{T_s Q_m}{\eta_m A_B} \tag{14}$$

where the dimensionless wave overtopping rate Q_m^* is the ratio between Q_m and the rate ($\eta_m A_B / T_s$) associated with the water volume increase rate in the bay caused by the stillwater level $\eta_o(t)$ in the ocean. Eq. (14) implies that the ratio (η_p / η_m) depends on the three dimensionless parameters K^*, η_m^* and Q_m^*. The ratio (η_p / η_m) increases with the increase of Q_m^* as indicated in Figure 6.2. For small β, the ratio (η_p / η_m) can exceed unity for Q_m^* = 0.5 and 1.0. The ratio then decreases with the increase of β monotonically.

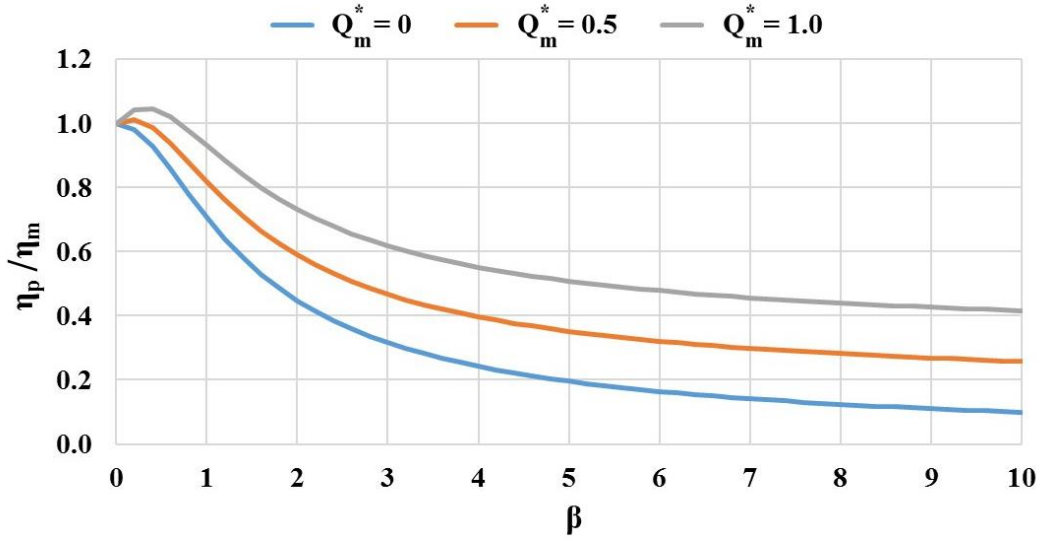

Figure 6.2 Ratio (η_p / η_m) of the peak stillwater elevations in the bay and ocean as a function of β for the dimensionless wave overtopping rate Q_m^* = 0, 0.5, and 1.0

The velocity $U(t)$ in the inlet channel can be estimated using Eq. (15) derived from Eq. (2) for the given analytical expressions of $\eta_o(t)$ and $\eta_B(t)$

$$U(t) = \left\{\frac{2g\left[\eta_o(t)-\eta_B(t)\right]}{K}\right\}^{1/2} \quad \text{for } \eta_o(t) > \eta_B(t) \tag{15}$$

$$U(t) = -\left\{\frac{2g\left[\eta_B(t)-\eta_o(t)\right]}{K}\right\}^{1/2} \quad \text{for } \eta_B(t) > \eta_o(t)$$

6.3 Effect of Wave Overtopping on Bay Peak Stillwater Elevation

Table 6.1 compares the measured and analytical η_p at tide gauges I, R, and D with the calibrated K^* for storm 20 (Hurricane Sandy) with η_m = 1.85 m, T_s = 13.4 h, and η_m^* = 0.81. The value of β at each gauge is calculated using Eq. (9). The computed Q_m = 1380 m^3/s for Hurricane Sandy yields Q_m^* = 0.48 in Eq. (14). The analytical η_p for Q_m^* = 0 in Eq. (14) corresponds to the analytical solution with no wave overtopping. The agreement between the measured and analytical η_p is better for Q_m^* = 0.48 (Q_m^* =0) at gauges I and D (gauge R). The wave overtopping rate Q_m = 1380 m^3/s increases the analytical η_p by about 0.2 m (20%) at Gauge D in Rehoboth Bay and about 0.1 m (10%) at gauges I and R in Indian River Bay. Rehoboth Bay is affected more by wave overtopping because of the larger calibrated K^* and reduced penetration of storm surge through Indian River Inlet from the ocean. The increase of η_p due to wave overtopping is much smaller than (V_o/A_B) = 1.3 m because the

Table 6.1 Measured and analytical peak stillwater elevations η_p at tide gauges I, R, and D for Hurricane Sandy with η_m = 1.85 m, T_s = 13.4 h, and Q_m^* = 0.48

Tide Gauge	K^*	β	Measured η_p (m)	Analytical η_p (m)	
				$Q_m^* = 0$	$Q_m^* = 0.48$
I	1.5	0.54	1.75	1.63	1.76
R	1.3	0.48	1.66	1.67	1.79
D	5.1	1.28	1.34	1.14	1.36

increased $\eta_B(t)$ in the bay reduces the stillwater elevation difference between the ocean and bay, resulting in the reduced water flux in the inlet channel from the ocean to the bay.

Chapter 7

HYPOTHETICAL STORM SANDYPLUS (SANDY + 0.4m)

Computation is also made for a hypothetical storm called SandyPlus. The still water elevation η_o for Hurricane Sandy is increased by 0.4 m for the entire 72-h duration as shown in Figure 7.1.

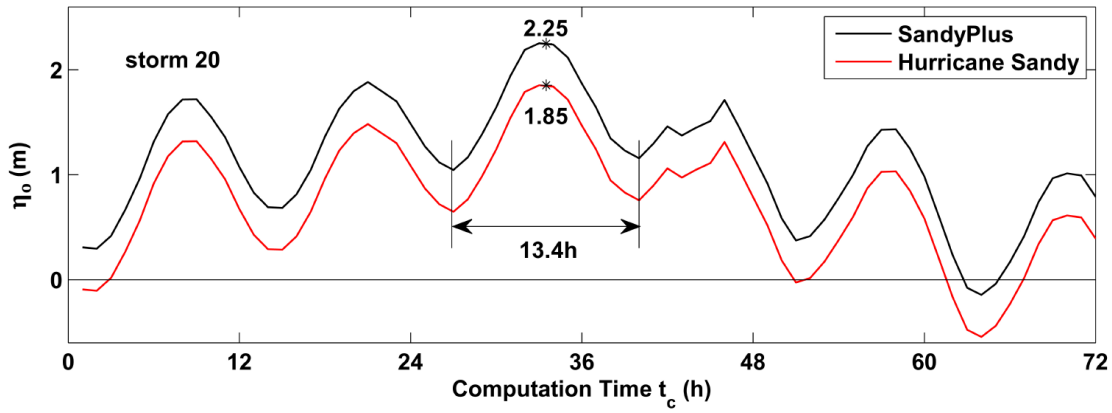

Figure 7.1 The still water elevation η_o for SandyPlus with 0.4 m increase of the still water elevation η_o of Hurricane Sandy.

7.1 Hypothetical Storm SandyPlus

The surge duration T_s = 13.4 h between the two low water levels remains the same. The offshore wave conditions are kept the same. The peak stillwater elevation η_m for SandyPlus is η_m = 2.25 m, corresponding to that of the 500-yr storm in Table 4.1. The stillwater elevation in the bay is assumed to be the same as η_o for the CSHORE computation of the barrier beach profile evolution and wave overtopping for

L1 – L14. During CSHORE computation for SandyPlus, the barrier beach was not submerged and the computed results are plotted and tabulated in the same way as in Chapter 5.

7.2 Computed Beach Profile Evolutions

The computed beach profile evolution along each of L1 – L14 for SandyPlus is examined by plotting the cross-shore variations of $z_b(x,t_c)$ at t_c = 0, 24, 48, and 72 h in Figures 7.2 – 7.4. The initial bottom elevation z_b (t_c = 0) for SandyPlus is the same as that for Hurricane Sandy. The computed profile changes for SandyPlus occur mostly during the day of the storm peak during t_c = 24 – 48 h. Comparing with the computed beach profile for Hurricane Sandy, the beach profile change for SandyPlus is more pronounced as expected.

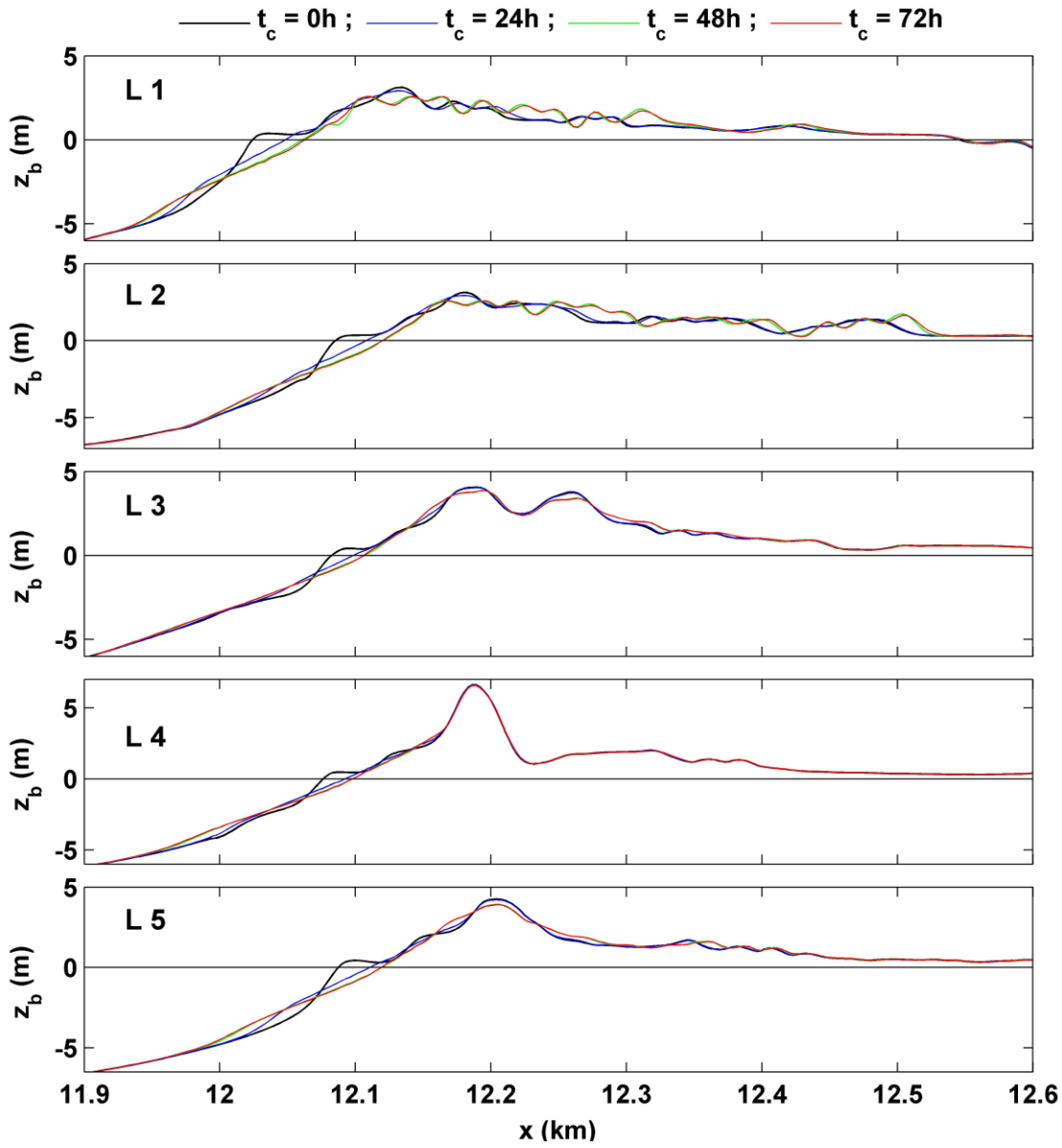

Figure 7.2 Initial (t_c = 0) and computed beach profiles at computation time t_c = 24, 48, and 72h along cross-shore lines L1, L2, L3, L4 and L5 for SandyPlus

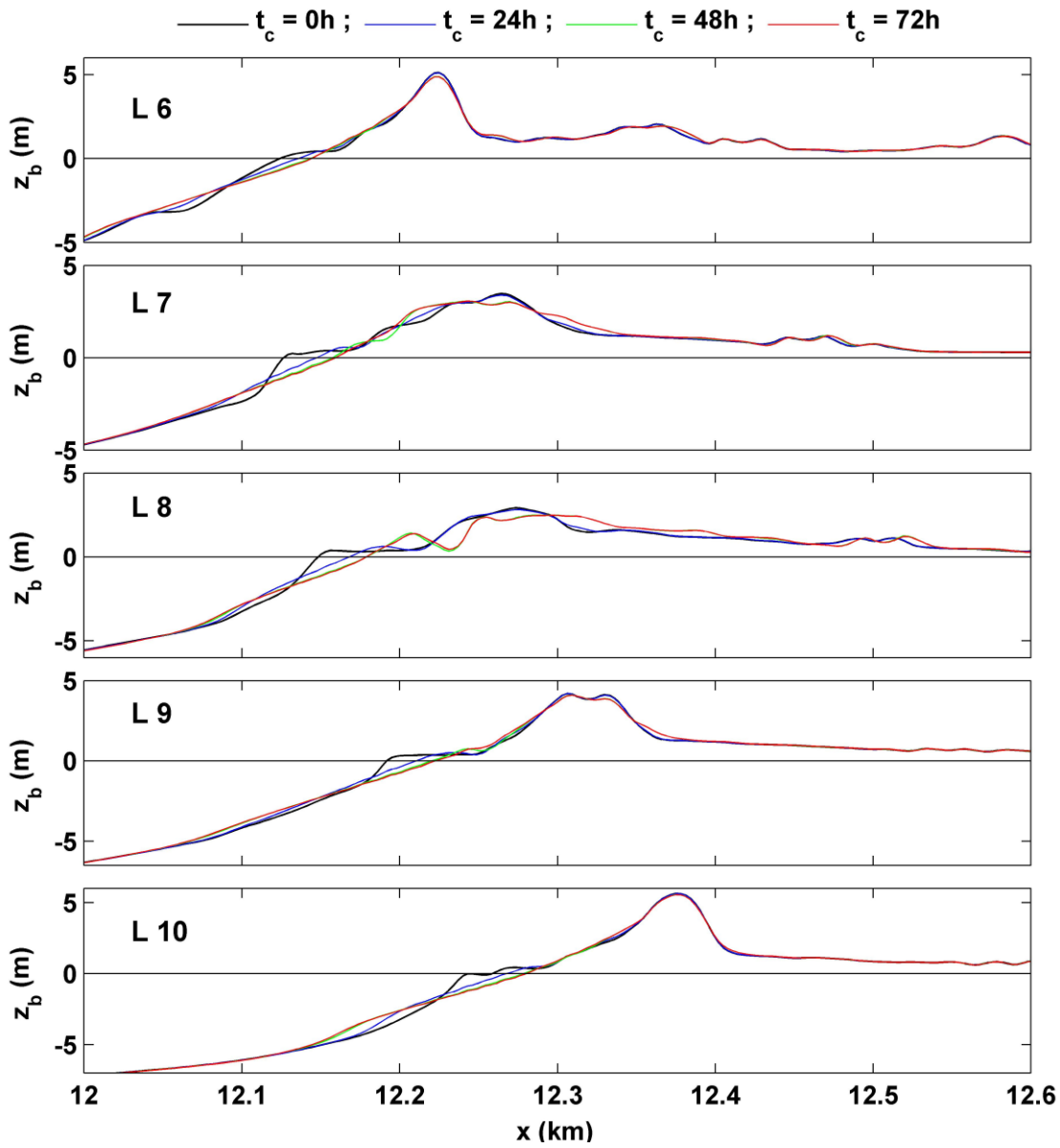

Figure 7.3 Initial (t_c = 0) and computed beach profiles at computation time t_c = 24, 48, and 72h along cross-shore lines L6, L7, L8, L9, and L10 for SandyPlus

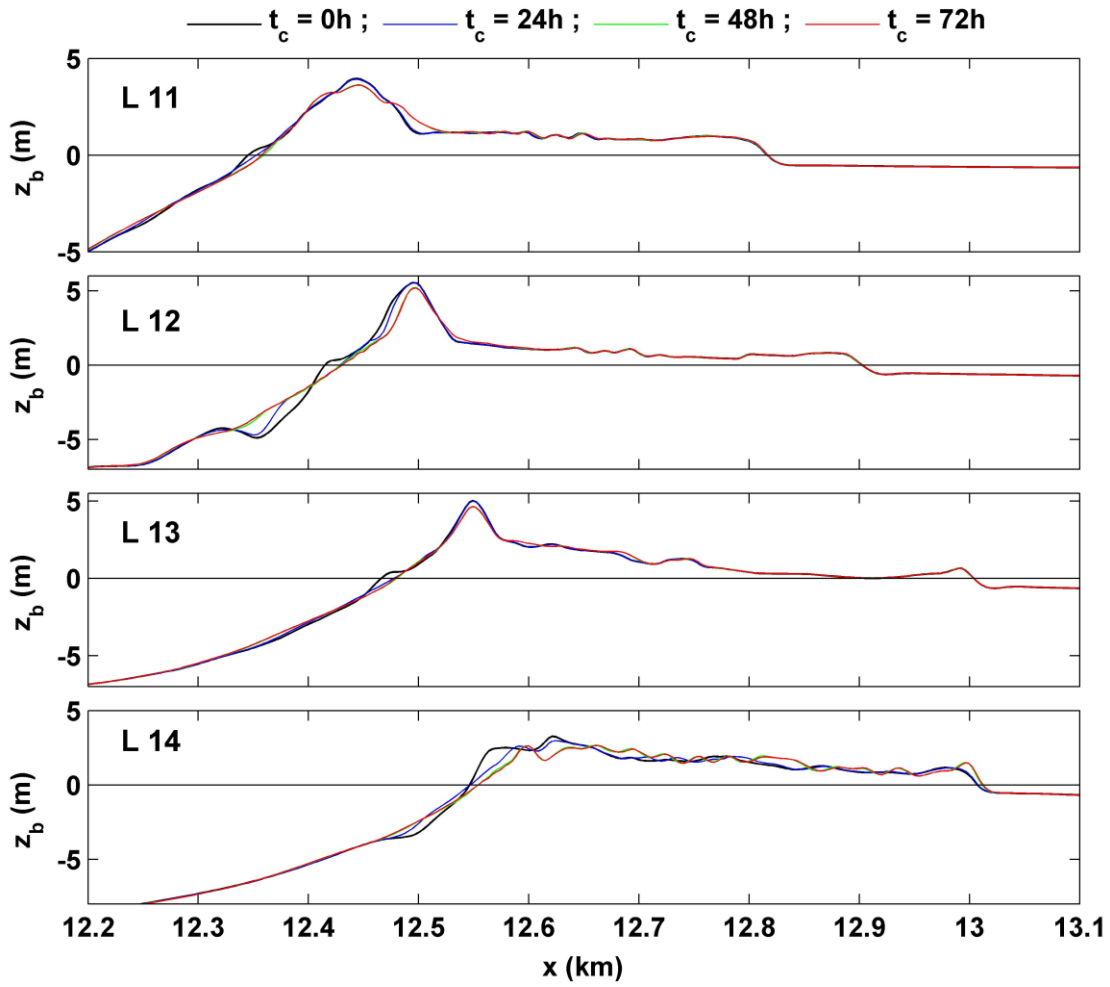

Figure 7.4 Initial (t_c = 0) and computed beach profiles at computation time t_c = 24, 48, and 72h along cross-shore lines L11, L12, L13, and L14 for SandyPlus

7.3 Cross-shore and Longshore Sand Transport

Figures 7.5 – 7.11 show the initial ($t_c = 0$) and final (t_c = 72 h) profiles along L1 – L14 for SandyPlus. The computed net cross-shore transport is slightly positive in the offshore zone of dominant by positive bed load transport and becomes negative in the zone dominated by suspended sand transported offshore by return (undertow) current induced by breaking waves. The differences of bed load volume v_{bx}, suspended load volume v_{sx}, and net volume v_x between SandyPlus and Hurricane Sandy are relatively small.

The longshore bed load and suspended load transport for SandyPlus are positive (northward) under the incident waves from the southeast as for Hurricane Sandy. The computed longshore sand transport takes place predominantly seaward of the dune crest and the volume v_y is much larger than the cross-shore transport volume v_x on the beach seaward of the dune crest. The longshore suspended load volume v_{sy} and net volume v_y for SandyPlus are larger than those of Hurricane Sandy.

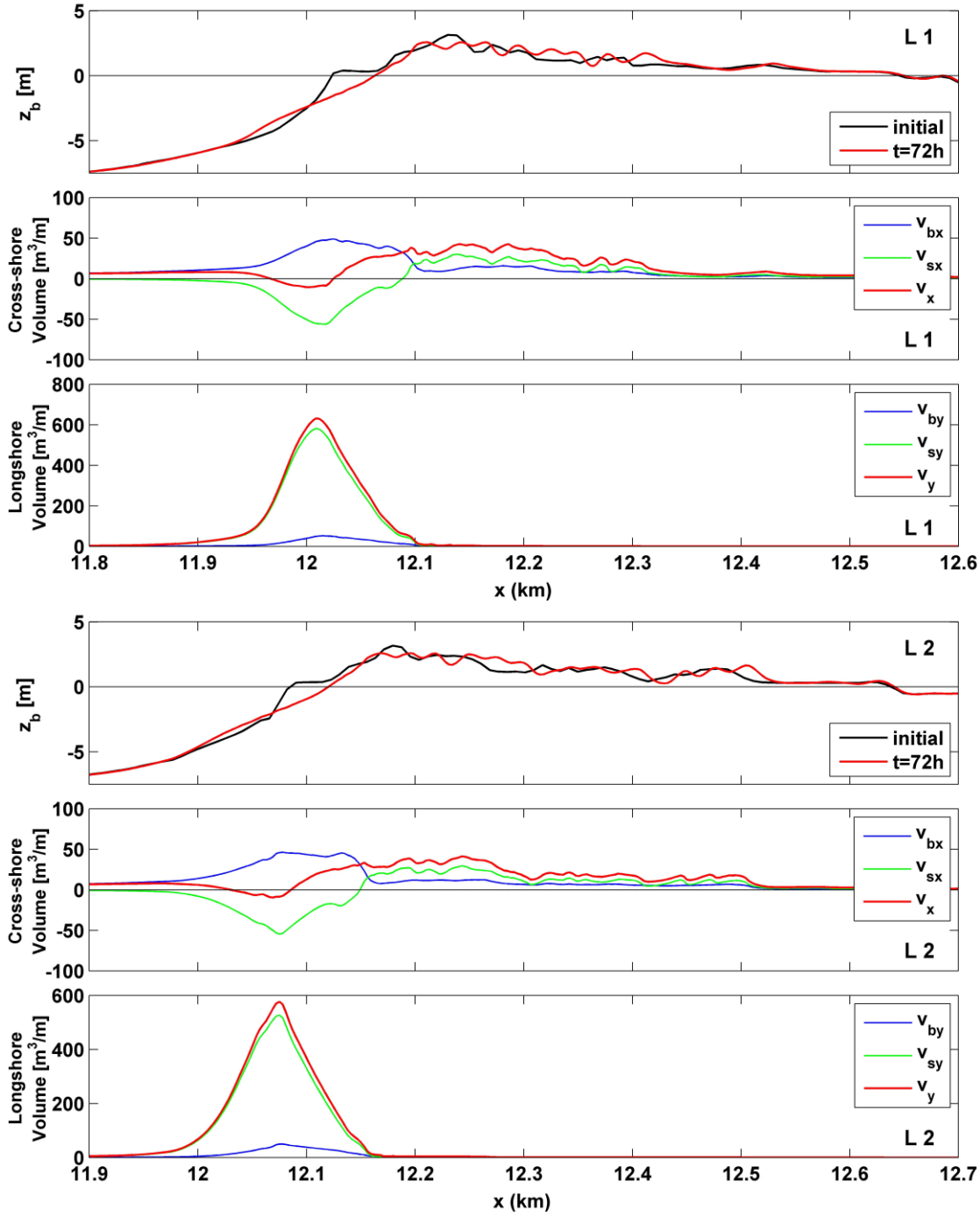

Figure 7.5 Initial and final profiles z_b, cumulative cross-shore sand transport volumes v_{bx}, v_{sx}, and v_x per unit width and cumulative longshore sand transport volumes v_{by}, v_{sy}, and v_y per unit width for cross-shore lines L1 and L2 in the case of SandyPlus

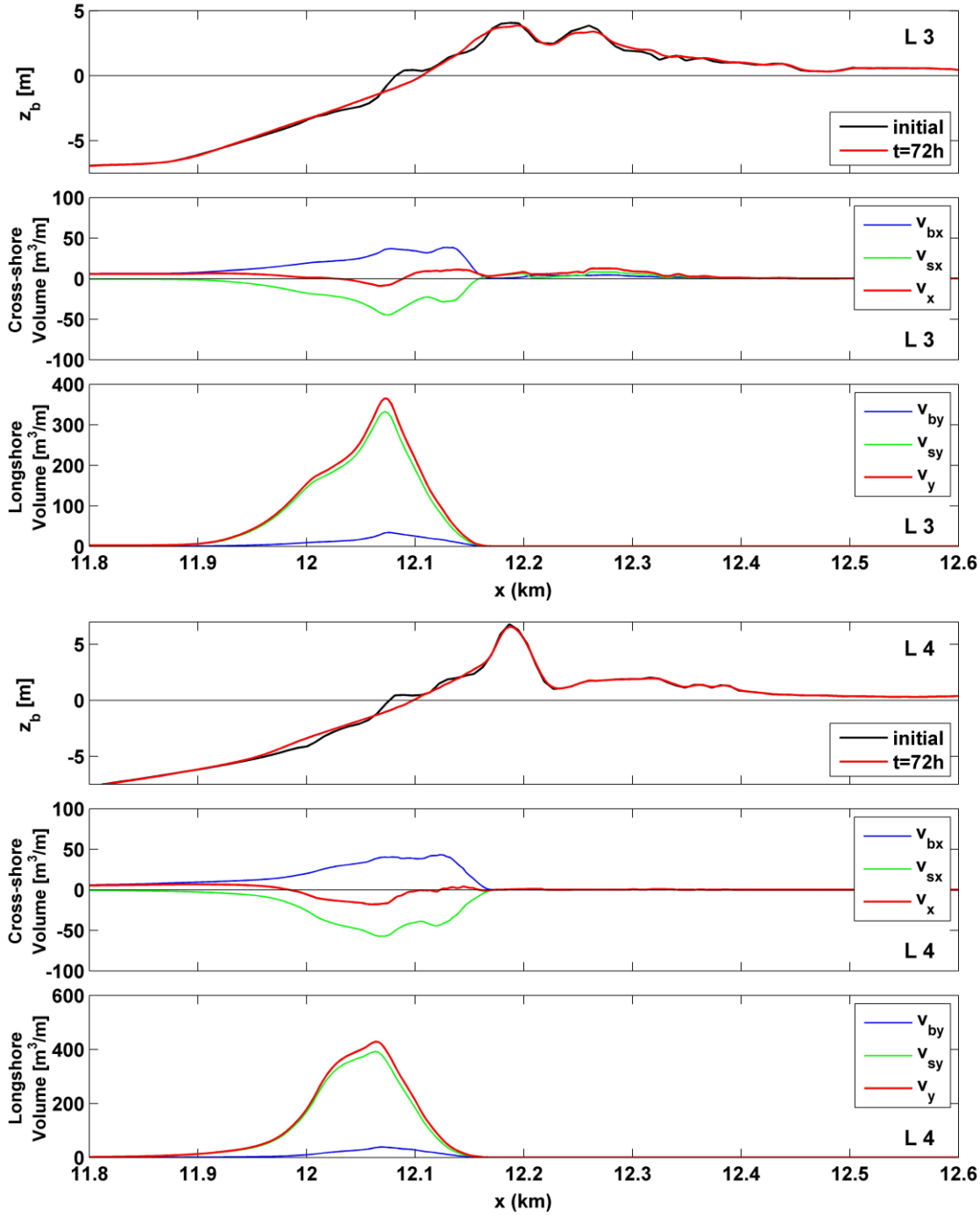

Figure 7.6 Initial and final profiles z_b, cumulative cross-shore sand transport volumes v_{bx}, v_{sx}, and v_x per unit width and cumulative longshore sand transport volumes v_{by}, v_{sy}, and v_y per unit width for cross-shore lines L3 and L4 in the case of SandyPlus

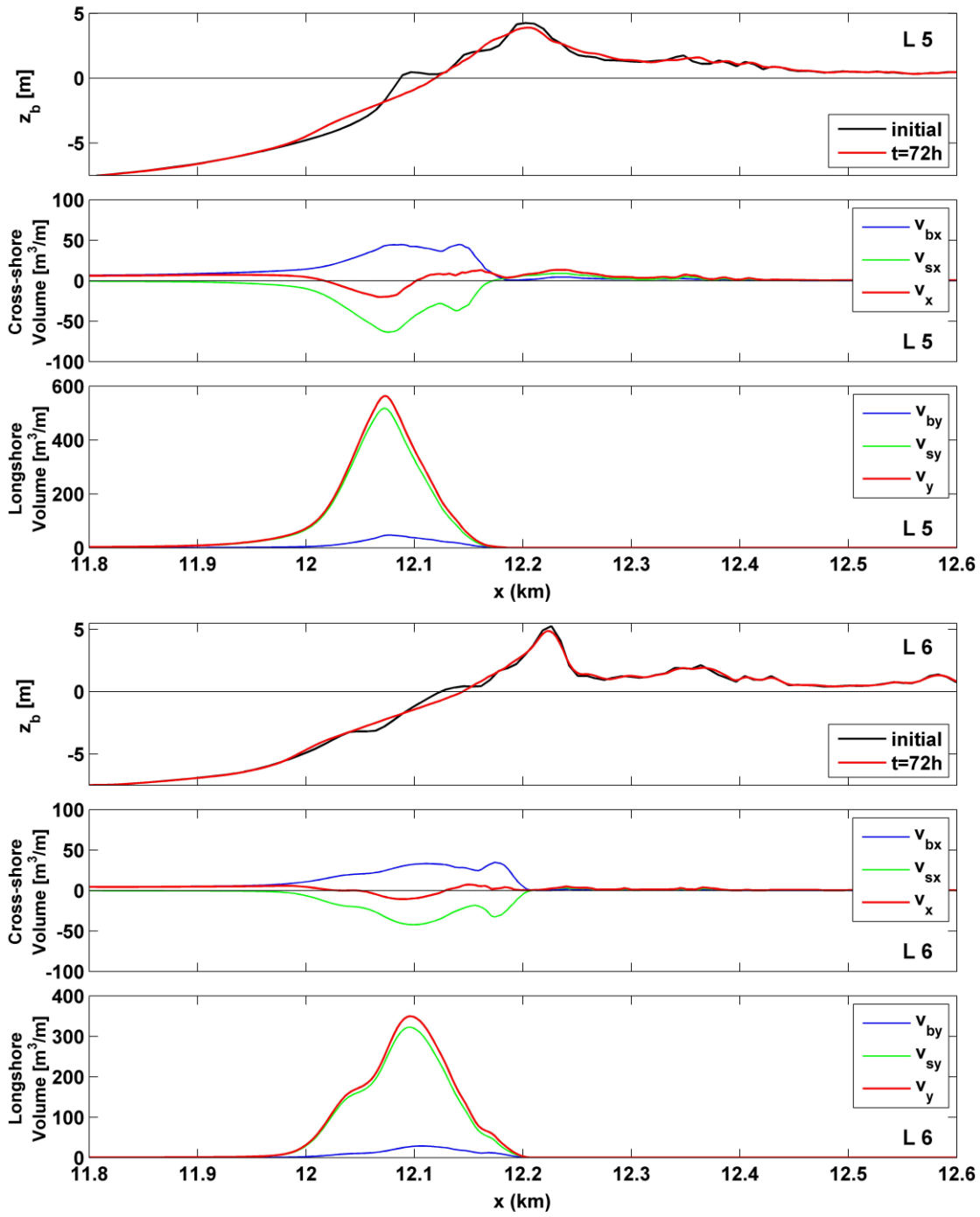

Figure 7.7 Initial and final profiles z_b, cumulative cross-shore sand transport volumes v_{bx}, v_{sx}, and v_x per unit width and cumulative longshore sand transport volumes v_{by}, v_{sy}, and v_y per unit width for cross-shore lines L5 and L6 in the case of SandyPlus

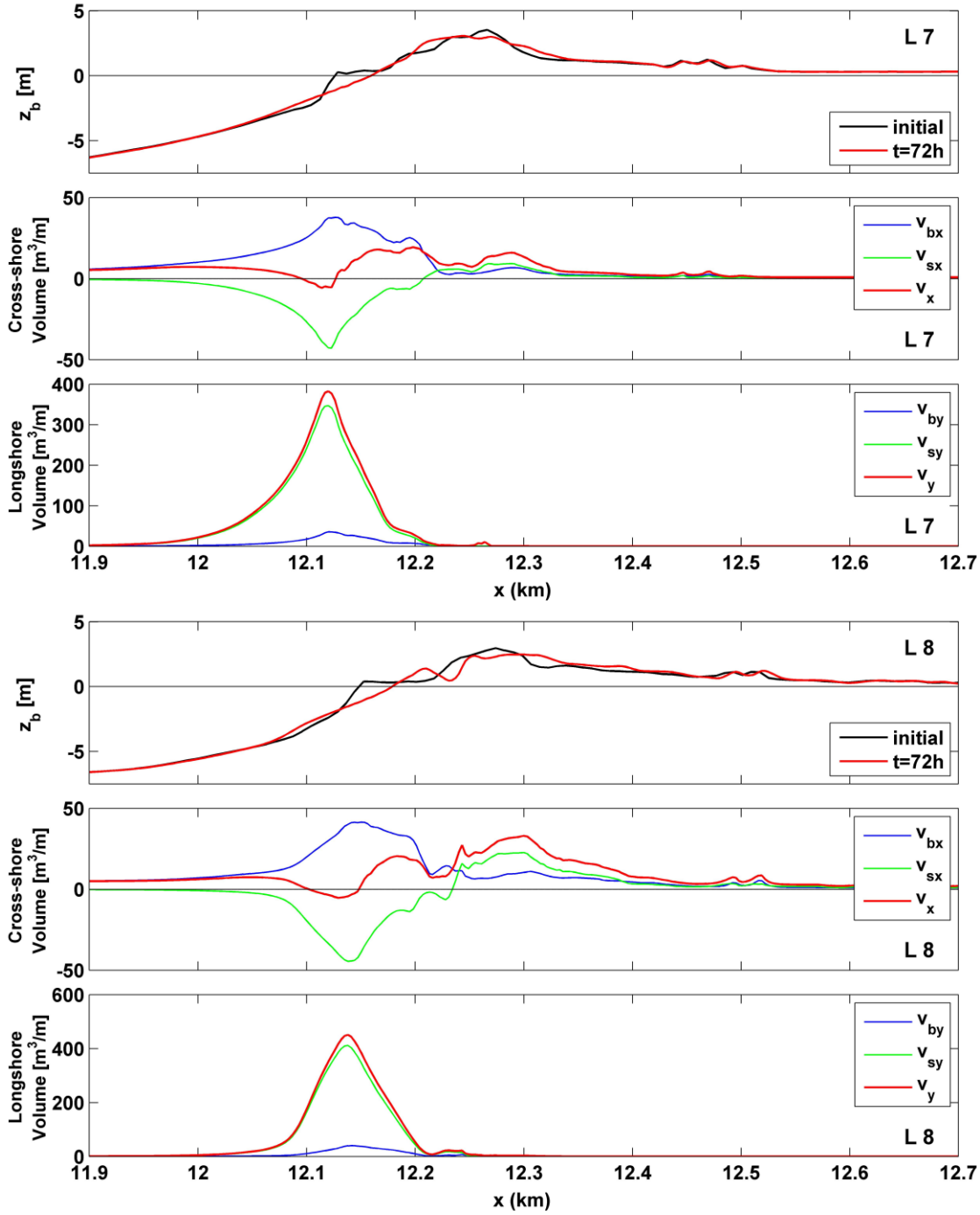

Figure 7.8 Initial and final profiles z_b, cumulative cross-shore sand transport volumes v_{bx}, v_{sx}, and v_x per unit width and cumulative longshore sand transport volumes v_{by}, v_{sy}, and v_y per unit width for cross-shore lines L7 and L8 in the case of SandyPlus

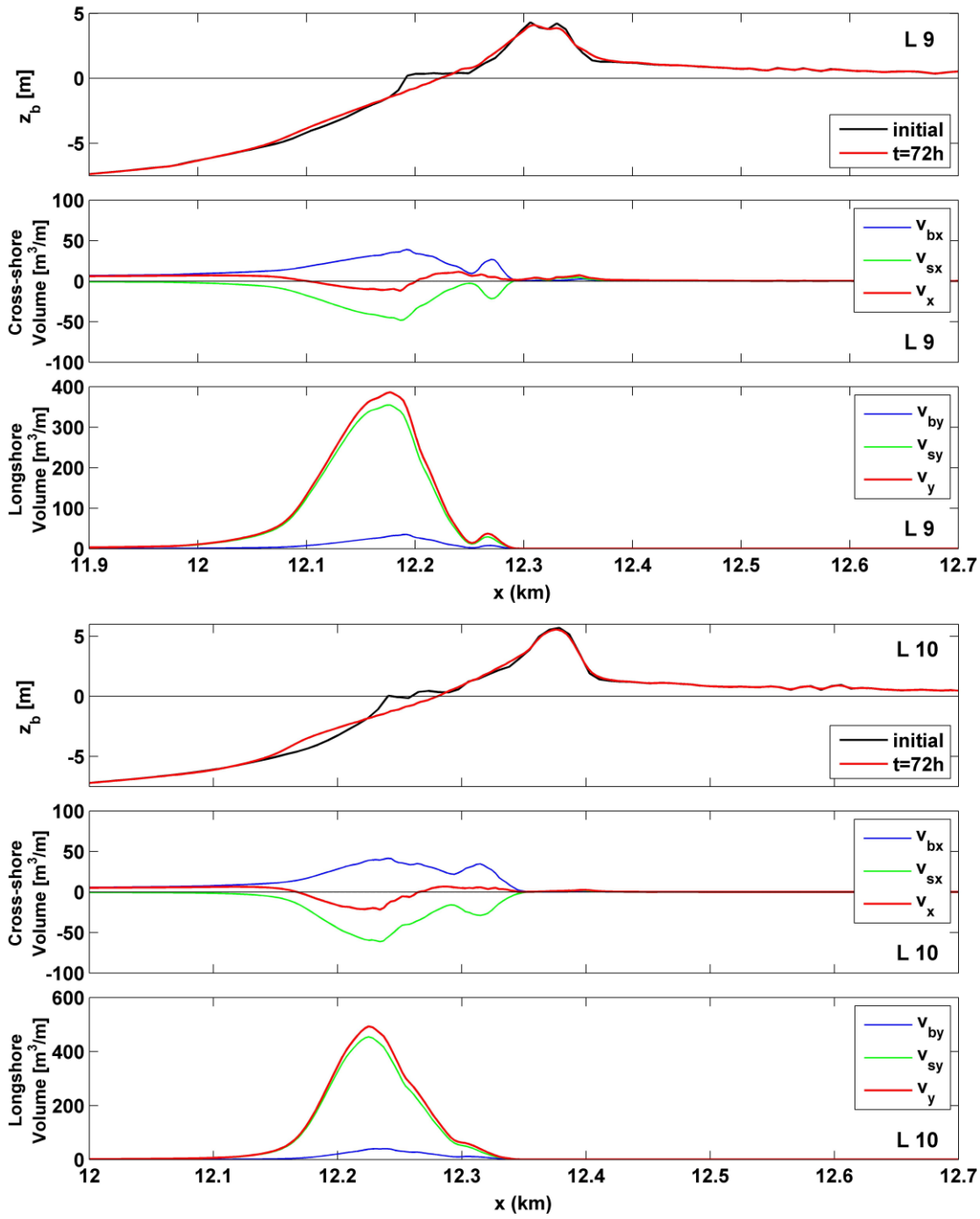

Figure 7.9 Initial and final profiles z_b, cumulative cross-shore sand transport volumes v_{bx}, v_{sx}, and v_x per unit width and cumulative longshore sand transport volumes v_{by}, v_{sy}, and v_y per unit width for cross-shore lines L9 and L10 in the case of SandyPlus

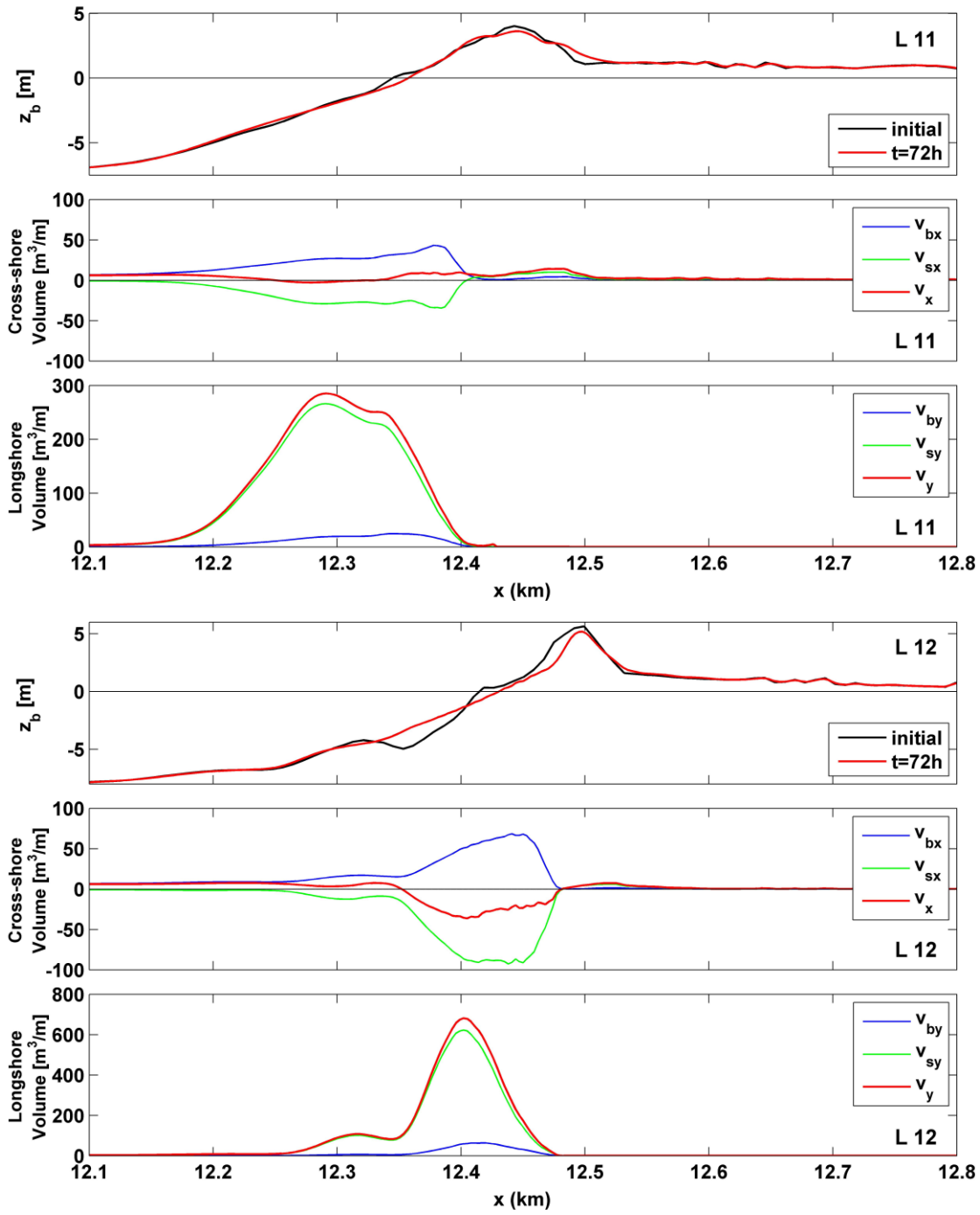

Figure 7.10 Initial and final profiles z_b, cumulative cross-shore sand transport volumes v_{bx}, v_{sx}, and v_x per unit width and cumulative longshore sand transport volumes v_{by}, v_{sy}, and v_y per unit width for cross-shore lines L11 and L12 in the case of SandyPlus

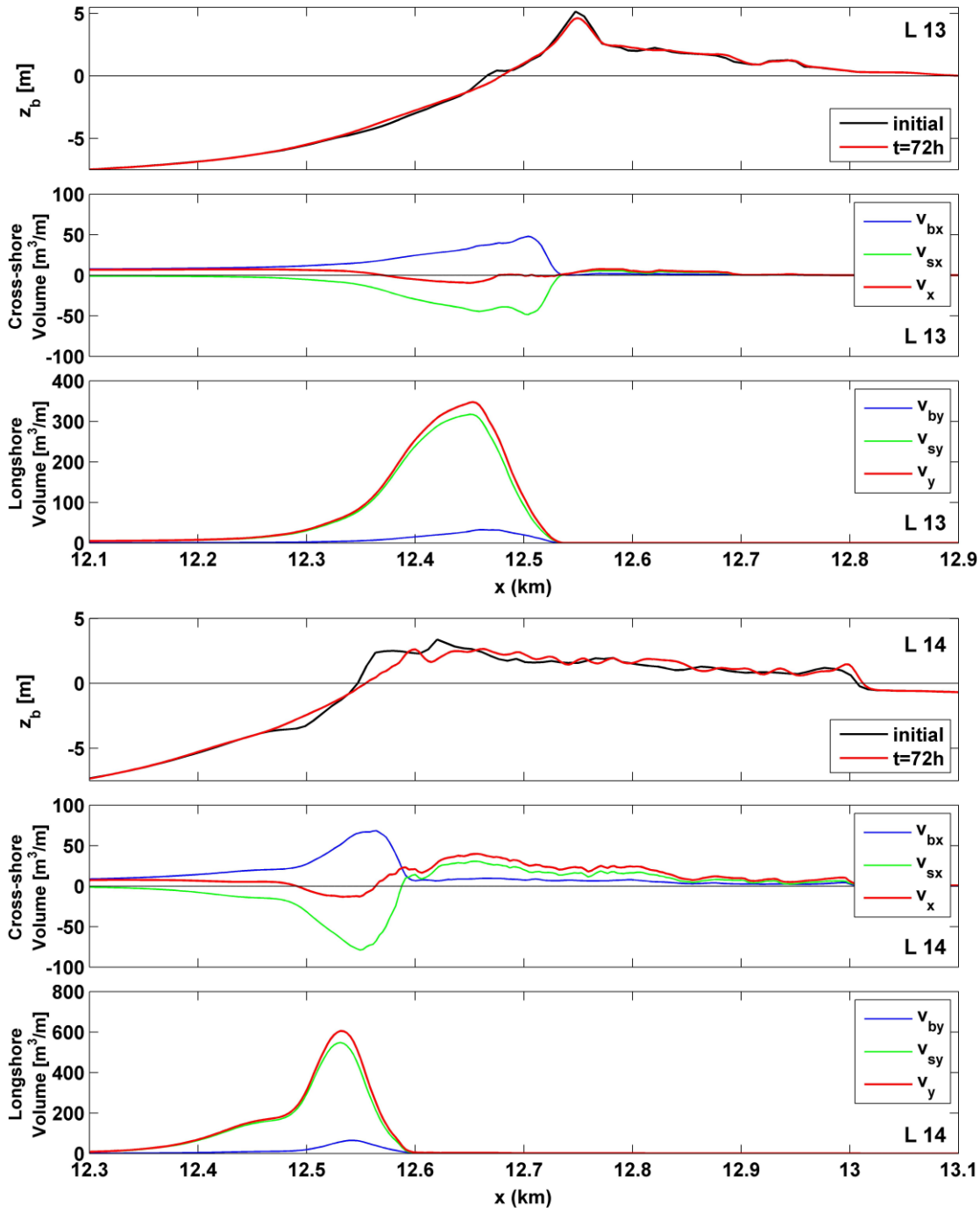

Figure 7.11 Initial and final profiles z_b, cumulative cross-shore sand transport volumes v_{bx}, v_{sx}, and v_x per unit width and cumulative longshore sand transport volumes v_{by}, v_{sy}, and v_y per unit width for cross-shore lines L13 and L14 in the case of SandyPlus

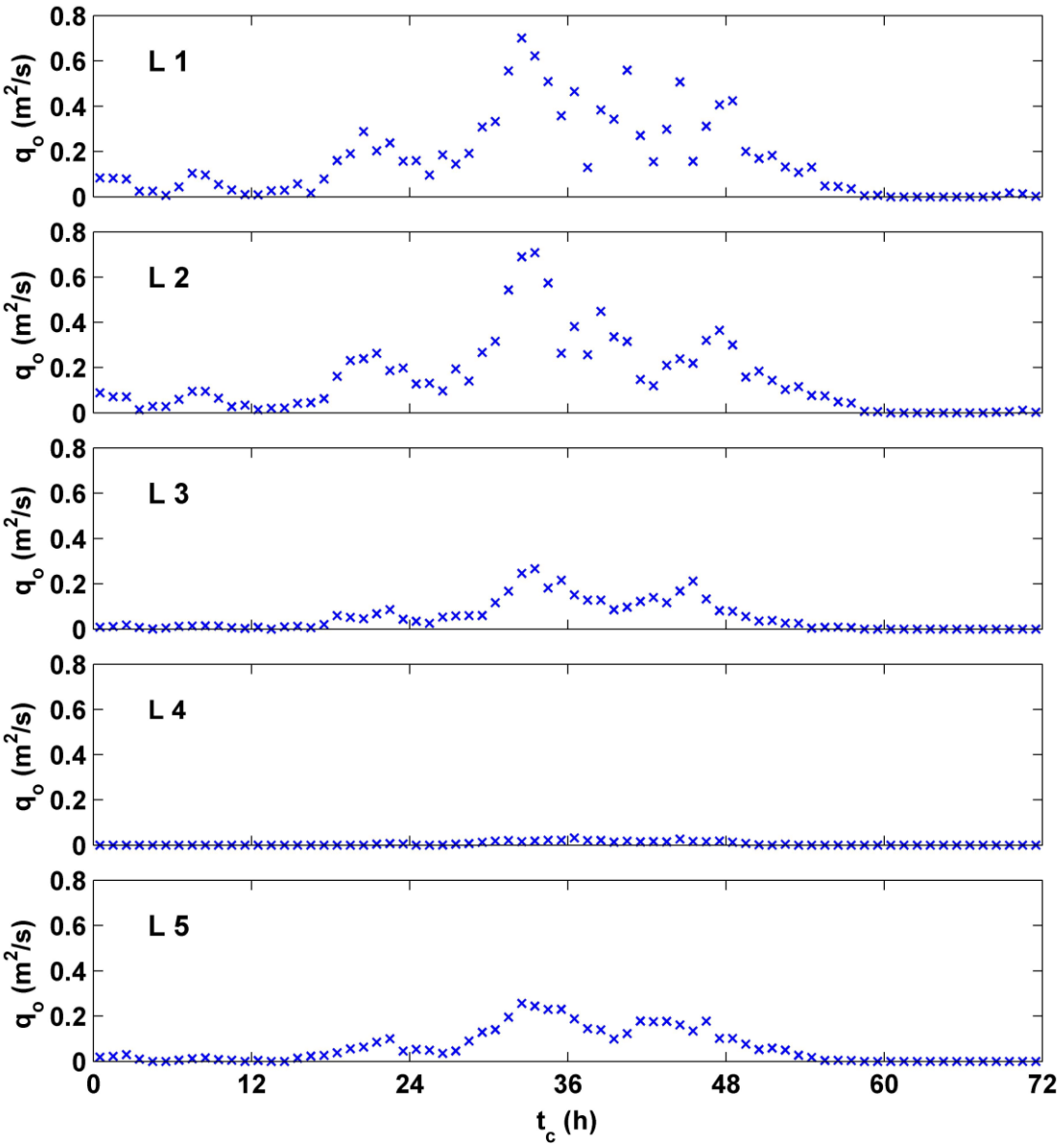

Figure 7.12 Computed temporal variation of hourly wave overtopping rate q_o per unit width along cross-shore lines L1, L2, L3, L4, and L5 for SandyPlus

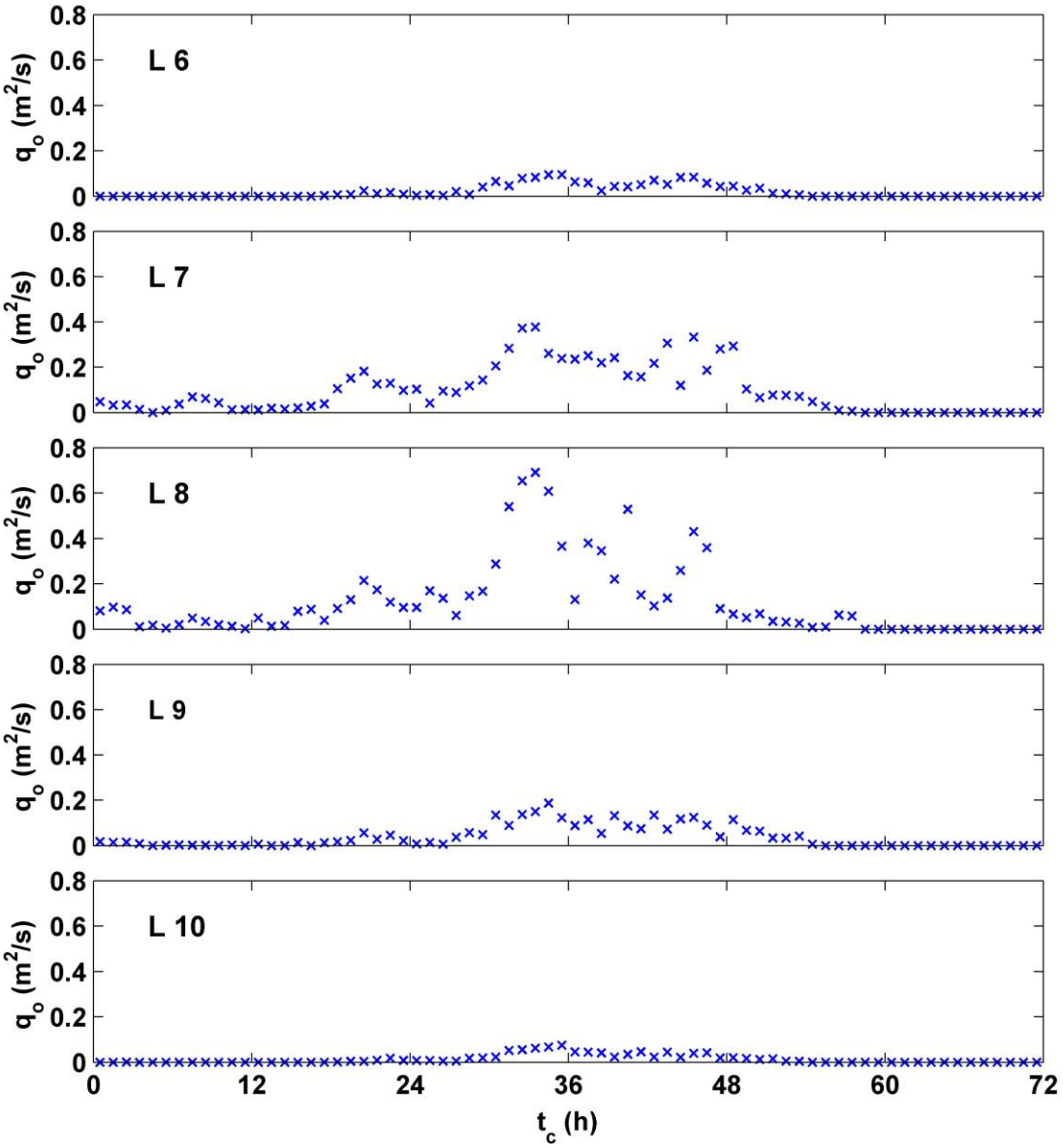

Figure 7.13 Computed temporal variation of hourly wave overtopping rate q_o per unit width along cross-shore lines L6, L7, L8, L9, and L10 for SandyPlus

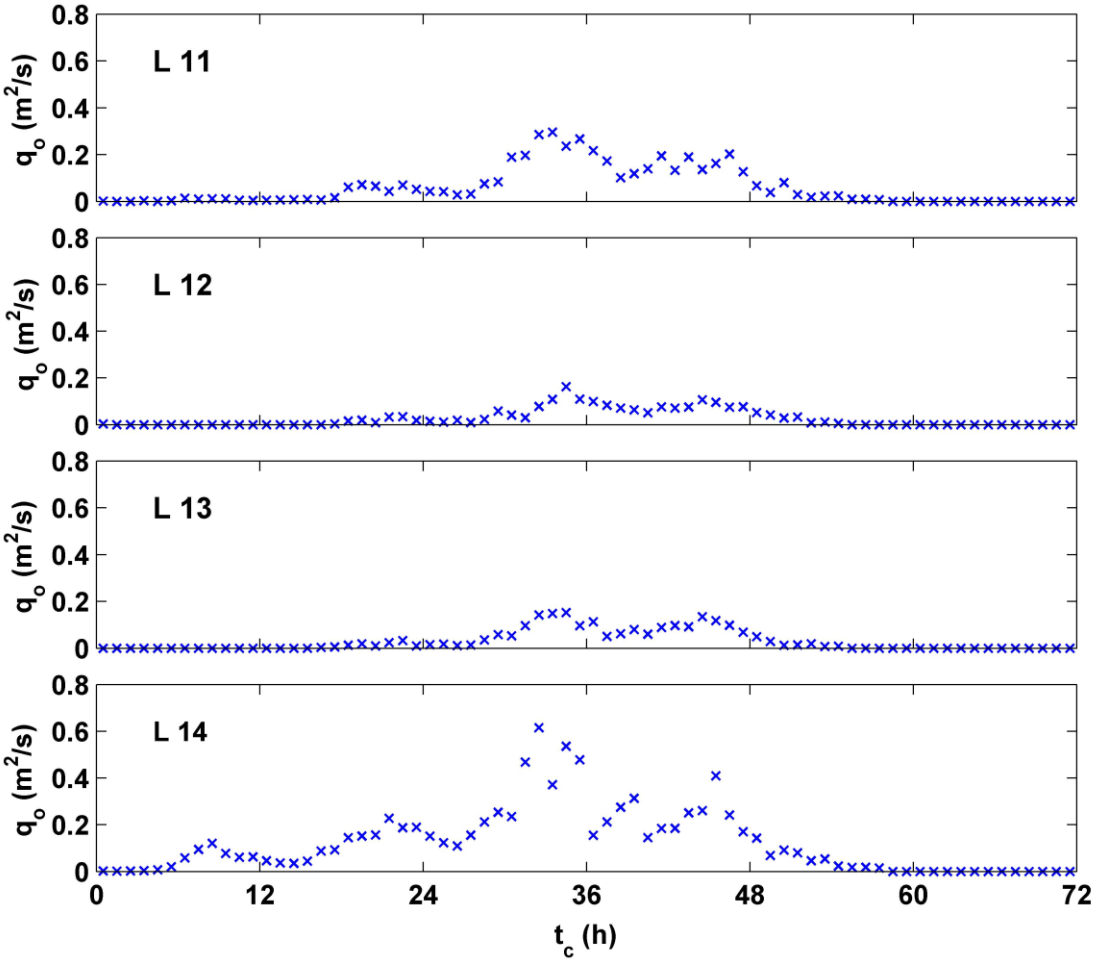

Figure 7.14 Computed temporal variation of hourly wave overtopping rate q_o per unit width along cross-shore lines L11, L12, L13, and L14 for SandyPlus

7.4 Computed Wave Overtopping Rates

Figures 7.12 – 7.14 show the hourly variation of the wave overtopping rate q_o for L1 – L14 for SandyPlus. The peak hourly wave overtopping rate q_o is increased up to 0.8 m^2/s, larger than 0.6 m^2/s for Hurricane Sandy. For L4, L6 and L10, wave

overtopping and overwash remain small. The computed wave overtopping occurs mostly during t_c = 24 – 48 h on the day of the storm peak as expected.

7.5 Dune Crest Lowering and Cross-sectional Area

Table 7.1 lists the dune crest elevations z_c and cross-sectional area A_d of the initial and final beach profile, as well as the wave overtopping volume v_o per unit alongshore length for L1 – L14 for SandyPlus. The initial dune crest elevations z_c are the same, while the initial cross-sectional area A_d is smaller for SandyPlus because of

Table 7.1 Alongshore variation of dune crest elevation z_c (m), dune cross-sectional area A_d (m^2), and wave overtopping volume v_o (m^3/m) per unit width for SandyPlus

Line	Initial Profile		Final Profile		Overtopping
	$\mathbf{z_c}$ **(m)**	$\mathbf{A_d}$ **(m^2)**	$\mathbf{z_c}$ **(m)**	$\mathbf{A_d}$ **(m^2)**	$\mathbf{v_o}$ **(m^2)**
1	3.12	13.3	2.59	2.4	42353
2	3.13	9.0	2.59	2.2	39052
3	4.06	38.9	3.86	52.1	13888
4	6.62	80.2	6.56	83.6	1461
5	4.24	37.3	3.90	47.8	16108
6	5.11	47.7	4.87	39.5	5130
7	3.47	31.3	3.07	21.0	25638
8	2.92	10.0	2.48	4.3	32465
9	4.19	25.1	4.10	30.8	9946
10	5.63	71.8	5.55	76.3	3371
11	3.96	42.0	3.62	41.1	16003
12	5.55	65.6	5.17	42.2	6915
13	5.01	40.0	4.63	32.0	7762
14	3.26	15.5	2.62	1.9	32315

the higher peak stillwater elevation η_m for the same initial beach profile for L1 – L14. The computed final dune crest elevations z_c for L1 – L14 are higher than 2.48 m and above the peak stillwater elevation η_m = 2.25 m. The computed final cross-sectional area A_d becomes much smaller for the lines with large wave overtopping. The computed overtopping volume v_o is larger in Table 7.1. The differences between the initial and final values of z_c and A_d increase with the increase of v_o as shown in Figure 7.15. The total wave overtopping volume $V_o = 130 \times 10^6$ m^3 for SandyPlus is 34% larger than that for Hurricane Sandy.

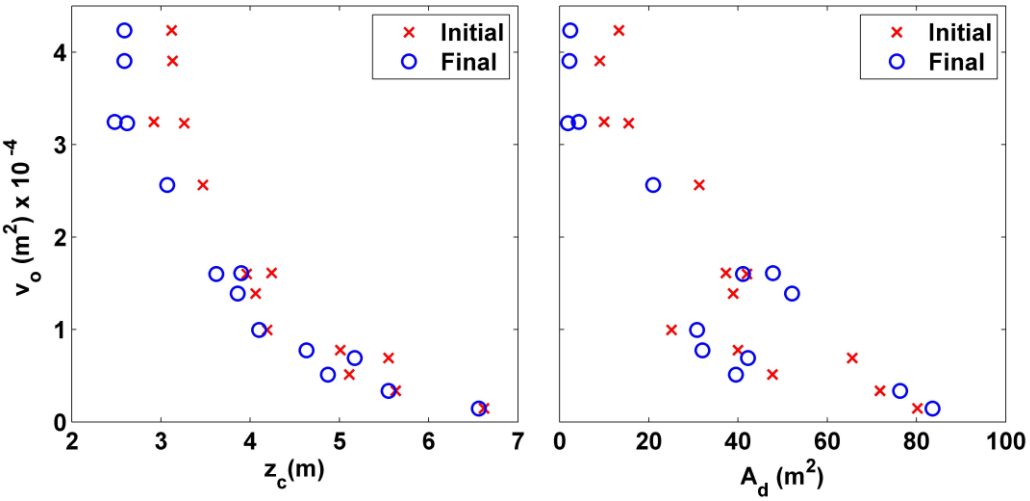

Figure 7.15 Wave overtopping volume v_o as a function of initial and final values of dune crest elevation z_c and dune cross-sectional area A_d for SandyPlus

7.6 Bay Peak Stillwater Elevations

Figure 7.16 shows the assumed and fitted stillwater elevation η_o and the computed and fitted rate Q_o for SandyPlus. The maximum wave overtopping rate Q_m

= 2230 m^3/s is 62% larger because of the 0.4-m increase of the stillwater level in the ocean.

The peak stillwater elevation η_p in the bay is calculated using Eq. (14) with Eqs. (9) and (10) where η_m = 2.25 m T_s = 13.4 h, η_m^* = 0.99, and Q_m^* = 0.64 for SandyPlus. Table 7.2 lists the analytical η_p at gauges I, R, and D for Q_m^* = 0 and 0.64. The value of β is larger in Table 7.2 than Table 6.1 because of the increase of η_m^*. The increment of η_p due to wave overtopping is the difference between the values of η_p for Q_m^* =0 and 0.64. The increment of η_p is larger in Table 7.2 than Table 6.1 because of the increased wave overtopping. The peak stillwater elevations η_p at gauges I and R in Indian River Bay are almost the same as η_m = 2.25 m in the ocean, whereas the elevation η_p at gauge D in Rehoboth Bay is about 0.6 m lower than η_m = 2.25 m if the calibrated K^* = 5.1 is reliable for SandyPlus. It is necessary to elucidate the physical reason of K^* = 5.1 in comparison to K^* = 1.3 – 1.5 in Indian River Bay.

Table 7.2 Analytical Peak Stillwater Elevation η_p at Tide Gauges I, R, and D for SandyPlus with η_m = 2.25 m, T_s = 13.4 h and Q_m^* = 0.64

Tide Gauge	**K^***	**β**	**Analytical η_p (m)**		**η_p increment (m)**
			$Q_m^* = 0$	**$Q_m^* = 0.64$**	
I	1.5	0.63	1.91	2.15	0.24
R	1.3	0.56	1.97	2.19	0.22
D	5.1	1.44	1.29	1.66	0.37

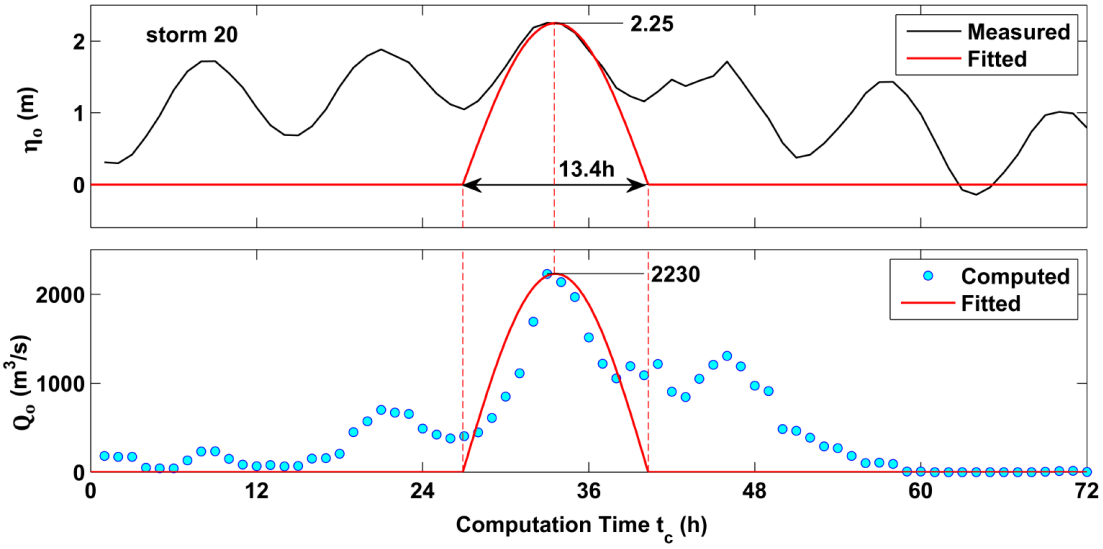

Figure 7.16 Measured and fitted ocean stillwater elevation η_o and computed and fitted wave overtopping rate Q_o over barrier beach of 7.2-km alongshore length for SandyPlus

Chapter 8

CONCLUSIONS

A simple analytical model for a small bay with a tidal inlet channel is developed to predict the peak stillwater elevation η_p in the bay caused by a storm. The storm tide in the ocean is represented by the peak stillwater elevation η_m and surge duration T_s. A simple analytical equation for the ratio (η_p/η_m) is derived as a function of the surge steepness parameter η_m^* related to η_m and T_s and the inlet and bay parameter K^* which is assumed constant for a specific location inside the bay. The model is applied to the Delaware Atlantic coast where Rehoboth Bay and Indian River Bay are connected to the Atlantic Ocean through the Indian River Inlet. The hourly stillwater elevation in the ocean is represented by the tide gauge data at Lewes with the record length of 94 years. Three tide gauges have been in operation in the combined bay since 2005. 27 storms identified during 2005 – 2015 are used to calibrate K^* for each of the bay gauges. The calibrated values of K^* for the two gauges in Indian River Bay are consistent with the value based on tidal hydraulics modeling. The agreement between the measured and analytical η_p is within errors of 10% for these two gauges. The calibrated K^* for one gauge in Rehoboth Bay is much larger and the agreement is within errors of 30%. Detailed numerical modeling or extension of the analytical model to two bays may explain the difference among the three gauge data. The analytical model with the calibrated K^* is used to estimate the statistical values of η_p corresponding to those of η_m at Lewes for the recurrence interval up to 500 years. The estimated values of η_p for the different recurrence intervals are

sensitive to the surge steepness parameter η_m^* and hence the surge duration T_s associated with the statistical η_m. A joint probability analysis of η_m and T_s at Lewes will be required for the more accurate prediction of η_p in the bay.

The most severe storm among the 27 storms during 2005 – 2015 is Hurricane Sandy in 2012. The barrier beach between the ocean and bay was overwashed during Hurricane Sandy. The cross-shore numerical model CSHORE is used to predict wave overtopping of the barrier beach during Hurricane Sandy where the offshore wave data and the merged bathymetry and topography data are available for Hurricane Sandy. CSHORE predicts the wave overtopping rate over the barrier beach whose profile is changed by cross-shore sand transport. The total overtopping water volume over the barrier beach of 7.2-km alongshore length is predicted to be of the order of 10^8 m^3. This water volume is equivalent to the stillwater elevation increase of 1.3 m over the entire bay surface area. The analytical model including wave overtopping predicts the peak stillwater elevation increase of 0.1 – 0.2 m in the bay because the increased bay water level reduces the water flux in the inlet channel from the ocean to the bay. The predicted wave overtopping volume per unit alongshore length and the degree of dune crest lowering are large at sections of low dune crests. However, the dunes on the wide barrier beach are durable and do not fail rapidly.

The analytical model is also applied for a hypothetical storm SandyPlus. The stillwater elevation η_o for Hurricane Sandy is increased by 0.4 m for the entire 72-hour duration. The same surge duration T_s and offshore wave conditions as Hurricane Sandy are used for SandyPlus. The bay stillwater elevation is assumed to be the same as the ocean stillwater elevation. The computed total wave overtopping volume for SandyPlus is 34% larger than that for Hurricane Sandy. The peak stillwater elevations

η_p in Indian River Bay are almost the same as η_m = 2.25 m in the ocean, except for gauge D in Rehoboth Bay with the predicted η_p being 0.6 m lower than η_m = 2.25 m. The analytical model coupled with the cross-shore numerical model CSHORE is useful in evaluating bay flooding risk during extreme storms in efficient manners. The utility of this coupled approach will need to be demonstrated at other field sties with tide gauge data in the bay and ocean.

REFERENCES

Cañizares, R., and Irish, J.L. (2008). "Simulation of storm-induced barrier island morphodynamics and flooding." Coastal Eng., 55, 1089-1101.

Dean, R.G., and Dalrymple, R.A. (2002). Coastal processes with engineering applications, Cambridge University Press, Cambridge, U.K.

ESRI [ArcGIS® software]. Environmental Systems Research Institute, Redlands, CA.

Federal Emergency Management Agency (FEMA) (2011). Coastal construction manual: Principles and practices of planning, siting, designing, constructing, and maintaining buildings in coastal areas. 4th edition, FEMA P-55.

Figlus, J., and Kobayashi, N. (2008). "Inverse estimation of sand transport rates on nourished Delaware beaches." J. Waterway, Port, Coastal, Ocean Eng., 134(4), 218-225.

Figlus, J., Kobayashi, N., Gralher, C., and Iranzo, V. (2011). "Wave overtopping and overwash of dunes." J. Waterway, Port, Coastal, Ocean Eng., 137(1), 26-33.

Irish, J.L., and Cañizares, R. (2009). "Storm-wave flow through tidal inlets and its influence on bay flooding." J. Waterway, Port, Coastal, Ocean Eng., 135(2), 52-60.

Johnson, B.D., Kobayashi, N., and Gravens, M.B. (2012). "Cross-shore numerical model CSHORE for waves, currents, sediment transport and beach profile evolution." Final Rep. No. ERDC/CHL TR-12-22, U.S. Army Corps of Engineers, Coastal and Hydraulics Laboratory, Vicksburg, MS.

Judge, E.K., Overton, M.F., and Fisher, J.S. (2003). "Vulnerability indicators for coastal dunes." J. Waterway, Port, Coastal, Ocean Eng., 129(6), 270-278.

Keshtpoor, M., Puleo, J.A., and Shi, F. (2014). "Downdrift beach erosion adjacent to the Indian River Inlet, Delaware, USA." Shore & Beach, 82(1), 31-41.

Keshtpoor, M., Puleo, J.A., Shi, F., and Ma, G. (2015). "3D numerical simulation of turbulence and sediment transport within a tidal inlet." Coastal Eng., 96, 13-26.

Kobayashi, N. (2016). "Coastal sediment transport modeling for engineering applications." J. Waterway, Port, Coastal, Ocean Eng., 10.1061/(ASCE)WW.1943-5460.0000347.03116001.

Kobayashi, N., and Jung, H. (2012). "Beach erosion and recovery." J. Waterway, Port, Coastal, Ocean Eng., 138(6), 473-483.

Kobayashi, N., Pietropaolo, J., and Melby, J.A. (2013). "Deformation of reef breakwaters and wave transmission." J. Waterway, Port, Coastal, Ocean Eng., 139(4), 336-340.

Larson, M., and Kraus, N.C. (1989). "SBEACH: Numerical model for simulating storm-induced beach change. Report 1: Empirical foundation and model development." Tech. Rep. CERC-89-9, Coastal Engineering Research Center, Vicksburg, MS.

Mei, C.C. (1989). The applied dynamics of ocean surface waves. World Scientific, Singapore.

Nadal-Caraballo, N.C., Melby, J.A., and Gonzalez, V.M. (2016) . "Statistical analysis of historical extreme water levels for the U.S. North Atlantic coast using Monte Carlo life-cycle simulation." J. Coastal Res., 32(1), 35-45.

NOAA (National Oceanic and Atmospheric Administration). (2015). "Center for Operational Oceanographic Products and Services." http://tidesandcurrents.noaa.gov/ (Dec. 24, 2015).

NOAA (National Oceanic and Atmospheric Administration). (2016). "National Centers for Environmental Information (NCEI). http://www.ncei.noaa.glov/ (Feb. 23, 2016).

USACE (United States Army Corps of Engineers). (2016). "Wave Information Study Stations (WIS)." http://frf.usace.army.mil/cgi-bin/wis/ (July 1, 2016).

USGS (United Stated Geological Survey). (2016). http://maps.waterdata.usgs.gov/mapper/index.html (Feb. 1, 2016).

WL|Delft Hydraulics (2001). "User manual Delft 3D-Flow." WL|Delft Hydraulics, Delft, The Netherlands.